Aus dem Adolf-Butenandt-Institut der Ludwig-Maximilians-Universität München
Lehrstuhl: Stoffwechselbiochemie
Vorstand: Prof. Dr. rer. nat. Dr. h.c. Christian Haass

ALS and FTLD associated FUS in zebrafish - investigating disease mechanisms *in vivo*

- Dissertation -
zum Erwerb des Doktorgrades der Naturwissenschaften (Dr. rer. nat.)
an der Medizinischen Fakultät der Ludwig-Maximilians-Universität zu München

vorgelegt von
Laura-Carolin Hasenkamp
aus Düsseldorf
2015

Gedruckt mit Genehmigung der Medizinischen Fakultät
der Ludwig-Maximilians-Universität München

Betreuer:	Prof. Dr. rer. nat. Dr. h. c. Christian Haass
Zweitgutachterin:	Dr. rer. nat. Dorothee Dormann
Dekan:	Prof. Dr. med. dent. Reinhard Hickel
Tag der mündlichen Prüfung:	04.04.2016

Eidesstattliche Versicherung

Ich, Laura-Carolin Hasenkamp, erkläre hiermit an Eides statt, dass ich die vorliegende Dissertation mit dem Thema

'ALS and FTLD associated FUS in zebrafish - investigating disease mechanisms *in vivo*'

selbstständig verfasst, mich ausser der angegebenen keiner weiteren Hilfsmittel bedient und alle Erkenntnisse, die aus dem Schrifttum ganz oder annähernd übernommen sind, als solche kenntlich gemacht und nach ihrer Herkunft unter Bezeichnung der Fundstelle einzeln nachgewiesen habe.

Ich erkläre des Weiteren, dass die hier vorgelegte Dissertation nicht in gleicher oder ähnlicher Form bei einer anderen Stelle zur Erlangung eines akademischen Grades eingereicht wurde.

München, den

(Laura-Carolin Hasenkamp)

However bad life may seem, there is always something you can do, and succeed at. While there is life, there is hope. **Stephen Hawking**

Table of contents

List of figures

List of abbreviations

+/+	wildtype
+/-	heterozygous
-/-	homozygous
aa	amino acid
AD	Alzheimer's disease
AdOX	adenosine-2,3-dialdehyde
aFTLD-U	atypical FTLD with Tau-negative, ubiquitin-positive inclusions
ALS	Amyotrophic lateral sclerosis
ALS-Ci/Bi	ALS with cognitive and behavioral impairment
ALS-FTLD	clinical presentation with similarly strong signs of ALS and FTLD
ALS-FUS	ALS with FUS-positive inclusions
APS	ammonium persulfate
bp	base pair
bvFTD	behavioural variant of Frontotemporal dementia
C. elegans	*Caenorhabditis elegans*
$CaCl_2$	calcium chloride
Cas9	CRISPR-associated 9
CHMP2B	charged multivesicular body protein 2B
CLIP	cross-linking and immunoprecipitation technology
CMV	cytomegalovirus
CNS	central nervous system
CO_2	carbon dioxide
CRISPR	clustered regularly interspaced short palindromic repeats
crRNA	CRISPR RNA
CT	computed tomography
$CuSO_4$	copper sulfate
DAB	3,3'-diaminobenzidine
dATP	deoxyadenosine triphosphate
dCTP	deoxycytosine triphosphate
DEPC	diethylpyrocarbonate

dGTP	deoxyguanosine triphosphate
DMEM	Dulbecco's Modified Eagel's Medium
DMSO	dimethyl sulfoxide
DNA	deoxyribonucleic acid
dNTP	deoxynucleoside triphosphates
DTT	dithiothreitol
dTTP	deoxytyrosine triphosphate
dpf	days post fertilization
DPR	dipeptide-repeat
DSB	double-strand breaks
EDTA	ethylenediaminetetraacetic acid
eGFP	enhanced GFP
Eif2α	eukaryotic translation initiation factor 2α
ELISA	enzyme-linked immunosorbent assay
EMG	electromyography
ENU	N-ethyl-N-nitrosouresa
ER	endoplasmic reticulum
EST	expressed sequence tag
EWS	Ewing's sarcoma
FACS	fluorescence-activated cell sorting
fALS	familial ALS
FBS	fetal bovine serum
FDA	US Food and Drug Administration
FTD	Frontotemporal dementia
FTLD	Frontotemporal lobar degeneration
FTLD-FUS	FTLD with FUS-positive inclusions
FTLD-MND	FTLD with symptoms of motor neuron disease
FUS	human fused in sarcoma gene
FUS	human fused in sarcoma protein
fus	zebrafish fused in sarcoma gene
Fus	zebrafish fused in sarcoma protein
Gal4	yeast transcription activator protein Gal4
GFP	green fluorescent protein
GRN	progranulin
gRNA	guide RNA
GSK-3β	glycogen synthase kinase-3 β
GuHCl	guanidine hydrochloride
H_2O_2	hydrogen peroxide

H_2O	water
H3	histone 3
HDR	homology-directed repair
hnRNP	heterogeneous nuclear ribonucleoprotein
hpf	hours post fertilization
HRM	high resolution melting
HRP	horseradish peroxidase
HSP	heat shock protein
IHC	Immunohistochemistry
IMI	Institute of Molecular Immunology
ISH	*in situ* hybridisierung
ISV	intersegmental blood vessels
KCl	potassium chloride
kDa	kilo-Dalton
KD	knockdown
KH_2PO_4	monopotassium phosphate
KI	knockin
KO	knockout
liq. N_2	liquid nitrogene
LC	low complexity
LDH	lactate dehydrogenase
LMN	lower motor neuron
Luc	luciferase
mAb	monoclonal andibody
MAPK	mitogen-activated protein kinase
MAPT	*microtubule associated protein tau* gene
Met	methionine
$MgCl_2$	magnesium chloride
$MgSO_4$	magnesium sulfate
MND	motor neuron disease
MO	morpholino
mpf	months post fertilization
mRNA	messenger RNA
MRI	magnetic resonance imaging
MW	molecular weight
MZT	maternal to zygotic transition
NaCl	sodium chloride
Na_2HPO_4	disodium hydrogen phosphate

NaN_3	sodium acid
NaOAc	sodium acetate
NCS	newborn calf serum
ND	neurodegenerative disease
NGS	next generation sequencing
NHEJ	non-homologous end joining
NMD	nonsense-mediated mRNA decay
NLS	nuclear localization signal
NTNG1	Netrin G1
o/n	overnight
OPTN	optineurin
ORF	open reading frame
OVA	ovalbumin
PAGE	polyacrylamide gel electrophoresis
PAM	protospacer-adjacent motif
PB	phosphate buffer
PBP	Progressive bulbar palsy
PBS	phosphate buffered saline
PCR	polymerase chain reactions
PD	Parkinson disease
PET	positron emission tomography
PFA	paraformaldehyde
PI	protease inhibitor
PI3K	Phosphatidyl inositol-3 kinase
PLS	Primary lateral sclerosis
PMA	Progressive muscular atrophy
PNFA	Progressive nonfluent aphasia
PPA	Primary progressive aphasia
PTU	phenylthiourea
PTZ	pentylenetetrazole
qPCR	quantitative PCR
RAN	repeat-associated non-ATG
RE	restriction endonucleases
RFLP	restriction fragment length polymorphism
RGEN	RNA-guided endonuclease
RGG	arginine-glycine-glycine motif
RIPA	radioimmunoprecipitation assay buffer
RNA	ribonucleic acid

ROS	reactive oxygen species
RRM	RNA recognition motif
RT	room temperature
sALS	sporadic ALS
SD	Semantic dementia
SD	standard deviation
SDS	sodium dodecyl sulfate
S.E.M.	standard error of the mean
SP	signal peptide
spCas9	*Streptococcus pyogenes*-derived Cas9
SSRI	selective serotonine reuptake inhibitor
STAT3	signal transducer and activator of transcription 3
TAF15	TATA-binding protein-associated factor
TALE	transcription activator-like effector
TALEN	transcription activator-like effector nuclease
TAR	transactive response
TARDBP	human TAR-DNA-binding protein gene encoding TDP-43
Tardbp	zebrafish TAR-DNA-binding protein gene
Tardbpl	zebrafish TAR-DNA-binding protein like gene
TBP	TATA-binding protein
TDP-43	TAR-DNA-binding protein of 43kDa
TEMED	tetramethylethylenediamine
TFEB	transcription factor EB
TILLING	targeted induced local lesions in genomes
TMEM106b	transmembrane protein 106B
TNFα	tumor necrosis factor α
TNFR	TNF receptor
TPP1	tripeptidyl peptidase 1
tracrRNA	trans-activating crRNA
TREM2	triggering receptor expressed on myeloid cells 2
TRN	Transportin
TUNEL	TdT mediated dUTP biotin nick end labeling
TX100	Triton X 100
UBQLN2	ubiquilin 2
UAS	upstream activation sequence
ubi	Ubiquitin
UMN	upper motor neuron
VCP	valosin-containing protein-1

wpf	weeks post fertilization
wt	wildtype / wildtypic
Xenopus	*Xenopus laevis*
ZFN	zinc-finger nuclease
ZnF	zinc-finger

1 Abstract

Amyotrophic lateral sclerosis (ALS) and Frontotemporal lobar degeneration (FTLD) are neurodegenerative diseases, characterized by selective and progressive loss of neurons. Several gene mutations were found to co-segregate with the diseases. Mutations in the *FUS* gene were found to cause about 5% of all inherited forms of ALS and 1% of sporadic cases with no family history. Moreover, FUS positive inclusions in the cytosol of neurons and glial cells are another hallmark of ALS cases with FUS mutations besides the specific degeneration of motor neurons. Additionally, FUS positive inclusion were also found in a subset of FTLD cases, subsequently termed FTLD-FUS. However, exact molecular pathomechanisms leading to insoluble FUS inclusions and death of neurons are elusive.

To clarify the physiological function of FUS and to test whether loss of FUS is necessary and sufficient to elicit ALS and/or FTLD related pathology, I studied FUS loss of function consequences in an *in vivo* approach using the zebrafish as a small vertebrate model. Additionally, ZFN mediated genomic editing the endogenous zebrafish *fus* locus in a way that resembeled an ALS patients mutation allowed to recapitulate pathomechanisms on molecular and cellular levels *in vivo*, devoid of unspecific toxic side effects often generated by transgenic overexpression.

Interestingly, complete loss of function mutants were not identified with the ZFN set used in this study, reflecting putative crucial functions of zebrafish *fus* during germ cell development, whereas embryonic depletion of *fus* via knockdown has no obvious phenotypic consequences. However, I generated a zebrafish model carrying an ALS patient like mutation, the $Fus^{mde1500}$ premature stop allele, resulting in a C-terminally truncated Fus protein lacking the entire nuclear localization signal (NLS) and parts of the arginine rich (RGG3) domain. Strikingly, the $Fus^{mde1500}$ mutant protein recapitulates some features of the pathologic FUS protein in ALS and FTLD patients including a tendency to become insoluble and partial cytosolic redistribution upon transgenic expression in zebrafish and primary cortical neurons. Remarkably, $Fus^{mde1500}$ mutant zebrafish exhibit no obvious phenotypes, indicating that pathogenicity of the $Fus^{mde1500}$ mutant protein is not sufficient to elicit ALS/FTLD reminiscent symptoms and pathol-

ogy in zebrafish. Thus, besides the $Fus^{mde1500}$ mutation additional challenges such as cellular and/or environmental stress are necessary to induce pathogenesis in zebrafish. Taken together, I generated $Fus^{mde1500}$ mutant zebrafish reflecting a biochemical and cell biological model suitable to analyze influences of aging and other risk factors on pathogenesis of FUSopathies in a preconditioned whole organisms approach.

2 Zusammenfassung

Amyotrophe Lateralsklerose (ALS) und Frontotemporale Lobärdegeneration (FTLD) sind neurodegenerative Erkrankungen, die durch den voranschreitenden und selektiven Verlust von Neuronen gekennzeichnet sind. Verschiedene Gene wurden bisher mit den Erkrankungen in Verbindung gebracht und bestimmte Mutationen in diesen Genen segregieren mit der Manifestation der Symptome. Mutationen im *FUS* Gen treten in ca. 5% aller erblich bedingten Formen von ALS auf, während ca. 1% in sporadischen Fällen ohne familiären Kontext gefunden wurden. Darüber hinaus sind FUS positive Einschlüsse im Zytosol von Neuronen und Glia Zellen neben dem spezifischen Absterben von Motorneuronen ein Charakteristikum von ALS Fällen mit *FUS* Mutationen, entsprechend ALS-FUS genannt. Zusätzlich dazu wurden FUS positive Einschlüsse auch in einem Teil von FTLD Fällen gefunden, die daraufhin als FTLD-FUS Fälle kategorisiert wurden. Allerdings sind die exakten molekularen Grundlagen und Pathomechanismen, die zu unlöslichen FUS Einschlüssen und dem Absterben von Neuronen führen, unbekannt.

Um die physiologische Funktion von FUS zu klären und zu untersuchen, ob ein Verlust dieser Funktion ausreicht um ALS und FTLD ähnliche Symptome auszulösen, wurden embryonal FUS defiziente Zebrafische analysiert. Darüber hinaus sollte der endogene genomische *fus* Lokus mit Hilfe der Zinkfinger Nuklease Technologie so editiert werden, dass eine ALS ähnliche FUS Mutation entsteht, um potentielle Pathomechanismen auf molekularer und zellulärer Ebene zu analysieren und dabei unspezifische Toxizitätseffekte durch transgene Überexpression zu vermeiden.

Interessanterweise konnten keine Mutanten mit einem kompletten FUS Funktionsverlust identifiziert werden, was auf eine wichtige Rolle von FUS bereits in der Keimzellentwicklung hindeutet, wohingegen der embryonale Verlust von *fus* über knockdown keinen phenotpyischen Effekt zeigt. Allerdings konnte das $Fus^{mde1500}$ Allele generiert werden, dass durch ein frühes Stopp Codon gekennzeichnet ist und zu einem C-terminal verkürzten Fus Protein führt, dem das nukleäre Lokalisationssignal (NLS) und Teile der Arginin reichen RGG3 Domäne fehlt. Das mutante $Fus^{mde1500}$ Protein spiegelt einige der Eigenschaften wider, die das pathologische humane FUS Protein in ALS und FTLD

Fällen besitzt, darunter die Tendenz zur Unlöslichkeit und die partielle Lokalisierung in zytosolischen Kompartimenten bei transgener Expression in Fischen und primären Neuronen. Dennoch zeigen mutante $Fus^{mde1500}$ Zebrafische keinen ausgeprägten Phänotyp, was dafür spricht, dass die Pathogenizität des mutanten $Fus^{mde1500}$ Proteins gering ist und nicht ausreicht, um ALS oder FTLS ähnliche Symptome und Pathologie in Zebrafischen auszulösen. Daher sind zusätzlich zur $Fus^{mde1500}$ Mutation weitere Faktoren z.B. zellulärer und Umwelt-bedingter Stress notwendig, um in Zebrafischen eine ALS/FTLD-ähnliche Pathogenese zu induzieren.
Zusammengenommen habe ich im Rahmen dieser Doktorarbeit mutante $Fus^{mde1500}$ Zebrafische generiert, die als biochemisches und zelluläres Model dienen können, um in einen durch die $Fus^{mde1500}$ Mutation prädispositionierten Kontext den Einfluss des Alterns und anderer Risikofaktoren auf die Pathogenese von FUSopathien zu untersuchen.

3 Introduction

3.1 Neurodegenerative Diseases

The term 'Neurodegenerative Diseases' comprises a group of fatal diseases characterized by progressive degeneration of neurons in the central nervous system (CNS) leading to impairments in cognitive function, motor function or to behavioral changes. So far, only symptomatic therapy is possible to diminish patients' suffering. With aging being the major risk factor for most neurodegenerative diseases, they are an important public health issue creating immense medical, social and financial burdens for aging societies. Besides neuronal degeneration, formation of insoluble protein aggregates is a common feature in neurodegenerative diseases such as Alzheimer's disease (AD), Parkinson disease (PD), Polyglutamine diseases, Prion disorders, Frontotemporal dementia (FTD) and Amyotrophic lateral sclerosis (ALS). Therefore, these diseases are often referred to as proteinopathies. Despite a shift from rather descriptive to a more mechanistic research in the field of human neurodegeneration and the identification of key components of pathological protein aggregates, exact molecular mechanisms leading to neurotoxicity and cell loss are still elusive. Moreover, it is yet unclear, whether oligomerized and/or aggregated proteins are the toxic species [1] or rather act as a beneficial entity by trapping harmful species [2] or whether protein aggregates are innocent bystanders and toxicity is meditated by different components such as aberrant RNA molecules [3]. The identification of pathogenic gene mutations sheds light on cellular processes involved and thereby paves the way for effective therapeutic strategies.

In general, patients suffering from different neurodegenerative diseases present with various clinical symptoms and harbor divers pathologies, except from the common hallmarks of aggregation of proteins and neuronal degeneration. Despite the variety of often overlapping clinical characteristics, single neurodegenerative diseases can be differentiated pathologically. Unfortunately, this diagnosis is often only possible *post mortem* via autopsy followed by immunohistochemistry.

The diversity of symptoms is of special interest in two neurodegenerative diseases, Amyotrophic lateral sclerosis (ALS) and Frontotemporal lobar degeneration (FTLD),

being discussed as a disease continuum with the individual diseases representing two endpoints of the same syndrome [4].

3.2 Frontotemporal lobar degeneration

The term Frontotemporal lobar degeneration (FTLD) describes the neuropathological feature of a group of disorders comprised as frontotemporal dementia (FTD). FTLD is characterized by selective loss of neurons in the frontal and temporal lobe of the cortex, leading to impaired social behavior and/or speech and language dysfunction [5].
FTLD was first described in 1892 by neurologist and psychiatrist Arnold Pick. Later, Alois Alzheimer identified characteristic protein inclusions in these patients. After AD, FTLD is the second most common dementia in patients under 65 years of age with a estimated prevalence of 10-20 per 100,000 and an incidence of 3.5-4.1 per 100,000/year [6].

3.2.1 Clinical classification & symptoms

According to the clinical symptoms, FTLD is classified into 3 different variants, namely behavioral variant of FTD (bvFTD), being the most frequent variant with up to 50%, Progressive non fluent aphasia (PNFA) and Semantic dementia (SD), together accounting for the other half of FTLD patients. Patients suffering from bvFTD present with behavior and personality changes such as disinhibition, apathy, lack of emotional concern, hyperorality, stereotypic behavior as well as decline in executive function, whereas cognitive function is largely preserved [6]. Patients with SD show strong impairment in language comprehension and anomia, whereas patients suffering from PFNA present with loss of motor speech fluency and agrammatism, with relatively intact language comprehension [6]. PNFA and SD are combined in the term 'Primary progressive aphasia' (PPA) and often further subdivided into nonfluent/agrammatic variant PPA, semantic variant PPA and logopenic variant PPA, taking clinical presentation, pathology and genetics into account [7].
Diagnosis of FTLD is based on clinical features and neuroimaging results using magnetic resonance imaging (MRI), computed tomography (CT) and/or positron emission tomography (PET) [7]. This differential diagnosis excludes other potential symptoms-underlying disorders and is substantiated by postmorten neuropathological examination.
Despite intensive research during the last decades, FTLD is still incurable and no

mechanistic treatment strategy to decelerate or even prevent degeneration of cortical neurons is available. The only chance to alleviate patients' suffering is a symptomatic treatment using psychotropic drugs e.g. selective serotonin reuptake inhibitors (SSRI) or atypical antipsychotics for behavioral abnormalities.

3.3 Amyotrophic lateral sclerosis

Amyotrophic lateral sclerosis is a rare neurodegenerative disease characterized by muscle wasting (amyotrophic) due to the degeneration of upper and lower motor neurons and their lateral corticospinal tracts and axons (lateral sclerosis), respectively [8]. Consequently, voluntary muscle movements are impaired, eventually resulting in paralysis and death due to respiratory failure.
ALS was first described by Jean Martin Charcot in 1869 and is also known as Lou Gehrig's disease. Epidemiological studies show an estimated incidence of 2.7 per 100,000/year and a prevalence ranging from 1.1 to 8.2 per 100,000 [9].

3.3.1 Clinical classification & symptoms

ALS is the most common form of motor neuron diseases (MNDs). Under this umbrella term, several diseases are grouped, all characterized by progressive degeneration of lower motor neurons (LMNs) and/or upper motor neurons (UMNs). Interestingly, only ALS manifests with LMN and UMN dysfunction, whereas Primary lateral sclerosis (PLS) and Pseudo bulbar palsy have only UMN involvement and Progressive muscular atrophy (PMA) and Progressive bulbar palsy (PBP) show only LMN involvement.
Usually, early symptoms start focally resulting in a unilateral disease onset, whereas during disease progression symptoms disseminate, creating a bilateral clinical sign presentation. The majority of patients (approximately 70%) present with so called limb-onset, defined as degeneration of UMNs and LMNs in the limbs, resulting in weakness of limb muscles and locomotion deficits [10]. Approximately 25% show a bulbar-onset form with UMNs and LMNs dysfunction of cranial nerve nuclei, resulting in dysarthria and dysphagia, while the remaining 5% have initial trunk or respiratory involvement [10]. Regardless of the type of onset, symptoms progressively spread throughout the body leading to inhibition of all voluntary muscle control including respiratory muscles at late stages, resulting in respiratory failure in the majority of cases.
ALS is diagnosed according to the *El Escorial World Federation of Neurology Criteria of the Diagnosis of Amyotrophic Lateral Sclerosis*, short: *El Escorial criteria*. These

criteria demand the evidence of LMN and UMN degeneration as well as the absence of any evidence for another underlying disease [11], [12]. Extensive muscle wasting, muscle weakness, aberrant motor unit activity and spontaneous discharges of a single denervated muscle fiber (fibrillations) in combination with spontaneous discharges of motor units (fasciculations) are signs of LMN involvement, evident during anamnesis and diagnosed by electromyography (EMG). UMN involvement displays in spasticity and progressive degeneration of motor cortex, evidenced by neuroimaging using MRI and PET. Other diseases such as myopathies, sensory nerve damages or dementias must be excluded via electrophysiology, neuroimaging and cognitive testing [13]. Similar to FTLD a more precise diagnosis can only be obtained after autopsy and neuropathological examination.

Regardless of several clinical studies to mechanistically treat ALS, no therapeutic benefit was observed, except for the FDA approved drug Riluzole [13]. Riluzole (Rilutek, Safoni-Aventis) is an inhibitor of glutamate release and modifies ALS in a neuroprotective manner by decreasing glutamate mediated excitotoxicity, thereby extending survival of ALS patients by 3-6 months. Other than that, only symptomatical treatment ist available [14].

3.4 Overlap of ALS and FTLD

In the traditional view, ALS and FTLD are two neurodegenerative diseases that represent two distinct disorders. Recent research suggests however, that these two diseases rather represent one broad neurodegenerative disorder with ALS and FTLD being extreme ends of a disease continuum with overlapping clinical symptoms, pathology and genetics (see Figure 3.1).

Patients usually present with clinical symptoms, reflecting ALS or FTLD or mixed forms e.g. ALS with slight cognitive or behavioral impairment (ALS-Ci/Bi), forms with similarly strong symptoms of both, ALS and FTLD (ALS-FTLD), or FTLD with symptoms of motor neuron dysfunction (FTLD-MND). Approximately 14% of ALS patients develop symptoms that meet the clinical criteria of FTLD, whereas far more (30-50%) show subtle cognitive or behavioral impairment [15], [16], [4]. On the other hand, 12-16% of initially diagnosed FTLD patients present with symptoms of ALS, whereas up to one third show signs of either upper or lower motor neuron dysfunction [4], [17], [18]. These observations indicate an overlap of clinical symptoms in ALS and FTLD (see Figure 3.1A). Additionally, ALS and FTLD share common neuropathology, since many proteins that aggregate in ALS, e.g. dipeptide-repeat proteins (DPR), TAR

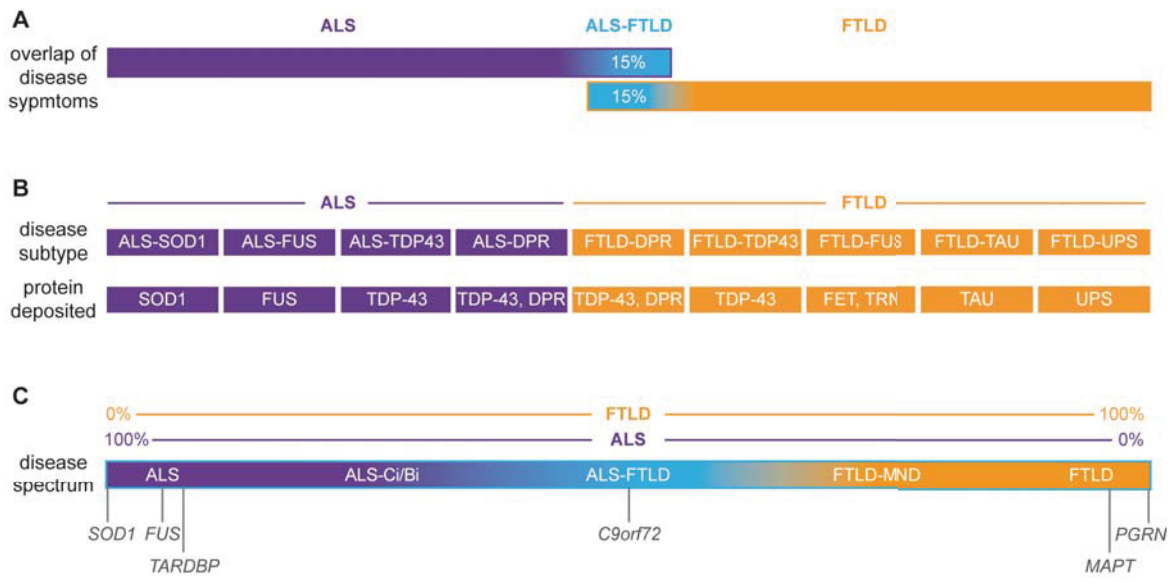

Figure 3.1: ALS and FTLD as disease continuum with overlapping clinical symptoms, pathology and genetics. A Clinical overlap. About 15% of ALS patients present with FTLD symptoms, whereas more then 50% have subtle cognitive or behavioral impairment [15], [16], [4]. Vice versa, about 15% of FTLD patients have classical ALS, whereas more show signs of non-classical ALS with mainly lower motor neuron impairment [17], [18], [4] (also see section 3.4). **B** Pathological overlap. Disease subtypes are classified according to the main deposited protein [19]. Note that TDP-43, DPR and FUS pathology is observed in ALS and FTLD. *Rare cases of FTLD-DPR show mainly DPR and only minimal TDP-43 pathology [20] (also see subsection 3.4.1).**C** Genetic overlap. Selected disease causing genes are blotted along the disease spectrum according to the percentage of mutations found in either ALS or FTLD [8] (also see subsection 3.4.1).

DNA-binding protein 43 (TDP-43), and Fused in sarcoma (FUS), also are deposited in FTLD. These finding have triggered a recent reclassification of ALS and FTLD subtypes according to the main deposited protein [19] (see Figure 3.1B). Moreover, genetic studies revealed ALS or FTLD causing mutations in the same genes, speaking for a genetic overlap of the two diseases (see Figure 3.1C). Particularly, mutations in the *C9orf72* gene are equally likely to cause ALS, or FTLD, or ALS-FTLD, whereas mutations in the *GRN* gene encoding progranulin or *microtubule-associated protein tau (MAPT)* encoding the microtubules-associated protein Tau account for only FTLD and mutations in *SOD1* encoding the copper/zinc superoxide dismutase 1 cause pure forms of ALS (see Figure 3.1C). Note that mutations in the FUS coding *FUS* gene and the TDP-43 coding *TARDBP* gene usually cause ALS but were also found in rare cases of FTLD, although a definite diagnosis by autopsy is missing in most cases [21], [22], [23]. Moreover, aggregated proteins in ALS and FTLD cases are often the gene products of the same genes harboring the disease-associated mutations. Taken together, clinical, pathological and genetical evidence point to a broad ALS-FTLD disease spectrum.

3.4.1 Molecular pathology and genetics in ALS and FTLD

Intensive research in the ALS and FTLD field identified key components of protein inclusions, thereby revealing first hints in the basics of the underlying molecular mechanisms of ALS and FTLD (see Figure 3.1). Moreover, genetic studies of familial ALS and FTLD revealed distinct mutations in several genes to cause ALS or FTLD or both in a mainly dominant manner. Approximately 10% of ALS cases are familial forms (fALS), whereas the majority (90%) are sporadic ALS (sALS) cases [8]. In FTLD, up to 40% are inherited cases (fFTLD), whereas the remaining 60% have no family history (sFTLD) [24]. In contrast to familial forms of ALS and FTLD, sporadic cases show no family history, but few cases habor mutations in the same genes as in fALS and fFTLD and patients present with symptoms indistinguishable from familial forms. However, the majority of sporadic ALS and FTLD cases have so far unknown genetic causes [25]. Incomplete family history, *de novo* mutations, non paternity, and incomplete penetrance are reasons for misclassification [4], though. Together with the constant identification of new histological markers, genetic causes and risk factors, existing disease classifications need to be continually reevaluated and updated.

Despite the many connective features of molecular pathology and genetics in ALS and FTLD, some pathogenic mutations and pathologic proteins are unique to either ALS or FTLD. Mutations in *MAPT* for example cause pure forms of FTLD with Tau positive inclusions [26], [27], [28], [29], [30], [31], consequently termed FTLD-Tau, that make up to 45% of all FTLD cases. Similar to *MAPT*, mutations in *GRN* also cause pure forms of FTLD, however patients show TDP-43 positive inclusions (FTLD-TDP) [30], [31] instead of Tau pathology. Mutations in other genes known to cause FTLD also elicit TDP-43 pathology, including *valosin-containing protein (VCP), C9orf72*, and in rare cases *ubiquilin 2 (UBQLN2)*, and *TARDBP* [37]. Tau pathology-negative FTLD cases including FTLD-TDP were termed atypical FTLD with ubiquitin positive inclusions (aFTLD-U). With emerging evidence from neuropathological studies, aFTLD-U has been reclassified according to the predominantly deposited protein besides ubiquitin, yielding new classes of FTLD, e.g. FTLD-TDP (45%) and FTLD-FUS (9%) [19], [32]. About 1% of all FTLD cases show inclusions positive for proteins of the ubiquitin-proteasome pathway (UPS), with neither TDP-43, nor FUS, nor Tau co-staining and are hence comprised as FTLD-UPS [19] (see Figure 3.1B).

Similar to the FTLD classification, pathological subtypes of ALS are defined by the major aggregating protein. Interestingly, ubiquitin immunoreactive inclusions were also found in ALS, characterizing pathogenic aggregates in all forms of ALS [33]. Apart

from that, TDP-43 positive inclusions are found in 97% of ALS, thus representing the most abundant aggregated protein after ubiquitin. In 2008, mutations in the TDP-43 coding *TARDBP* gene were identified to be causative for ALS [48], [49], [50], [51] with TDP-43 positive inclusions (ALS-TDP). Besides *TARDBP*, mutations in *(VCP), ataxin 2 (ATXN2), angiogenin (ANG), optineurin (OPTN), (UBQLN2)* and *profilin 1 (PFN1)* also cause ALS-TDP with TDP-43 pathology [37].

One of the genes linked to FTLD and ALS-FTLD mixed forms as well as identified as the most frequent genetic cause of ALS is the *C9orf72* gene [52], [53], [54], [55]. Interestingly, hexanucleotide GGGGCC repeats are localized in the upstream *C9orf72* region. The number of repeats ranges from 0-20 under healthy conditions to pathological expansion of over thousand repeats in disease [52], [53]. Interestingly, repeat associated non-ATG (RAN) translation of this locus yields several dipeptide repeat proteins (DPRs), which are deposited in ALS and FTLD subtypes with *C9orf72* mutations [56], [57], [58]. Additionally, TDP-43 is found aggregated in most DPR-positive inclusions carriers [20], [59].

In contrast, mutations in the *copper/zinc superoxide dismutase 1 (SOD1)* were found to cause pure ALS with aggregates immunoreactive for SOD1 and ubiquitin (ALS-SOD1) [34], but devoid of TDP-43 [35], [36].

In 2009 FUS, encoded by Fused in sarcoma (*FUS*) gene, was found to aggregate in pathological inclusions in about 1% of ALS cases, hence called ALS-FUS [37], [8] and in 9% of FTLD subtypes, namely Tau and TDP-43-negative aFTLD-U cases, basophilic inclusion body disease (BIBD) and neuronal intermediate filament inclusion disease (NIFID), thus comprised as FTLD-FUS [38], [39], [40]. Besides ALS and FTLD, FUS is also deposited in predominantly nuclear inclusions in other neurodegenerative disease such as Huntington's disease and spinocerebellar ataxia types 1-3 [32], together with ALS-FUS and FTLD-FUS referred to as FUSopathies, accordingly. Strikingly, not only deposited FUS protein was found to play a role in pathogenesis of ALS and FTLD, but also mutations in the *FUS* gene were identified to cause ALS-FUS [41], [42]. *FUS* mutations were also found in rare cases of FTLD-FUS, but pathogenicity of these mutations is yet unclear since no definite autopsy-based clinical FTLD diagnosis of these cases is available [21]. Importantly, composition of FUS-positive inclusions in ALS-FUS and FTLD-FUS is very distinct. FTLD-FUS is characterized by a selective deposition of FUS and the two other members of the FET protein family (FUS, Ewing sarcoma protein (EWS) and TATA-binding protein associated factor 15 (TAF15)) in contrast to ALS-FUS inclusions that are immunoreactive for FUS but none of the other FET family members [43], [37]. Moreover, Transportin (TRN), the FET family nuclear

import factor, is co-deposited in FUS inclusions of FTLD-FUS cases, but not in ALS-FUS [44]. Additionally, FUS, EWS and TAF15 proteins are hypomethylated when aggregated in FTLD-FUS, whereas in ALS-FUS, FUS protein is highly methylated [45]. These distinct features of FUS positive inclusions in ALS-FUS and FTLD-FUS indicate different underlying mechanisms of inclusion formation.

3.5 Fused in sarcoma/Translocated in sarcoma

Fused in sarcoma/Translocated in sarcoma (FUS/TLS) was initially identified as part of fusion oncogenes in several sarcomas [60], [61]. Later, mutations in *FUS* were found to be a hallmark of ALS-FUS, together with FUS protein containing inclusions [41], [42], also found in FTLD-FUS [38], [39], [40].
FUS is part of the FET (former TET) protein family, consisting of 3 similar DNA/RNA-binding proteins, FUS, EWS and TAF15. Like FUS, EWS and TAF15 were first identified as fusion oncogenes in various cancers [62]. Interestingly, recent findings indicate that all 3 FET family members play a role in ALS and FTLD pathogenesis since FET proteins co-deposit in FTLD-FUS [43]. Moreover, few case studies of ALS patients even report mutations in EWS and TAF15 [63], [64].
FUS is an ubiquitously expressed 526 amino acid long multi domain nuclear protein (Figure 3.2).

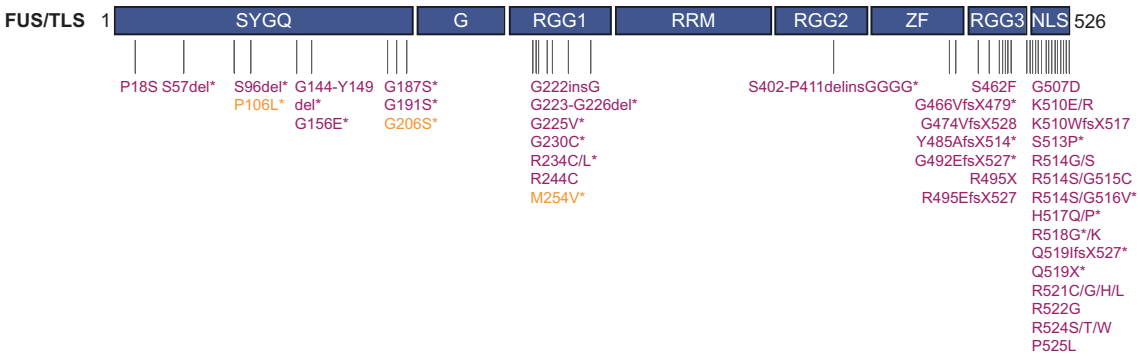

Figure 3.2: Fused in sarcoma/translocated in sarcoma (FUS/TLS). Graphic illustration of domain structure of FUS with mutations identified in ALS (purple) and rare cases of FTLD (orange). Asterisks indicate mutations reported in single cases without family history. del = deletion; ins = insertion; fs = frameshift; X = stop; SYGQ = serine, tyrosine, glycine, glutamine; G = glycine; RGG = arginine glycine glycine motif; RMM = RNA recognition motif; ZF = zinc finger; NLS = nuclear localization signal.

The N-terminal serine, tyrosine, glycine, and glutamine (SYGQ) rich domain has transcriptional properties e.g. acts as a potent transcriptional activator [65]. Moreover, the SYGQ domain is predicted to feature prion-like properties and is necessary and suffi-

cient for *in vitro* aggregation of FUS protein [66], [67]. In addition, FUS exhibits DNA and RNA-binding capacity, mediated by several arginine-glycine-glycine box (RGG) rich domains, an RNA recognition motive (RRM) and a zinc finger (ZnF) domain [68], [69]. Moreover the very C-terminal part of the protein harbors a non-classical nuclear localization signal (NLS), comprising a proline-tyrosine motif (PY-NLS) and parts of one of the RGG domains [70], [71]. This PY-NLS mediates nuclear import via direct binding to the nuclear import receptor transportin (TRN), also known as Karyopherin β2 [72].

3.5.1 FUS' pathogenicity

Mutations in *FUS* were found to account for about 4% fALS and 1% sALS [32]. Importantly, fALS mutations predominantly cluster in the very C-terminal part of FUS, containing the non-classical NLS, whereas many sporadic mutations also localize to the SYGQ and the first RGG domain (Figure 3.2). *In vitro* studies overexpressing mutant FUS constructs show that fALS mutations disrupt the amino acid sequence of the NLS, thereby affecting its binding properties towards TRN, resulting in impaired nuclear import and cytosolic redistribution of the FUS protein [70]. Interestingly, the degree of cytosolic redistribution of the different FUS mutation constructs reflects the impact on TRN binding and correlates with the severeness of different ALS causing mutations regarding age of onset and disease progression [70]. Many of the N-terminal sALS mutations were found only in single cases, so it remains unclear, whether these mutations are causative [73]. However, sALS mutation in *FUS* mostly cluster in the prion like low complexity (LC) domain, potentially interfering with aggregation properties of the FUS protein.

In FTLD-FUS, usually no underlying mutations of *FUS* disrupt the NLS function and nuclear import. Also general TRN-dependent nuclear import deficits can be excluded since other TRN targets are unaffected [44]. Instead, cytosolic redistribution of FUS is thought to be mediated by insufficient arginine methylation of RGG domains in FUS, leading to an overly tight binding to TRN and an impaired nuclear import and accumulation of FUS in the cytoplasm [37].

In addition to redistribution of FUS in ALS-FUS and FTLD-FUS, a so called '2nd hit' theory is being discussed, implying that besides mutation and mislocalization of the FUS protein to the cytosol another event, e.g. environmental stress, has to take place to generate insoluble cytosolic inclusions and elicit motor neuron toxicity. Work in cell culture showed that upon cellular stress (heat shock, oxidative stress, endoplasmatic

reticulum (ER) stress) mutant cytosolic FUS accumulates in stress granules (SG) [70], [74]. SGs reversibly form upon stress conditions and serve as a storage entities for mRNAs and RNA-binding proteins during stress response [75]. Interestingly, insoluble inclusions in ALS-FUS and FTLD-FUS contain characteristic markers of SG, indicating that SGs might be a precursor to pathologic inclusions [73].
In general, two different potential FUS pathomechanisms are under debate, namely gain-of-function and loss-of-function mechanisms. In a gain-of-function model, toxicity is mediated by aberrant accumulation and aggregation of FUS in the cytosol, whereas loss-of-function describes a toxicity mediated by loss of physiological FUS functions in the nucleus due to mislocalisation. It is currently unclear whether gain or loss of function or a combination of both mechanisms are responsible for FUS induced pathology (also see subsection 3.5.3).

3.5.2 FUS' physiological function

FUS protein function is crucial for several nuclear and cytosolic processes that include DNA/RNA metabolic steps like DNA repair, transcription, RNA splicing and transport.
FUS was identified as POMp75 protein important for DNA homologous pairing and DNA double strand break repair [76], [77]. Moreover, FUS knockout mice show enhanced radiation sensitivity, defects in spermatogenesis and B lymphocyte development and genomic instability, strengthening its important role in DNA damage response and maintenance of genomic integrity [78], [79].
FUS has been shown to associate with RNA polymerase II and its general transcription factor TFIID [80] and is able to inhibit RNA polymerase III, potentially via direct interaction with TATA binding protein (TBP) [81], speaking for a general role of FUS in transcription regulation. Moreover, FUS might directly control transcription of specific genes through its interaction with certain nuclear hormone receptors [82] and specific FUS response elements in several target genes [83].
Mass spectrometry studies found FUS as P2 component of the heterogeneous nuclear ribonucleoprotein (hnRNP) complex H [84], indicating a role of FUS not only in transcription but also in heterogeneous nuclear RNA processing and maturation. The hnRNP complex, consisting of more than 30 different proteins, is involved in pre-mRNA splicing and in transporting fully processed mRNA to the cytoplasm [69]. Additional evidence for FUS' function in splicing comes from proteomic analysis of the human spliceosome that identified FUS as a component of the splicing machinery [85], [86].

Also the association with several other spliceosomal small nuclear ribonulear proteins [87] and the influence of FUS on selection of 5' splice sites during alternative splicing [88] identifies FUS as splice factor.
Consequently, FUS has been shown to directly bind RNA, preferentially along long intronic regions, leading to a sawtooth like binding pattern that is thought to stabilize nascent RNA during transcription and/or splicing [89]. Moreover several RNA binding motives for FUS have been described, ranging from G/C rich [90] or C/U rich [91] regions to GGU [92], GGUG [87], or GUGGU motives [89]. Also RNA secondary structure has been found to affect binding to FUS since RNAs containing short stem loop motives were identified to bind FUS with higher affinities than other or no secondary structures containing RNAs [93], [90].
The role of FUS in RNA binding and alternative splicing has been extensively investigated in the recent years by analyzing RNA targets of FUS to gain insights into potential physiological roles of FUS in the nervous system. Independent studies were performed using several different systems (*in vitro* using stably transduced HEK cells expressing human FUS [93] or FUS knockdown mouse embryonic stem cell derived neurons [91], mouse embryonal FUS knockout brains [92], *in vivo* FUS kockdown using stereotactic injections, FUS knockout brain derived cultured mouse neurons [89] or FUS knockdown in primary cortical mouse neurons [90] amongst others) combining cross-linking and immunoprecipitation (CLIP) technologies with next-generation sequencing, thus yielding direct binding and splicing targets of FUS. Gene ontology analysis of the identified targets revealed an impact of FUS in axonogenesis, axon guidance, cell adhesion, neuron protection, vesicle transport and cytoskeletal organisation. Interestingly, overlap of different studies was small and only few targets were found independently in more than one study [94]. Moreover, different exons were identified to be alternatively spliced within the same target by different studies [94]. Some of these targets were described previously, e.g. Nd1-L [95] or could be validated in independent studies, e.g. *MAPT* [96]. The *MAPT* gene consists of 16 exons and is mainly expressed in the nervous system. Tau shows a complex and tight regulation of alternative FUS dependent splicing of an N-terminal cassette (exons 2 and 3) and exon 10 that leads to six different isoforms (0N3R, 1N3R, 2N3R, 0N4R, 1N4R, 2N4R)[94]. Interestingly enhanced expression of 4R Tau isoforms including exon 10 results in impaired axonal growth and neurodegeneration both in the presence and absence of overt Tau aggregation [96], [97], [98], [99], [26].
FUS continuously shuttles between nucleus and cytoplasm and was also shown to play important roles outside the nucleus [100]. In cultured hippocampal neurons, FUS is

localized in dendritic granules and spines upon synaptic stimulation, together with the accumulation of mRNAs [101], pointing to a role of FUS in mRNA transport. Interestingly, FUS was also shown to interact with axonal transport factors kinesin [102] and myosin-Va [103] and to transport the mRNA of the actin stabilizing protein Nd1-L [95]. Additionally, depletion of FUS in cultured hippocampal neurons leads to abnormal dendritic and spine morphology [104] and severely enlarged axonal growth cones [96], indicating that FUS is important in maintaining neuronal morphology und synaptic function.

3.5.3 FUS animal models

Several animal models of FUS have been generated to better understand physiological functions of FUS and to thereby get insights of molecular mechanisms that turn dysfunctional in ALS-FUS and FTLD-FUS. To do so, two approaches are being applied. Firstly, overexpression of wildtype FUS or ALS relevant mutations mimick a gain of function situation, where cytotoxicity is thought to be mediated by additional aquired function(s) in the cytosol due to mislocalization and aggregation of FUS in patients. Secondly, elimination of endogenous FUS generates a loss of function situation, where essential (nuclear) functions of FUS can no longer be maintained, hypothetically resulting in neuronal dysfunction. Gain of function and loss of function are both being discussed as potential pathomechanisms leading to FUS mediated pathology (also see subsection 3.5.1).

In *C. elegans* overexpression of wildtype FUS and several ALS-associated mutations results in cytoplasmic mislocalization of FUS mutations according to the severeness of phenotype seen in humans [105]. Moreover, overexpression of mutant FUS is more toxic than wildtype FUS, but results in progressive motor defects, paralysis and a shorter live span in both cases [105].

In drosophila, knockdown of the human *FUS* orthologue *cabeza (caz)* results in decreased adult viability, diminished locomotor speed, and reduced life span [106] and shortening of motor neuron terminal branches [107]. Interestingly, overexpression of wildtype but not mutant human FUS could rescue this phenotype [106], indicating that the ALS mutations convey loss of function. Overexpression of human wildtype and ALS related FUS mutants showed that mutant FUS is partially localized to the cytosol, whereas wildtype FUS is purely nuclear. Moreover mutant FUS is more toxic than wildtype and results in degeneration of motor neurons and reduced life span [108], [109].

In zebrafish, both FUS overexpression and Morpholino (MO) mediated transient knockdown studies have been performed. Knockdown of zebrafish *fus* results in motor neuron axon outgrowth phenotype and motor deficits [110]. Strikingly, overepression of an ALS-related mutation R521H resulted in very similar phenotypes [110]. Interestingly, this mutation failed to rescue the knockdown phenotype when co-expressed [110].
In mice, two independend studies generated *Fus* knockout lines. Inbred stains of *Fus*-/- mice show B-lymphocyte development defects, high incidence of chromosomal instability, e.g. karyotypic abnormalities and fail to suckle, resulting in perinatal death [78]. In outbred *Fus*-/- strains reduced fertility in females, dysfunctional spermatogenesis resulting in male sterility, increased sensitivity to ionizing irradiation and impaired pairing of homologous DNA molecules during meiosis was reported [79]. In both lines, no neurodegenerative phenotypes have been described, but overlapping phenotypes point to a crucial function of FUS in maintenance of genomic stability. Primary neurons derived from *Fus*-/- mice show low spine densitiy and abnormal spine morphology [111]. Overexpression of wt human FUS in mice results in progressive limb paralysis, synaptic denervation and motor neuron degeneration in spinal cord and focal muscle atrophy [112].
In rats overexpression of wt FUS as well as the ALS mutation R521C lead to loss of neurons in brain and spinal cord, accompanied by denervation of neuromuscular junctions and paralysis [113]. Interestingly, mutant FUS causes severe phenotypes, whereas overexpression of wildtype FUS results in moderate but significant neurodegeneration [113].
Taken together, existing FUS animal models display conflicting results. To better recapitulate the disease situation *in vivo*, targeted genomic editing should be utilized to generate models that harbor ALS mutations controlled by the endogenous FUS locus. This genetic approach will shed light into putative gain or loss of function mechanisms leading to FUS pathogenesis and disease.

3.6 Zebrafish

3.6.1 Zebrafish as model organism

Zebrafish (*Danio rerio*) as a small vertebrate model has long been the system of choice for a wide spectrum of biological questions to be investigated *in vivo* at cellular and subcellular resolution [114]. Zebrafish are small, easy to handle and grow, fertile within three months of age and highly reproductive, providing more than two hundred embryos

per week per healthy pair of adult fish. Another advantage is the rapid development of the embryo, e.g. gastrulation is complete within ten hours after fertilization and heart beating starts at the end of the first day of an embryo's life. Moreover, most organs are formed and functional within the first five days of development. Zebrafish embryos develop *ex utero* and together with the characteristic transparency within the first days of development, they are very well suited for cell biological studies. Additionally, minimal invasive experimental manipulations such as targeted mutagenesis, introduction of exogenic DNA and RNA interference technology are feaasible due to the easy accessibility of the embryo. Moreover, comparison of the zebrafish genome to the human genome shows that approximately 70% of human genes have at least one obvious zebrafish orthologue [115], indicating a broad conservation of gene function between species.

Historically, zebrafish research started in 1930s with classical developmental and embryological studies [116]. Since then the zebrafish has been extensively used to study cell fate and migration during early development, organogenesis and regeneration mechanisms, amongst others and has become a valuable tool in biomedical research. Since 1990 large genetic screens identified several mutations in genes that are orthologues to human genes, allowing to study gene function on a cellular level *in vivo*. Moreover, several of these mutants serve as model for human monogenic diseases, elucidating basic molecular mechanisms underlying these diseases. To date, zebrafish models for a variety of human diseases exist, including cancer [117], cardiovascular diseases [118], immunological diseases, inflammation, wound healing and regeneration [116], metabolic disorders such as diabetes type I and II, obesity and artherosclerosis [119], [120], muscle diseases [121] and neurodegeneration [122], [123].

Also, high throughput small molecule screening is possible in zebrafish due to its unique features. Since 2000, chemical screens were successfully performed to identify the therapeutical relevance of known and novel compounds for certain indications as well as their potential toxicity and teratogenicity [124]. These chemical screens yield not only new lead compounds but also insights into conserved physiological processes in vertebrates [125], [124], [126], [127], [128], further solidifying the role of zebrafish in pharmaceutical drug discovery and biomedical research.

3.6.2 Mutagenesis in zebrafish

Genetic manipulations generating loss of function situation are employed to analyze the resulting phenotype and conclude about physiological functions of the gene. In

zebrafish genetic manipulation is feasible either by performing forward genetic screens or by using the recently established reverse genetics techniques. The term forward genetics describes the approach of random mutagenesis followed by screening for desired phenotypes and identification of the underlying mutations and loci. In contrast, reverse genetics is the targeted mutagenesis of desired genes and subsequent analysis of resulting phenotypes.

Forward genetics mutagenesis of zebrafish made use of chemical mutagens like ethylnitrosourea (ENU) [129], [130] or retroviral techniques [131]. Both approaches result in mosaic P0 founder fish that are breed to generation F2 or F3 and then analyzed for phenotypes, followed by identification of the underlying mutation. This time, cost and labor-intensive approach of forward genetic screening was long time the only way to generate heritable gene mutations in zebrafish.

The only alternative to forward genetic screening has long been to transiently ablate protein function using targeted knockdown via antisense morpholinos (MO) or antisense gripNAs. However, transient non-heritable knockdown approaches are susceptible to off-side targets and can only temporarily either block translation or interfer with splicing [132].

Classical reverse genetics using targeted mutagenesis was not possible in zebrafish due to lack of embryonic stem cell cultures, unlike other model organisms such as mice where targeted genomic editing has been successfully performed via homologous recombination. Instead, Targeting Induced Local Lesions in Genomes (TILLING) was the reverse genetics strategy of choice in fish. TILLING allows to identify mutations in specific genes of interest in chemically mutagenized populations [133] and was firstly used in zebrafish in 2002 [134]. Similar to forward genetic screens, fish are mutagenized using ENU or retroviral techniques and analyzed for mutations in genes of interest as early as F1 generation, prior to being breed to homozygousity and analyzed for phenotypes. In 2008 engineered zinc finger nucleases (ZFNs) were found to be functional in zebrafish, allowing targeted, heritable gene disruption in zebrafish for the first time [135], [136]. This finding paved the way for the discovery of several other genome editing tools such as transcription activator like effector nucleases (TALENs) and clustered regularly interspaced short palindromic repeats/CRISPR associated 9 (CRISPR/Cas9) and their utilization in zebrafish to perform genomic editing via targeted mutagenesis [137], [138], [139], [140], [141], [142], [143], [144]. ZFNs, TALENs and CRISPR/Cas9 all consist of a sequence-specific DNA-binding entity and a double strand cleaving DNA nuclease [145] (see Figure 3.3A). Introduction of double strand breaks into the genome elicits two repair mechanisms in the affected cell, namely non-homologous end joining

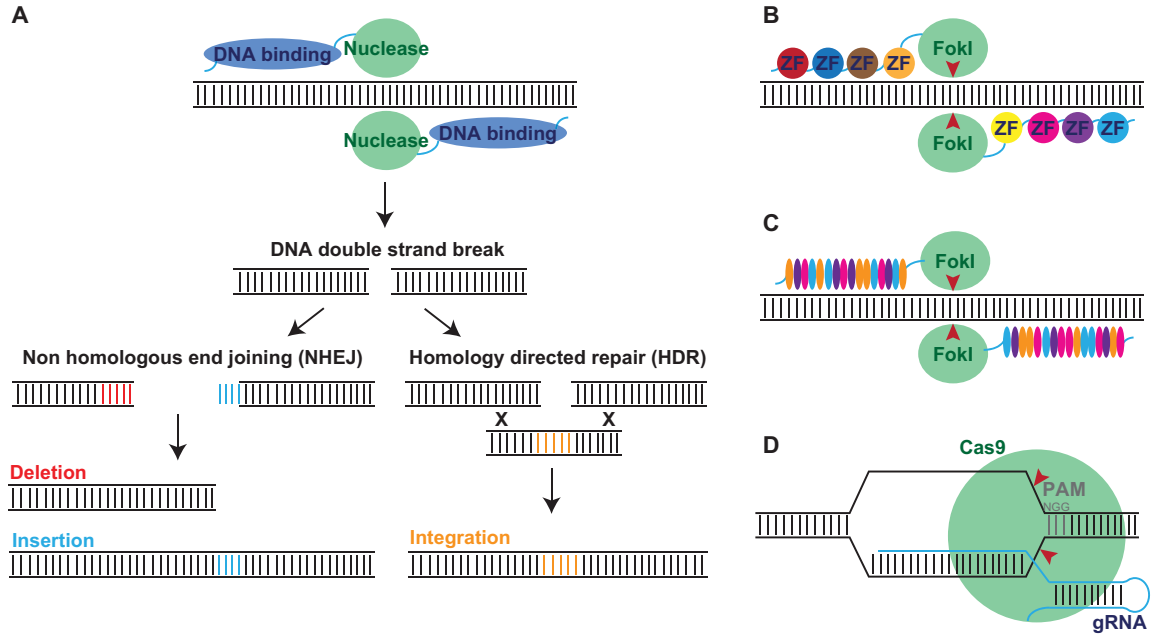

Figure 3.3: Genome editing strategies. A Schematic illustration of genome editing via targeted mutagenesis. DNA cleaving entity (green) is directed to a specific genomic locus via sequence specific DNA binding elements (blue). When heterodimerized, nuclease introduces DNA double strand breaks that elicit two DNA repair mechanisms: NHEJ and HDR. NHEJ is error prone and frequently generates small deletions (red) or insertions (cyan), leading to frame shift or premature stop codons and loss of protein function (knockout) due to nonsense mediated RNA decay. HDR utilizes a homologous template DNA strand to repair double strand breaks, allowing to integrate exogenic DNA from a donor sequence with flanging homology arms, yielding knockins. **B** Zinc finger nucleases (ZFNs). Left and right subunit heterodimerize, initiating DNA cleavage by FokI endonuclease (FokI). ZFN arrays are composed of three to six zinc finger motives (ZFs), each binding three nucleosides. **C** TALENs. Like with ZFNs, DNA cleavage only occurs upon heterodimerization of left and right subunit of FokI. Each of the 16 TALEs per subunit recognizes 1 DNA nucleoside. **D** CRSIPR/Cas9. Cas9 nuclease (Cas9) is recruited to genomic target site via binding of 20 nucleotide long targeting sequence containing guided RNA (gRNA). Arrowheads (red) indicate approximate position of double strand break.

(NHEJ) and homology directed repair (HDR). The former ligates broken DNA strands without template and is therefore error prone due to frequent insertions and deletions (indels) of basepairs (bps), resulting in frameshifts or premature stop codons and subsequent degradation of the transcripts via nonsense-mediated RNA decay (NMD) or truncated proteins, respectively. This phenomenon can be utilized to generate knockout (KO) animals and mutant alleles can be identified via sequence analysis. In contrast to NHEJ, HDR needs homologous DNA template and can therefore be exploited to introduce exogenic DNA into a desired locus, resulting in knock-in (KI) animals [141], [146], [147], [145].

3.6.2.1 ZFNs

ZFNs are engineered chimeric proteins, composed of the catalytic active nuclease domain of a FokI endonuclease fused to an array like arrangement of three to six Cys2His2 zinc finger modules, with each module recognizing three bps of the DNA target sequence (see Figure 3.3B). The catalytic nuclaese moiety is composed as heterodimer, allowing DNA cleavage only if both nuclease subunits are brought together in close proximity via the sequence specific zinc finger arrays, thereby reducing off-target events. The design, however, is complex since affinity of single zinc finger modules is context dependent, thus difficult to predict *in silico*, therefore demanding initial *in vitro* testing [148], [149].

Nevertheless, work flow is comparatively easy: DNA constructs encoding ZFNs are transcribed *in vitro* and injected into zygotic zebrafish embryos, where they are translated *in vivo* and introduce DNA double strand breaks. Each affected cell within the embryo repairs the DNA damage independently using either HDR or NHEJ, generating a mosaic P0 generation embryo harboring different mutantations within the same genomic locus. Back-crossings with wildtype fish yield a non mosaic F1 generation, being heterozygous for one specific allele. Genotyping of F1 generation fish allows to analyze induced alleles prior to phenotyping, which usually starts in the F2 generation when homozygosity is achieved.

So far, ZFNs have been successfully used in cell culture systems and *in vivo* to study gene function in the model organism of interest, including targeted gene disruption, gene correction (allele editing) and gene addition [149]. In zebrafish, only the disruption of native genes using ZFNs could successfully been shown since NHEJ seems to be the favored repair mechanism and HDR is rare in this context. Interestingly, efficiencies of introduced loss of function mutations vary, depending on the zinc finger selection strategy, *in vitro* validation assays for zinc finger affinities, target site and model system [145].

3.6.2.2 TALENs

Transcription activator like effector nucleases (TALENs) are engineered chimeric proteins similar to ZFNs with a FokI endonuclease subunit fused to a DNA binding entity, which in case of TALENs is the plant pathogen *Xanthomonas*-derived transcription activator like effector (TALE) (see Figure 3.3C). TALEs consist of four different repeats, each being 33-35 amino acids long and containing two variable amino acids at position 12 and 13 that mediate specific binding to one of the four different DNA nucleosides.

About 16 TALE repeats are fused to each of the two FokI nuclease subunits. Pairs of TALEN are designed in a way that the two FokI subunits form a heterodimer when aligning at the desired genomic locus, thereby introducing sequence specific DNA double strand breaks and drastically reducing the chance of obtaining off-site targets. In contrast to ZFNs, nucleoside binding of single TALE repeats is not context dependent, making the design much easier. Generation of TALE repeats requires extensive cloning, though [145], [150]. Mutagenesis, breeding, genotyping and phenotyping of zebrafish is similar to the ZFN approach (see subsubsection 3.6.2.1).

3.6.2.3 CRISPR/Cas9 system

The CRISPR/Cas9 system differs from the other genomic editing tools due to the fact that the DNA binding entity is a RNA, that guides the *Streptococcus pyogenes* derived SpCas9 nuclease to the desired genomic locus, thus mediating sequence specificity. This guiding RNA, (guide RNA, gRNA), binds DNA via Watson-Crick base pairing, a highly specific and predictable mechanism (see Figure 3.3D). The archaea derived CRISPR/Cas9 system is reminiscent of an innate immune system [151] and was successfully modified for applications in eukaryotes [152], [145]. Generation of gRNAs and Cas9 protein is simple and less cost and labor intensive than ZFNs and TALENs since almost no sequence requirements limit the design, except for a two nucleotide SpCas9 specific NGG protospacer adjacent motif (PAM) next to the 20 nucleotide long target sequence. Moreover, gRNA and Cas9 mRNA can easily be transcribed *in vitro* and injected into zebrafish zygotes. Off-site events are likely to be more frequent than with ZFNs and TALENs due to the comparatively short target region used with CRISPR/-Cas9 system. However, due to outcrossing and elimination of undesired off-target mutations in zebrafish, these are neglectible [145]. Moreover, efficiency is comparable to TALENs [153]. The CRISPR/Cas9 system has recently been used in zebrafish to introduce mutations in specific loci via NHEJ and for generation of KI animals, exploiting the HDR DNA repair mechanism [140], [141], [142], [143], [144]. Again, workflow of obtaining mutant zebrafish using the CRISPR/Cas9 is similar to the ZFN approach, once gRNAs and Cas9 are injected into zebrafish zygotes (see subsubsection 3.6.2.1).

3.6.3 Modelling ALS/FTLD in zebrafish

Despite the intensive research and remarkable clinical and pathological characterization of neurodegeneration associated genes, their physiological function is largely elusive. Besides other animal models, zebrafish have been used to study function of neurode-

generation associated proteins *in vivo*. Two main strategies have been employed to do so. Firstly, overexpression of genes via RNA or DNA injection, where mimicking of potential toxic effects due to overly expressed or mislocalized proteins generates a gain of function situation. Secondly, a loss of function situation can be achieved by ablation of gene expression via transient knockdown using morpholinos (MOs) or gripNAs (see subsection 3.6.2) or stable knockout of genes using targeted mutagenesis (see subsection 3.6.2).

To recapitulate hallmarks of the ALS/FTLD disease contiuum, several studies were performed in zebrafish. ALS causing mutant SOD1 protein has been overexpressed, eliciting ALS like phenotypes including neuromuscular junction alterations, motor neuron loss, muscle atrophy, paralysis and premature death [154], [155]. Furthermore, zebrafish orthologues of the FTLD-associated *granulin (GRN) grna* and *grnb* have been knocked out recently, resulting in neither spinal motor neuron axonopathies nor a reduced number of myogenic progenitor cells, in spite of the previously reported phenotypes for *grna* and *grnb* MO-mediated knockdown embryos, probably owing to unspecific toxicity of MOs [156]. Similarly, ALS and FTLD related TDP-43 protein has been studied in zebrafish. Two zebrafish orthologues, *tardbp* and *tardbpl*, exist with *tardbpl* being alternatively spliced upon *tardbp* ablation, thus compensating for *tardbp* gene function [145], [157], [158]. Consequently, only knockout of both *tardbp* and *tardbpl* lead to severe dysfunction involving spinal motor neuron axon length, muscle atrophy, vasculature mispatterning, blood circulation and eventual lethality [157]. In addition, overexpression of human wildtype and mutant TDP-43 as well as transient knockdown of zebrafish *tardbp* has been studied. Interestingly, MO-mediated knockdown of zebrafish *tardbp* alone was reported to result in reduced length and aberrant branching of primary spinal motor neuron axons [159]. Surprisingly, injection of human wildtype and mutant TDP-43 mRNA into zebrafish embryos elicit similar motor neuron defects [159], [160], with mutant TDP-43 evoking more severe phenotpyes [159]. Also, ALS and FTLD related FUS protein has been studied in zebrafish. Transient MO mediated knockdown of the only FUS homologue *fus* results in reduced but hyperbranched motor neuron axons and abnormal motor behaviour [110]. Remarkably, also overexpression mutant FUS mRNA harboring the ALS causing mutation R521C (see Figure 3.2) yields reduced, hyperbranched motor neuron axons and motor deficits [110].

However, beforehand described transient *knockdown* or overexpression studies display a major drawback which is unspecific toxicity, due to off-site target effects or global degradation machinery breakdown or simply interfering with absolute protein levels.

To circumvent these unwanted side effects, clean genetic approaches utilizing genome editing (see subsection 3.6.2) will be the future strategy of choice to analyze disease mechanism and progression.

4 Objectives

Identification of ALS causing mutations in the *FUS* gene and pathologically deposited FUS protein in ALS and FTLD was a major breakthrough in the molecular understanding of these neurodegenerative diseases.

Currently, two potential mechanisms explaining FUS mediated pathology are under debate. Firstly, FUS fulfills crucial nuclear functions for sustained neuronal homeostasis and depletion from the nucleus is thought to result in a loss of function, leading to cell death. Secondly, mutant and redistributed FUS might obtain toxic function in the cytosol driving neuronal cell death, thus resembling gain of function [161]. However, the physiological role of FUS and the underlying cellular mechanisms linking mislocalization of mutant FUS to pathologic inclusion formation and neuronal degeneration are still unknown. Therefore, the ultimate goal of this study was to elucidate the physiological function of FUS and shed light on molecular mechanisms underlying FUS-mediated pathology.

To investigate the physiological function of FUS and to test whether loss of this function is necessary and sufficient to elicit ALS and/or FTLD-related pathology, I aimed to study FUS loss of function consequences *in vivo* using zebrafish as a small vertebrate model. Besides transient embryonic silencing of *fus* via knockdown, loss of FUS should be achieved via stable and heritable ablation of FUS using ZFNs, at that time the only genome targeting technique established for applications in zebrafish.

Additionally, I aimed to generate a zebrafish *fus* allele resembeling an ALS patients mutation to recapitulate pathomechanisms on cellular and molecular but levels devoid of unspecific toxic side effects often generated by transgenic overexpression. Since classical knockin strategies were not established in zebrafish at that time, ZFN mediated targeted mutagenesis should be performed and alleles should be screened for premature stop codons yielding truncated proteins rather than frameshift mutations and RNA decay as in the knockout approach.

Moreover, after generation of *fus* mutant zebrafish, resulting phenotypes were analyzed to investigate the impact of the induced mutations on the physiological functions of *fus* and Fus protein pathogenicity. Particularly, ALS relevant effects such as mutant Fus

protein localization, aggregation potential, inclusion formation, spinal motor neuron morphology, muscle, and vessel development were of special interest.
Since FUS positive inclusions are not only found in ALS and FTLD cases, but also in a wide spectrum of polyglutamine diseases such as Huntington's disease and spinocerebellar ataxia [32], results of this study will provide new profound insights in molecular mechanism of FUS mediated pathology not only in ALS/FTLD but have an impact on other FUSopathies, thereby allowing to eventually develop successful treatment strategies for all these diseases.

5 Material and Methods

5.1 Material

5.1.1 Zebrafish lines

The following zebrafish lines were used:

Zebrafish line	**Origin (Reference)**
wildtype-line AB	G. Streisinger, Institute of Neuroscience, University of Oregon, Eugene, USA
wildtype-line TLF	C. Nüsslein-Volhard, MPI for Developmental Biology, Tübingen, Germany

5.1.2 Cells

Human cervical carcinoma cells (HeLa) were obtained from DSMZ, #ACC 57. Primary rat cortical neurons were dissected and cultured from E18 Sprague-Dawley rat embryos, supplied by Charles River Laboratories.

5.1.3 ZFNs

CompoZr Zinc finger nuclease plasmids containing coding sequences to specifically target zebrafish *fus* gene at exon 14 were obtained from Sigma Aldrich.

***fus* ZFN set**	**binding and *cut site***
PZFN1/PZFN2	GGCTTCGATCGAGGTG*gtttcc*GTGGTCGTGGTGGTGATC

5.1.4 gripNAs

gripNAs were purchased from Gene Tools. Sequences are given in 5'-3' orientation.

Targeted site	Sequence
fus ATG gripNA	GCCCAAACATGGCGTCAA
fus intron13-exon14 splice gripNA	GTGTAGGTGGTTTTGGTG

5.1.5 Vectors and plasmids

The following vectors and plasmids were used:

Vector	Insert	Origin
pCR8/GW/TOPO	-	Invitrogen
pCRII TOPO	-	Invitrogen
pCSeGFP-Dest	n-terminal GFP tag	Lawson Lab [162]
pTolDestR4-R2pA	-	Lawson Lab [162]
pENTR5'-ubi	*zebrafish ubiquitin promotor*	Zon lab [163]
pCR8-zfFuswt	wildtype *zebrafish fus* cDNA	L. Hasenkamp
pCR8-zfFusF500X	mutant $Fus^{mde1500}$ *zebrafish fus* cDNA	L. Hasenkamp
pCS2eGFP-zfFuswt	wildtype *zebrafish fus* cDNA, n-terminal GFP-tag	L. Hasenkamp
pCS2eGFP-zfFusF500X	mutant $Fus^{mde1500}$ *zebrafish fus* cDNA, n-terminal GFP-tag	L. Hasenkamp
pCR8eGFP-zfFuswt	wildtype *zebrafish fus* cDNA, n-terminal GFP-tag	L. Hasenkamp
pCR8eGFP-zfFusF500X	mutant $Fus^{mde1500}$ *zebrafish fus* cDNA, n-terminal GFP-tag	L. Hasenkamp
pTol-ubi:eGFP-zfFuswt	wildtype *zebrafish fus* cDNA, n-terminal GFP-tag, *zebrafish ubiquitin promotor*	L. Hasenkamp

pTol-ubi:eGFP-zfFusF500X	mutant $Fus^{mde1500}$ *zebrafish fus* cDNA, n-terminal GFP-tag, *zebrafish ubiquitin promotor*	L. Hasenkamp

5.1.6 Oligonucleotides

Oligonucleotides were synthesized by Thermo Scientific or Sigma-Aldrich. Sequences are given in 5'-3' orientation. Abbreviation and number in the oligonucleotide name refer to the Schmid laboratory oligonucleotide database.

5.1.6.1 Cloning primers

oD45 zfFus ATG	ATGGCGTCAAATGATTATGGC
oD34 zfFus Stop	TTAGTAAGGGCGGTCTCTGC
oLH1 zFus_stop_F500X_rev	CTAACCACCTCGATCGAAGC
GATC T7-981079	TAATACGACTCACTATAG

5.1.6.2 Sequencing primers

GATC M13-FP	TGTAAAACGACGGCCAGT
GATC M13-RP	CAGGAAACAGCTATGACC
GATC SP6	ATTTAGGTGACACTATAGAA
GATC T7-981079	TAATACGACTCACTATAG
oLH1_A2 FUS_ZFN1_f1	CATGTGGAAATTTGAACTTC

5.1.6.3 Genotyping primers for RFLP

oLH1-A2 FUS_ZFN1_f1	CATGTGGAAATTTGAACTTC
oLH1-B4 FUS_ZFN1_r3	AAGTGGATTGATTACTGGTC

5.1.6.4 Genotyping primers for allele specific PCR

To amplify either the $Fus^{wildtype}$ or the $Fus^{mde1500}$ allele, two primers per PCR reaction were used:

Primer	Sequence	Amplified allele
oLH1-B5 FUS_ZFN1_f4	GGAAGTGGAGGAGGAATG	$Fus^{wildtype}$
oLH1-G3 zFus-F500X-/-_wtr1	GATCACCACCACGACCACGG	$Fus^{wildtype}$
oLH1-G5 zFus-F500X-/-_mutf1	CTTCGATCGAGGTGGTTAGG	$Fus^{mde1500}$
oD34 zfFus Stop	TTAGTAAGGGCGGTCTCTGC	$Fus^{mde1500}$

5.1.6.5 Genotyping primers for HRM analysis

oLH2_A11 Fus-HRM-for2	GTGGTTTTGGTGGAGAGC
oLH2_A13 Fus-HRM-rev1	TTCCAGGTCCAAATCCTC

5.1.6.6 Semiquantitative PCR primers

Primer	Sequence	Amplified gene
oA03 β-actin F	TGTTTTCCCCTCCATTGTTGG	*β-actin*
oA04 β-actin R	TTCTCCTTGATGTCACGGAC	*β-actin*
oLH2_A18 ntng1-for2	CTGACTTGCGAGTGTGAGCA	*ntng1*
oLH2_A19 ntng1-rev2	GGACACTGACAACGGACGTA	*ntng1*
oLH2_A20 mapta-for1	ATGTGCAGGCTAGATGTGGC	*mapta*
oLH2_A21 mapta-rev1	GAGCGATGCAGACACCTGG	*mapta*
oLH2_A24 Mapt1of2-for1	GGGCAACAGGTGAAGAAGGT	*maptb*
oLH2_A25 Mapt1of2-rev1	GGGACTTGCAGACGATGTCA	*maptb*

5.1.6.7 Quantitative PCR primers

oLH2_A35 qPCR-zfFus-for3	TGGTGGTGGTAGTGGCAACGGC
oLH2_A36 qPCR-zfFus-rev3	TGCACTGATTGCACTCGTTTCGCC
oKS A13 elf1a2 F	AGCAGCAGCTGAGGAGTGAT
oKS A14 elf1a2 R	GTGGTGGACTTTCCGGAGT
BS-G74 actb1 ex12a F	GATCTTCACTCCCCTTGTTCA
BS-G75 actb1 ex12a R	AAAACCGGCTTTGCACATAC

5.1.7 Bacteria

DH5α *E. coli* competent cells	Hanahan
One Shot TOP10 Chemically Competent *E. coli*, C4040	Invitrogen

5.1.8 Antibodies

5.1.8.1 Primary antibodies

The following antibodies were used for Western blotting (WB), immunohistochemistry (IHC) or immunofluorescence stainings (IF).

Antibody (Species)	**Dilution**	**Supplier**
α-actinin, A7811 (mouse)	IF: 1:500	Sigma-Aldrich
α-tubulin, T6199 (mouse)	WB: 1:10000	Sigma-Aldrich
Calnexin, SPA-860 (rabbit)	WB: 1:10000	Stressgen
eIF2α (mouse)	WB 1:2000	Cell Signalling
peIF2α (mouse)	WB 1:1000	Cell Signalling
F59-myosin (mouse)	IF: 1:100	DSHB
FLAG M2-Peroxidase, A8592	WB: 1:1000	Sigma-Aldrich
FUS sc47711 (mouse)	WB: 1:1000	Santa Cruz
FUS 3H2-11 (mouse)	IHC: 1:100	Institute of Molecular Immunology (IMI), Helmholtz Center Munich
FUS 2A10 (mouse)	IHC: 1:100	Institute of Molecular Immunology (IMI), Helmholtz Center Munich
FUS 2B6 (mouse)	IHC: 1:100	Institute of Molecular Immunology (IMI), Helmholtz Center Munich
GFP (mouse)	IF: 1:500	Neuromab
GFP (rabbit)	WB: 1:5000	Clonetech
Heat shock protein (HSP) 70 (rabbit)	WB: 1: 15000	Abcam
Heat shock protein (HSP) 40 (rabbit)	WB: 1: 5000	Enzo

Histone H3 (rabbit)	WB: 1:2000	Cell Signalling
LDH (rabbit) sc33781	WB: 1:1000	Santa Cruz
ZE-5 4D1 (rat IgG2c)	IF: 1:10	Institute of Molecular Immunology (IMI), Helmholtz Center Munich
zn1 (mouse)	IF: 1:100	DSHB
znp1 (mouse)	IF: 1:100	DSHB

Primary peptide antibodies generated by the IMI, Helmholtz Center Munich:

Antibody (Species)	**Dilution**	**Epitope**
Zebrafish Fus 3H2-11 (mouse IgG2b)	IHC: 1:100	GQSYSQPSAQNYSQQSYGG
Zebrafish Fus 2A10 (mouse IgG2a+b)	IHC: 1:100	GQSYSQPSAQNYSQQSYGG
Zebrafish Fus 2B6 (mouse IgG2a)	IHC: 1:100	AQSGGYSQQSSYSGYNQ

5.1.8.2 Secondary antibodies:

Antibody	**Dilution**	**Company**
Alexa Fluor 488 anti-mouse, A-11029	1:500	Invitrogen
Alexa Fluor 488 anti-rabbit, A-11034	1:500	Invitrogen
Alexa Fluor 555 anti-rat, A-21434	1:500	Invitrogen
anti-rabbit-HRP, W401B	1:10000	Promega
anti-mouse-HRP, W402B	1:5000	Promega

5.1.9 Chemicals

5.1.9.1 Chemicals and reagents

Acetic acid, 100063.2511	Merck

Acrylamide / bis solution, 10681.03	Serva
Agarose, 15510-027	Invitrogen
Ammonium persulfate (APS), 9592.2	Roth
Ampicillin, K029.2	Roth
Aqua Poly/Mount, 18606	Polysciences
β-Mercaptoethanol, 4227.1	Roth
Bacto agar, 214030	BD
Bacto trypton, 211699	BD
Boric acid, 100165.1000	Merck
Bovine serum albumin (BSA), A8022	Sigma-Aldrich
Bromophenol blue, 18030	Fluka
BseDI restriction enzyme	Fermentas
Calcium chloride ($CaCl_2$), 102382.0500	Merck
Chloroform/isoamylalcohol, X984.1	Roth
Citric acid monohydrate	Sigma-Aldrich
Collagenase, C9891	Sigma-Aldrich
Copper(II) sulfate ($CuSO_4$) 102790.0250	Merck
DanKlorix	Colgate-Palmolive
Deoxynucleoside triphosphates (dNTPs)	Thermo Scientific
dNTP mix, 11819362001	Roche
Dulbecco's modified Eagle medium (DMEM) Glutamax, 61965	Gibco
Diethylpyrocarbonate (DEPC), D5758	Sigma-Aldrich
10x DIG RNA labelling mix, 14300621	Roche
Dimethyl sulfoxide (DMSO), 317275	Merck
Disodium hydrogen phosphate (Na_2HPO_4), 106580.5000	Merck
Dithiothreitol (DTT) (100mM), Y00147	Invitrogen
6x DNA loading dye, R0611	Thermo Scientific
Dry ice	-

EDTA free Protease inhibitor cocktail tablets, 05056489001	Roche
Endothelial Cell Basal Medium, C-22010	Promocell
Ethylenediaminetetraacetic acid (EDTA), 108418.1000	Merck
80% ethanol, UN1170	CLN
Ethanol p.a., 100989.1011	Merck
Ethidium bromide, 2218.2	Roth
FastRuler high range DNA ladder, 500-10000bp, SM1123	Thermo Scientific
FastRuler middle range DNA ladder, 100-5000bp, SM1113	Thermo Scientific
FastRuler low range DNA ladder, 50-1500bp, SM1103	Thermo Scientific
Fetal bovine serum (FBS), F7524	Sigma-Aldrich
Fetal calf serum (FCS)	Life Technologies
Formic acid	Sigma-Aldrich
Gelatin, 104080.0100	Merck
Gelatin, from bovine skin, G9391-100G	Sigma
GeneRuler DNA ladder mix, SM0331	Thermo Scientific
GeneRuler express DNA ladder, SM1553	Thermo Scientific
Glycerol p.a., 3783.2	Roth
Glycine p.a., 04943	Biomol
5x GoTaq buffer, M791A or M792A	Promega
GoTaq DNA polymerase, M830B	Promega
Hydrochloric acid, 37%	Sigma-Aldrich
Hydrogen peroxide solution 30%	Sigma-Aldrich
Guanidine hydrochloride, G4505	Sigma-Aldrich
Immersol W 2010	Zeiss
Insect pins, 26002-10	Fine science tools
Isopropanol p.a., 109634.2511	Merck
Liberase TM, 05401119001	Roche
Lipofectamine 2000, 11668-019	Invitrogen
Liquid nitrogene (liq. N_2)	Linde

Loeffler's methylene blue solution, 101287	Merck
Low serum growth supplement kit, S-003-K	Life technologies
Magnesium chloride ($MgCl_2$), 105833.1000	Merck
Magnesium sulfate ($MgSO_4$), 105886.1000	Merck
Medium 199, 31150-022	Life technologies
Medium 200, M-200-500	Life technologies
MercaptoEtOH, 805740	Merck
Methanol p.a., 106059.2511	Merck
Methionine [S35]-label	Hartmann Analytik
Methyl cellulose, M0387	Sigma-Aldrich
Meyer's haematoxylin stain	e.g. Sigma-Aldrich
Milk powder, T145.2	Roth
Monopotassium phosphate (KH_2PO_4), 104877.1000	Merck
Neurobasal medium, 10888022	Life technologies
Newborn calf serum (NCS), N4762	Sigma-Aldrich
Non-essential amino acids (NEAA), 11140-035	Life Technologies
Nonidet P40 / NP40 / IGEPAL, 19628	USB
Normal goat serum	XX
Opti-MEM, 51985-026	Gibco
Paraffin wax	Sigma-Aldrich
Paraformaldehyde (PFA), P6148	Sigma-Aldrich
Penicillin-Streptomycin, 15140-122	Gibco
Pentylenetetrazole (PTZ), P6500	Sigma-Aldrich
Periodic acid	e.g. Sigma-Aldrich
Phenylthiourea (PTU), P7629	Sigma-Aldrich
Phenol/chloroform/isoamylalcohol, A156.1	Roth
PhosSTOP, 04906837001	Roche
Potassium chloride (KCl), 104936.1000	Merck
Protease inhibitor (PI) mix, 05056489001	Roche

Pronase, 11459643001	Roche
Proteinase K (PK), 03115852001	Roche
Precision plus protein all blue standard, 161-0373	Bio-Rad
Random hexamer primer, S0142	Thermo Scientific
Recombinant human VEGF165, 293-VE-010	R&D Systems
Restriction endonucleases	NEB, Thermo Scientific
RiboLock RNase inhibitor (40U xx), EO0382	Thermo Scientific
Ribonucleic acid from torula yeast, Type VI, R6625	Sigma
RNase H, 18021071	Invitrogen
SeeBlue Plus2 pre-stained standard, LC5925	Invitrogen
SOC-Medium, 15544-034	Invitrogen
Sodium acid (NaN_3), 106688.0100	Merck
Sodium acetate (NaOAc), 6779.1	Roth
Sodium chloride (NaCl), 3975.2	Roth
Sodium fluoride (NaF)	Sigma-Aldrich
Sodium dodecyl sulfate (SDS), 20765.03	Serva
Sodium deoxycholate D6750	Sigma-Aldrich
SP6 polymerase, EP0131	Fermentas
Spectinomycin, 85555	Fluka
Sulforhodamin B, S1402	Sigma
Sucrose, S1888	Sigma-Aldrich
T7 polymerase, EP0111	Fermentas
Tetramethylethylenediamine (TEMED), 2367.3	Roth
TissueTek O.C.T., 25608-9300	VWR
5x Transcription buffer, EP0111	Fermentas
Tricaine, A5040	Sigma-Aldrich
Trichloracetic acid, 1.00807.1000	Merck
Tris, 08003	AppliChem
Trisodium citrate dihydrate	Sigma-Aldrich

Triton X-100, 108603.1000	Merck
Trypsin EDTA or 2.5%, 15090046	Life technologies
Tween 20, 822184.0500	Merck
Vannas-Tübingen Spring Scissors, 15008-08	Fine science tools
Vectahield H-1000 mounting medium	Vectorlabs
Xylene, 108681.1000	Merck
Yeast extract, 212720	BD

5.1.9.2 Solutions and buffer

All solutions and buffers were prepared with H_2O that was desalted and purified using a Milli-Q system (electric resistance 18.2MΩcm at 25°C).

1%-2% agarose	1%-2% agarose 1x TBE
Ampicillin stock	100 mg/ml dissolved in dH_2O and sterile filtered
10% APS (stock)	10% APS in dH_2O stored at -20°C
Bleaching solution	1 l tap water, 380 µl DanKlorix
10x BSA stock	0.1 g/ml
Citrate buffer	11.5 ml 0.1M citric acid 88.5 ml 0.1M-trisodium citrate
DEPC-dH_2O	200 µl DEPC per 100 ml dH_2O incubate o/n at 37°C and autoclave
DMEM Glutamax, 61965	Gibco
GuHCl-stripping buffer	6M guanidine hydrochloride 20 mM Tris 0.2% Triton X-100/NP40 adjust to pH7.5
High salt buffer	50 mM Tris, pH7.4 750 mM NaCl 10 mM NaF 5 mM EDTA

High salt, 1% TX100 buffer	50 mM Tris, pH7.4 750 mM NaCl 10 mM NaF 5 mM EDTA 1% Tritonx100
HYB^-	125 ml 50% formamide 31.25 ml 20x SSC 2.5 ml 10%Tween-20 ad 250 ml dH_2O
HYB^+	HYB- 5 mg/ml torula (yeast) RNA 50 µg/ml heparin
4x Lämmli sample buffer	4 ml 20% SDS 4 ml glycerol 1 ml β-mercaptoethanol 1.25 ml 1M Tris, pH7.6 1 pinch bromophenol blue
Lysis buffer	10% PK stock in TE, pH8.0
6x Loading dye orange or blue	0.5% SDS 25% glycerol 25 mM EDTA in dH_2O pinch of Orange G or Bromophenol blue
Low salt buffer	10 mM Tris, pH7.4 5 mM EDTA
Low salt, 1% TX100 buffer	10 mM Tris, pH7.4 5 mM EDTA 1% TritonX100
NCST	10% NCS stock 0.1% Tween in 1xPBS
PBS	0.14 M NaCl 10 mM Na2HPO4 2.8 mM KH2PO4 2.7 mM KCl pH 7.4
PBST	0.1% Tween in 1x PBS

PBST/milk	3% milk powder 0.1% Tween in 1x PBS
4% PFA	4% PFA in 1x PBS incubate approx. 5 min at 80°C until PFA is dissolved cool to 4°C prior to usage or store at -20°C
PK stock	17 mg/ml PK in dH_2O
Pronase stock	30 mg/ml pronase in dH_2O
10x PTU	0.3 mg/ml in E3
PTZ stock solution (150mM)	5.18mg PTZ 10% DMSO in 250ml E3
PTZ working solution (5mM)	1:30 dilution of PTZ stock solution (150mM) in E3
RIPA	50 mM Tris-HCl, pH 8.0 150 mM NaCl 5 mM EDTA 1% NP-40 0.5% Deoxycholat 0.1% SDS
RIPA, 2% SDS	50 mM Tris-HCl, pH 8.0 150 mM NaCl 5 mM EDTA 1% NP-40 0.5% Deoxycholat 2% SDS
Running gel buffer	1.5 M Tris-Glycine, pH8.8
10x running buffer	29 g Tris 144 g glycine ad 1 l with dH_2O and autoclave
SDS running buffer	0.1% SDS in 1x running buffer
Spectinomycin stock	30mg/ml dissolved in dH_2O and sterile filtered
20x SSC	175.3 g NaCl 88.2 g Na-citrate ad 1000 ml dH_2O adjust to pH7 and autoclave
Stacking gel buffer	1 M Tris-Glycine, pH6.8

Staining buffer (NTMT)	100 mM Tris pH9.5 50 mM $MgCl_2$ 100 mM NaCl 0.1%Tween-20 1 mM Levamisol (add fresh)
Stripping buffer	62.5 mM Tris 2% SDS adjust to pH6.7 prior to use add 350 µl MercaptoEtOH per 50 ml stripping buffer
10x TBE	1080 g Tris 550 g Boric acid 400 ml 0.5 M EDTA, pH8.0 ad 10 ml dH_2O
TE pH8.0	10 mM Tris 1 mM EDTA adjust to pH8.0 and autoclave
10x transfer buffer	30.3 g Tris 144 g glycine ad 1 l with dH_2O adjust to pH8.3 and autoclave
50x tricain	2g tricain 10.5 ml 1 M Tris pH9.0 ad 500 ml with dH_2O adjust to pH7.0

5.1.9.3 Media

Media used for the cultivation of bacteria were autoclaved to prevent the growth of undesired organisms. After cooling sterile filtered antibiotics in the indicated concentrations were added.

E3	5 mM NaCl 0.17 mM KCl 0.33 mM $CaCl_2$ 0.33 mM $MgSO_4$

E3 Methylene blue	5 mM NaCl 0.17 mM KCl 0.33 mM $CaCl_2$ 0.33 mM $MgSO_4$ 0.002% Loeffler's methylene blue solution)
LB-Agar	1.5% Bacto Agar 1% Bacto Trypton 0.5% Yeast extract 17.25 mM NaCl in dH_2O Ampicillin 100 µg/ml or Spectinomycin 100µg/ml
LB-Medium	1% Bacto Trypton 0.5% Yeast extract 17.25 mM NaCl in dH_2O Ampicillin 100 µg/ml or Spectinomycin 100µg/ml

5.1.10 Kits

BCA Assay Protein Quantitation Kit, UP40840A	Uptima
DNA polymerase (Pfu)	Agilent
Gateway LR Clonase II Enzyme Mix, 11791-020	Invitrogen
cytoTox 96 non-radioactive cytotoxicity assay, G1780	Promega
GoTaq DNA Polymerase, M3175	Promega
iScript cDNA Synthesis Kit, 170-8891	BioRad
M-MLV Reverse Transcriptase, 28025-013	Invitrogen
MEGAClear Kit, AM1908	Ambion
mMESSAGE mMACHINE SP6 Kit, AM1340	Ambion
mMESSAGE mMACHINE T7 Kit, AM1344	Ambion
MessageMAX T7 mRNA transcription kit	Epicentre
NucleoBond Xtra Midi, 740410	Macherey-Nagel

NucleoSpin Gel and PCR Clean-up, 740609	Macherey-Nagel
NucleoSpin Plasmid, 740588	Macherey-Nagel
pCR8/GW/TOPO TA Cloning Kit, K250020	Invitrogen
Pierce ECL Plus Western Blotting Substrate, 32132	Thermo Scientific
RNAqueous-Micro Kit, AM1931	Ambion
RNase-free DNase Set, 79254	Qiagen
RNeasy Mini Kit, 74104	Qiagen
Supervision 2	DCS
SsoFast Eva Green Supermix, 172-5204	BioRad

5.1.11 Consumables

0.2 ml Strip tubes, AB-0266	Thermo Scientific
96-Well PCR Plate, AB-0600	Thermo Scientific
Blotting Paper, MN 218 B	Macherey-Nagel
Borosilicate glass capillaries, 1B120F-4	World Precision Instruments
Centrifuge tubes 15 ml, 50 ml	Sarstedt
Combitips Plus 0.5 ml, 5ml	Eppendorf
Cover slip	Thermo Scientific
Fluorodish Cell Culture Dish - 35 mm, FD3510-100	World Precision Instruments
Hard-Shell 384-Well PCR Plates, HSP-3805	BioRad
Microcentrifuge tubes 1.5 ml, 2.0 ml	Sarstedt
Microscope slide	Thermo Scientific
Microscope slide with wells	Thermo Scientific
Microseal B Film, MSB1001	BioRad
Multi-well plates (6, 12, 24, 48, 96)	Thermo Scientific
μ-slides, 80826	Ibidi
PCR Film, AB-0558	Thermo Scientific

PES membrane filter (0.45 µm)	VWR International
Petri dishes 60 mm, 100 mm	Sarstedt
Pipette tips 10 µl, 10 µl long, 200 µl, 1000 µl	Sarstedt
Pipette tips with filter (10 µl, 10 µl long, 20 µl, 100 µl, 300 µl, 1000 µl)	Sarstedt
Phase Lock Tubes 1.5 ml	Eppendorf
PVDF Membrane, Immobilon-P, IPVH00010	Millipore
sterile serological pipetts 5 ml, 10 ml, 25 ml	Sarstedt
Superfrost Plus slides, J1800AMN3	Thermo Scientific
Transfer pipettes	Sarstedt
X-ray films Kodak, BioMax MR Film, Cat8701302	Sigma Aldrich
X-ray films Super RX, 47410 19236	Fujifilm

5.1.12 Equipment

Accu jet pro	Brand
Agarose gel documentation device	Intas
Agarose gel systems	Peqlab
Benchtop centrifuge 5415D	Eppendorf
Benchtop cool centrifuge Biofuge fresco	Heraeus
Bio-ice cooling unit, 170-3934	Bio-Rad
C1000 Thermal Cycler	Bio-Rad
Cassette for x-ray film exposure	Radiographic Products
Casting stands	Bio-Rad
Casting frames	Bio-Rad
Celltram air microinjector, 5176	Eppendorf
Centrifuge multifuge 3 S-R	Heraeus
CO_2 Incubator	Binder
Cold-light source KL 1500 LCD	Zeiss

Dumont Forceps # 5 Titanium	Fine Science Tools
DMZ-Universal (needle) Puller	Zeitz-Instrumente
Foam Pads	Bio-Rad
Freezer -20°C	Liebherr
Freezer -80°C	Heraeus
Fridge	Liebherr
Gel Releaser, 165-3320	Bio-Rad
Gel dryer, model583	Bio-Rad
Hood for cell culture	Heraeus
iCycle-MyiQ	BioRad
Incubator 28°C, 37°C, 55°C	Binder or B. Braun Biotech International
Kontes Pellet Pestle, 1.5 ml	Fisher Scientific
Kontes Pellet Pestle Cordless Motor, K749540-0000	Fisher Scientific
Micro forge, MF-900	Narishige
Microwave	Sharp
Microinjector (Femto Jet)	Eppendorf
Microinjection molds	e.g. Eppendorf
Micro scales BP2215	Sartorius
MilliQ academics	Millipore
Mini gel holder cassette, 170-3931	Bio-Rad
Mini-PROTEAN Comb, 10-well and 15-well	Bio-Rad
Mini-PROTEAN 3 cell	Bio-Rad
Mini-PROTEAN Tetra cell	Bio-Rad
Mini trans-blot central core, 170-3812	Bio-Rad
Multipipette plus	Eppendorf
Nano Photometer	IMPLEN
Microtome	xx
PCR Plate Sealer	Eppendorf

PCR Thermocycler	Eppendorf, BioRad
pH Meter	WTW
Pipette 10 µl, 100 µl, 200 µl and 1000 µl	Eppendorf
Plate reader PowerWaveXS	BioTek
PowerPac Basic Power Supply, 164-5050	Bio-Rad
PowerPac HC Power Supply, 164-5052	Bio-Rad
Preserving boiler EKO 620	Petra
Rotors (TLA-55, SW28)	Beckmann Coulter
Scales BP3100S	Sartorius
Schott bottles	Schott
Sonifier (Cell Disruptor B15)	Branson
Shaker Duomax 1030	Heidolph
Shaker cold room	Bachofer
Short plates, 165-3308	Bio-Rad
Spacer plates 0.75 mm, 165-3310 and 1.5 mm, 165-3312	Bio-Rad
Spring Scissors, 3 mm Blades, Straight	Fine Science Tools
Spring Scissors, 5 mm Blades Angled	Fine Science Tools
Staining containers	Roth
Staining racks	Roth
Staining vials	Roth
Stereo Microscope Stemi 2000	Zeiss
Tea nets	-
Thermomixer comfort	Eppendorf
Thermomixer compact	Eppendorf
Ultracentrifuge	Beckmann Coulter
UV Detectionsystem	Intas
Vortexgenie2	Scientific Industries
Waterbath	GLF

5.1.13 Microscopes

Axiovert 135 (inverted) DIC	Zeiss
Cell Observer CSU-X1 Yokogawa Spinning Disk AxioCam MRm and Evolve 512	Zeiss
Confocal laser scanning microscope LSM 710	Zeiss
Fluorescence-Stereomicroscope MZ 16F	Leica
Fluorescence-Stereomicroscope MZ 16FA	Leica
Mikroskop Zeiss Axioplan 2 imaging AxioCam HRc	Zeiss
Stereomicroscope Zeiss Stemi 2000-C	Zeiss
ZebraBox Revolution, high sensitivity digital camera (30 frames/s)	ViewPoint

5.1.14 Hardware and software

Adobe Illustrator CS5	Adobe Systems Software
Adobe Photoshop CS5	Adobe Systems Software
Axiovision 4.0	Zeiss
Bio-Rad CFX Manager 2.0	Bio-Rad
CLC Main Workbench 6	CLC bio
Gen5	BioTek
GraphPad Prism 6	GraphPad Software
Leica Application Suite	Leica
Lightscanner HR 96, HRM analysis software	Idaho Technology Inc.
MacBookPro	Apple
Microsoft Office for Mac 2011	Microsoft
Papers2	Mekentosj
Zebralab tracking software 3,22,3,9	ViewPoint
Zen Black 2011	Carl Zeiss Microimaging
Zen Blue 2011	Carl Zeiss Microimaging

5.2 Methods

5.2.1 Molecular biological methods

5.2.1.1 Isolation of genomic DNA

For the isolation of genomic DNA from methanol fixed zebrafish embryos, larval and adult tissues, methanol was completely removed by pipetting and subsequent evaporation at 55°C. Then 50µl or 30µl of TE buffer containing 10% Proteinase K were added to the adult or larval and embryonic tissue, respectively and the samples were lysed at 55°C for at least 1h. Inactivation of Proteinase K was achieved by incubation at 95°C for 5-10min. Remaining debris was pelleted in a short centrifugation step. The supernatant containing genomic DNA was stored at -20°C or used for genotyping.

5.2.1.2 Genotyping *fus* ZFN mediated mutations

fus ZFN mediated mutations were identified via restriction fragment length polymorphism (RFLP). Genomic DNA was extracted from zebrafish embryos and fin biopsied tissue and Polymerase chain reaction (PCR) was performed with genotyping primers flanking *fus* target site containing DNA fragments. Per reaction 2µl of genomic DNA lysate were amplified with 0.2µl of GoTaq polymerase (5 units per 1µl), 0.34µl of 10mM dNTPs and 0.05µl of each forward and reverse primer (100mM) in 3.4µl 5×GoTaq buffer diluted in dH_2O were used. The following PCR programm was applied:

Cycle Step	Temperature	Time	No. of cycles
Initial Denaturation	94°C	2min	1
Denaturation	94°C	30s	35
Annealing	60°C	30s	
Extension	73°C	5min	
Final Extension	73°C	5min	1

Next, PCR amplicons were subjected to restriction digest with BseDI restriction enzyme. Per reaction, 5µl PCR product, 0.25µl BseDI restriction enzyme (10 units per 1µl), 0.25µl Tango restriction buffer diluted in dH_2O were incubated at 55°C for 3h. PCR and restriction digest products were analyzed by agarose gel electrophoresis.

5.2.1.3 Genotyping Fus^{mde1500} mutations

Fus^{mde1500} mutations were identified via PCR using allele specific primers. Per sample two consequent PCRs were performed and analyzed by gel electrophoresis. 1µl of genomic DNA lysate was amplified with 0.2µl of GoTaq polymerase (5 units per 1µl), 0.34µl of 10mM dNTPs and 0.05µl of each forward and reverse primer (100mM) specific for either the Fus^{wildtype} allele or the Fus^{mde1500} allele in 3.4µl 5×GoTaq buffer diluted in dH_2O per PCR reaction. The following PCR program was used:

Cycle Step	Temperature	Time	No. of cycles
Initial Denaturation	94°C	2min	1
Denaturation	94°C	30s	45
Annealing	62°C	30s	
Extension	73°C	10s	
Final Extension	73°C	5min	1

5.2.1.4 Large scale mutation screening using HRM analysis

For genotyping using HRM analysis, a PCR followed by melting curve anaylsis was performed using a PCR cycler and the Bioke Lightscanner device. Per reaction 2µl of genomic DNA lysate were amplified with 0.1µl of GoTaq polymerase (5 units per 1µl), 0.2µl of 10mM dNTPs, 1µl of each forward and reverse primer (2.5µM) and 1µl of LC Green reagent in 2µl 5×GoTaq buffer diluted in dH_2O were used. Before subjecting samples to PCR, wells were coated with 20µl of mineral oil to avoid evaporation. The following PCR program was applied prior to generation of melting curves using the Lightscanner:

Cycle Step	Temperature	Time	No. of cycles
Initial Denaturation	94°C	2min	1
Denaturation	94°C	30s	45
Annealing	65°C	30s	
Extension	73°C	10s	
Final Extension	73°C	5min	1

Lightscanner melting curve detection was set to start and stop temperatures of 75°C and 98°C, respectively with a general hold temperature of 72°C. Analysis of melting curve shifts by the Lightscanner software allowed identification of the mutations.

5.2.1.5 RNA extraction

RNA from zebrafish embryos, zebrafish larvae, and adult zebrafish tissues was extracted according to the protocol of the RNeasy Mini Kit including DNase treatment (RNase-free DNase Set). Microcentrifuge tubes containing shock frozen embryos, larvae, or tissues were kept on dry ice until homogenization. For all steps RNase free consumables and solutions were used. The tissue was disrupted with the tissue homogenizer in 350µl+ 350µl RLT buffer containing β-mercaptoethanol. After being extracted from tissue using the RNeasy Mini Kit RNA was eluted in 30-50µl RNase-free H_2O. RNA quality was examined by agarose gel electrophoresis and the concentration was determined using a NanoDrop device. All RNA solutions were stored at -80°C until further usage.

5.2.1.6 cDNA synthesis

cDNA synthesis was performed as described in the M-MLV Reverse Transcriptase kit. RiboLock RNase Inhibitor was utilized as RNase inhibitor. For cDNA used in qRT-PCRs 0.1µg total RNA and 0.1µg Random Hexamer Primer Mix was used. For cDNA used in semiquantitative RT-PCRs 2µg total RNA were used together with 0.5µg Random Hexamer Primer Mix. cDNA used for cloning of *fus* constructs was synthesized using up to 5µg of total RNA with 0.5µg of oligo (dT) primers selectively enriching for mature mRNAs followed by RNase H digest to remove RNA-DNA hybrids. A β-actin control PCR was used as a control for efficient cDNA synthesis.

5.2.1.7 Cloning of zebrafish *fus* contructs

Several zebrafish *fus* constructs were cloned using TOPO cloning (see subsubsection 5.2.1.8) and Gateway technology (see subsubsection 5.2.1.9). Fulllength $Fus^{wildtype}$ and $Fus^{mde1500}$ alleles were amplified via PCR from cDNA pools and cloned into pCR8/GW/TOPO vectors, serving as entry vectors. From there, Gateway reaction with pCS2+plasmids allowed to swap inserts and generate expression vectors with $Fus^{wildtype}$ and $Fus^{mde1500}$ constructs under the expression control of the pCS2+ CMV promotor. Moreover, destination vectors with a GFP tag 5' or 3' of the Gateway sites allow for N-terminal or C-terminal fusion of the gene of interest with GFP. 5' GFP containing pCS2+ vectors were utilized to tag $Fus^{wildtype}$ and $Fus^{mde1500}$ constructs N-terminally with GFP. These constructs were used to screen suitable antibodies detecting wildtype Fus protein as well as truncated mutant $Fus^{mde1500}$ protein. In addition, the multiple gateway reaction was used to clone GFP tagged $Fus^{wildtype}$ and $Fus^{mde1500}$

constructs under the control of the ubiquitin promotor, derived from a different entry vector. These plasmids were utilized to examine localization of Fus protein in zebrafish embryos and rat primary cortical neurons.

5.2.1.8 TOPO cloning

For molecular cloning of entry clones the pCR8/GW/TOPO TA Cloning Kit or the TOPO TA Cloning Kit, Dual Promoter were used. Proof-reading polymerases do not generate sticky required for topoisomerase reaction in both kits. Therefore sticky adenosine ends were added as described in the following reaction: 20µl purified PCR product, 5µl 5×GoTaq Buffer, 0.5µl 10mM dATP and 0.3µl GoTaq DNA Polymerase were incubated for 15min at 72°C. Then 1-4µl PCR product were used in a TOPO Cloning reaction following the manual of the respective Cloning Kit. The TOPO cloning reaction was incubated for up to 30min before transformation in chemically competent *E. coli* cells (see subsubsection 5.2.1.10).

5.2.1.9 Gateway cloning

To transfer DNA fragments from entry clones to expression clones the Gateway cloning system was used. 100ng/µl pCR8/GW/TOPO vector containing the DNA fragment of interest served as entry clone and 150ng/µl pCS2+ vector containing the Gateway cassette as destination vector. The Gateway cloning reaction was conducted as described in the user manual of the Gateway LR Clonase II Enzyme Mix. 1-5µl LR Clonase reaction were subsequently used for transformation in chemically competent *E. coli* cells (see subsubsection 5.2.1.10).
For multiple gateway cloning, a destination vector and several entry vectors are needed. To generate GFP tagged zebrafish *fus* contructs under the control of the ubiquitin promotor, pCS2eGFP-zfFuswt and pCS2eGFP-zfFusF500X vectros were used as templates to amplify GFP-Fus coding sequences via PCR and perform TOPO cloning to generate pCR8eGFP-zfFuswt and pCR8eGFP-zfFusF500X plasmids. 100ng/µl pCR8 containing zebrafish *fus* coding sequences N-terminally fused to GFP and 100ng/µl pENTR5'-ubi vector were used as entry vectors, while 200ng/µl pTolDestR4-R2pA vector served as destination vector. Cloning reaction was performed according to the manufacturers protocol.

5.2.1.10 Chemical transformation of bacteria

To transform plasmid DNA in bacteria, chemically competent DH5α or TOP10 *E. coli* cells were used. Cells were thawed on ice and 2-4µl of TOPO cloning reactions, 2µl of LR Gateway cloning reactions or 10pg-100ng plasmid DNA were added and incubated on ice for 30min followed by a heat-shock at 42°C for 30s and a quick chill on ice for 3min. To allow the bacteria to express resistance genes, 250µl SOC medium were added and bacteria were incubated at 37°C, 200rpm for 1h. Then 10-200µl of the transformation were spread on pre-warmed LB agar plates containing the appropriate antibiotic. When using the TOPO TA Cloning Kit Dual Promoter LB agar plates were coated with 40µl IPTG stock and 40µl X-Gal stock beforehand to allow blue/white selection. LB agar plates were incubated o/n at 37°C. If bacteria colonies were present, some were selected and analyzed for the integration of the correct plasmid by colony PCR (see subsubsection 5.2.1.12).

5.2.1.11 Gradient PCR

Gradient PCRs were performed to determine the optimal annealing temperature of a primer pair prior to using it for cloning or genotyping. A temperature gradient range from 50-70°C was tested as possible annealing temperatures, whereas temperature during other PCR cycle steps were kept constant. The extension time was adjusted to the expected size of the PCR product. PCR products were analyzed by agarose gel electrophoresis.

5.2.1.12 Colony PCR

Prior to sequencing, single clones were analyzed for the correct insert via colony PCR. Single clones were picked with pipette tips, 30µl LB medium with the appropriate antibiotic was inoculated and colony resuspensions were incubated at RT on the bench for 30min. Primers suitable to determine whether the insert of interest was integrated into the plasmid were selected. To analyze clones after integrating zebrafish *fus* constructs into TOPO vectors 2µl colony resuspension and 0.05µl of each forward and reverse M13 primers, together with 0.2µl of GoTaq polymerase (5 units per 1µl), 0.34µl of 10mM dNTPs and 3.4µl 5×GoTaq buffer diluted in dH_2O were used for one reaction. The following PCR programm was applied to amplify zebrafish *fus* coding sequences :

Cycle Step	Temperature	Time	No. of cycles

Initial Denaturation	94°C	2min	1
Denaturation	94°C	30s	25
Annealing	60°C	30s	
Extension	73°C	2min	
Final Extension	73°C	5min	1

After PCR products were analyzed by agarose gel electrophoresis and clones containing the correct insert were subjected to bacterial cultivation and DNA extraction (see subsubsection 5.2.1.13).

5.2.1.13 Bacterial cultivation and DNA extraction

After colony PCR and identification of promissing clones 3-5ml of LB medium containing the appropriate antibiotics were inoculated with 10µl of a single clone resuspension (see subsubsection 5.2.1.12) and incubated at 37°C, 200rpm, o/n for miniprep isolation of entry clone plasmids. Plasmid DNA was isolated as described in the NucleoSpin Plasmid protocol. The concentration was determined with a NanoDrop device and plasmids were sequenced by GATC to determine the correct sequence of the integrated insert of interest. Samples were stored at -20°C until further usage. For midiprep isolation of expression clone plasmids 200ml of LB medium containing the appropriate antibiotics were inoculated with 10µl of a single clone resuspension and incubated at 37°C, 200rpm, o/n. Plasmid DNA was isolated as described in the NucleoBond Xtra Midi protocol and dissolved in 200µl of sterile dH_2O. The concentration was determined with a NanoDrop device and plasmid solutions were stored at -20°C. Plasmids were sequenced by GATC and used for expression in zebrafish, HeLa cells or rat primary cortical neurons.

5.2.1.14 *ISH* probe generation

Sense and antisense probes for *in situ* hybridisations were generated similarly to a standard *in vitro* RNA transcription protocol. First, pCS2+ zf FUS construct (F62) was chosen as DNA template and linearized with BamHI or KnpI for generation of antisense or sense probe, respectively. 10µg DNA template with 20 units of the respecting enzyme were incubated in 1×restriciton buffer diluted in dH_2O at 37°C for 2h. Linearized template DNA was purified according to the NucleoSpin PCR Clean-up protocol and eluted in 25µl DEPC-H_2O prior to controling for efficient digest and measuring the

concentration using a Nano photometer device. In the next step, digoxygenin (DIG) labelled RNA was transcribed from the linearized DNA templates. 1µg linearized DNA template with 40 units of T7 RNA polymerase for antisense or T3 RNA polymerase for sense probes were incubated with 1×DIG labelling mix, 5mM DTT and 40 units of Ribolock RNAse inhibitor in 1×reaction buffer diluted in DEPC-H_2O at 37°C for 2h. Probes were recovered via precipitation. $\frac{1}{10}$vol 8M LiCl and $2\frac{1}{2}$vol of prechilled 100% ethanol were added and incubated for 1h at -20°C. Samples were centrifuged for 30min at 4°C at 13000rpm and the supernatant was discarded. 300µl 75% ethanol in DEPC-H_2O were added and samples were centrifuged for 5min at 4°C at 13000rpm. The supernatant was discarded and the pellet dried at RT, redissolved in 20µl DEPC H_2O and used for ISH (see subsubsection 5.2.3.9) after determination of concentration and quality via nano photometer and agarose gel electrophoresis, respectively.

5.2.1.15 Agarose gel electrophoresis

Agarose gel electrophoresis was performed to analyze and separate PCR products, to analyze restriction enzyme digests or to control RNA quality. Dependent on the size of the expected product 1-2% agarose gels containing ethidium bromide (approx. 1:50000) were used. Samples containing loading dye and a suitable DNA ladder were loaded onto the gel. Electophoresis was performed in 1×TBE buffer until a clear separation of the bands of interest was determined via UV detection and documented via image acquisition.

5.2.1.16 Gel extraction and PCR clean-up

After agarose gel eletrophoresis, samples were purified from the gel according to the NucleoSpin Gel Clean-up protocol. For direct purification of PCR amplicons after PCR the NucleoSpin PCR Clean-up protocol was used. Purified DNA was eluted in 30-50µl elution buffer NE and was either analyzed by sequencing or used for cloning.

5.2.1.17 Quantitative PCR

All primer pairs for quantitative PCR (qPCR) spanned an exon-exon junction with an intron larger than 1kb to exclude amplification of genomic DNA. Specificity of the primers was tested by qPCR on wildtype cDNA and verified by a single peak via melting curve analysis and one single band of the predicted size in agarose gelelectrophoresis. Additionally, the qPCR product was sequenced. qPCR was performed in 384-well format on a C1000 Thermal Cycler. To generate cDNA, 0.1µg total RNA of each

sample were transcribed with 0.1µg random hexamer primers and 20mM dNTPs. For a standard curve total RNAs of all samples were combined and a dilution series of 1:1, 1:10, 1:100, 1:1000 was transcribed with 0.1µg random hexamer primers and 20mM dNTPs. For the qPCR reaction on cDNA 1µl 1:25 diluted standard cDNAs and 1:100 diluted sample cDNAs plus 3µl mastermix, composed of 2.5µl SsoFast Eva Green Supermix, 0.25µl 10µM forward primer and 0.25µl 10µM reverse primer were used. Each reaction was performed in triplicates. The PCR program applied contained the following steps: 30s at 95°C, 55 cycles of 5s at 95°C and 10s at 60°C and a melting curve from 60°C to 95°C with increases of 0.5°C every 5s. The relative expression of each gene was calculated using the ΔΔCT-method and the normalized fold expression was calculated by normalization to the reference genes *eF1α* and *actin1β*.

5.2.1.18 Semiquantitative PCR

Semiquantitative PCR for *mapta*, *maptb*, *ntng1* and β-*actin* as loading control were performed. 1µl cDNA and 3.4µl 5×GoTaq Reaction Buffer, 0.34µl dNTPs (10mM), 0.05µl 100µM forward primer, 0.05µl 100µM reverse primer, 12.57µl dH_2O and 0.1µl GoTaq DNA Polymerase per reaction were subjected to the following PCR program:

Cycle Step	Temperature	Time	No. of cycles
Initial Denaturation	94°C	2min	1
Denaturation	94°C	30s	25
Annealing	65°C	30s	
Extension	73°C	5min	
Final Extension	73°C	5min	1

For all PCR products the same volume was analyzed via agarose gel electrophoresis.

5.2.1.19 Determination of protein concentration

For the determination of protein concentrations in zebrafish samples and cell culture lysates BCA Assay was applied as described in the protocol of the BCA Assay Protein Quantitation Kit. BSA was used for the standard curve and the colorimetric reduction of copper(II) sulfate containing BCA reaction solution by peptide bonds was measured with a plate reader at 562nm.

5.2.1.20 SDS-polyacrylamide gel electrophoresis

SDS-polyacrylamide gel electrophoresis (SDS-PAGE) was performed to separate proteins according to their molecular weight (MW). The percentage of the running gel was chosen depending on the expected MW of the protein of interest (http://www.thermoscientificbio.com/uploadedFiles/Resources/general-recommendations-for-sds-page.pdf) . Recipes for three separating gels (25ml) and three stacking gels (6ml):

	7%	8%	12%	15%	Stacking gel
40% acrylamide	4.43ml	5.03ml	7.58ml	9.45ml	563µl
Running gel buffer	12.5ml	12.5ml	12.5ml	12.5ml	-
Stacking gel buffer	-	-	-	-	750µl
10% SDS	250µl	250µl	250µl	250µl	60µl
dH_2O	7.57ml	6.97ml	4.42ml	3.15ml	4.913ml
10% APS	250µl	250µl	250µl	250µl	60µl
TEMED	5µl	5µl	5µl	5µl	6µl

The PAGE equipment including denaturing gels was assembled and SDS running buffer was added. Wells were rinsed with SDS running buffer prior to loading of samples as well as Precision Plus Protein™ All Blue ladder. Electrophoresis was started with 80V, increased to 120-150V after the protein standard began to separate and was stopped when the region of interest showed sufficient separation. Gels were subsequently used for Western Blotting.

5.2.1.21 Western blotting

Wet Western blotting was used to transfer and immobilize proteins on a PVDF-membrane. Prior to blotting, pre-wetting (activation) of the PVDF-membrane in methanol was performed. Afterwards, the membrane was washed in dH_2O and incubated in 1×transfer buffer. Membranes and gels were assembled between foam pads and Whatman paper in a holder cassette. Next, proteins were transferred onto the PVDF-membrane in 1×transfer buffer at 400mA for 70min. After Western blotting, membranes were blocked by shaking incubation in PBST/milk for 1h at RT. Next, the blocked membrane was incubated in primary antibody diluted in PBST/milk, 0.05% NaN_3 at 4°C o/n. The next day the primary antibody was removed and kept for further use at 4°C, while the membrane was washed 4×15min in PBST. The secondary

antibody was applied diluted in PBST/milk for 1h at RT. After removal of the secondary antibody the membrane was washed 8×for 15min prior to immunodetection. For immunodetection ECL Plus was used as indicated in the manual. By catalyzing chemiluminescent substrates the horse radish peroxidase (HRP) moiety of the secondary antibody produces chemiluminescence that can be detected upon exposure to X-ray films. After immunodetection the membrane was washed three times for 5min in PBST. Before a second immunodetection the membrane was stripped to resolve formed antibody-antigen interactions
Stripping the membrane was achieved by horizontally shaking in 10ml GuHCl-stripping buffer plus 70µl β-mercaptoethanol (0.1M) at RT for 10min. Then the membrane was washed two times for 5min in PBST. A second round of 5min incubation in 10ml GuHCl-stripping buffer plus 70µl β-mercaptoethanol followed. Afterwards, the membrane was rinsed in PBST and washed five times for 5min in PBST. After being stripped and reblocked in PBST/milk, the PVDF membrane was ready for immunodetection with another antibody that serves as loading control, e.g. tubulin or actin.
For quantitative Western blotting HRP mediated luminescence directly correlating with protein levels was detected using LAS 4000 image reader instead of exposure to X-ray films and analyzed by Multi Gauge V3.0 software.

5.2.1.22 Subcellular fractionation

Frozen adult brain of zebrafish carrying homozygous, heterozygous $Fus^{mde1500}$ mutations or $Fus^{wildtype}$ alleles were homogenized using a tissue homogenizer device in 100µl of low salt buffer containing 1×Proteinase and Phosphatase Inhibitor. A 25µl aliquot of each sample was separated as total input. Samples were centrifuged at 5000×g at 4°C for 30min and supernatant was collected as low salt fraction. Two additional washing steps with the same buffer (low salt buffer) followed before the pellet was redissolved in 100µl low salt buffer containing 1% TritonX100 (TX100). Again samples were centrifuged at 5000×g at 4°C for 30min and supernatant was collected as low salt/TX100 fraction followed by 2×washing in low salt buffer containing 1% TX100. Lastly, pellets were redissolved in 100µl high salt buffer. All four fractions (total, low salt buffer fraction, low salt buffer/TX100 fraction, high salt fraction) for all three genotypes were subjected to the BCA assay to determine protein concentration. After adding 4×Lämmli buffer and boiling for 5min, 750rpm at 95°C 10µg of each sample according to the determined protein concentrations was loaded to a SDS-PAGE gel and subjected to Western blotting.

5.2.1.23 Solubility fractionation

Frozen adult zebrafish brains deriving from homozygous, heterozygous $Fus^{mde1500}$ mutants or wildtype siblings were sequentially extracted using buffers with increasing detergent concentrations. First, brains were homogenized in 200µl high salt buffer using tissue a homogenizing device. High salt buffer soluble proteins were extracted via ultracentrifugation at 100000×g at 4°C for 38min. Supernatant was collected as high salt buffer fraction. 2×washing steps with 200µl high salt buffer followed to make sure all proteins soluble in high salt buffer were extracted. Next, pellets were redissolved in 100µl high salt buffer with 1% TritonX100 and subjected to ultracentrifugation at 100000×g at 4°C for 38min. Supernatants were collected as high salt/TX100 buffer fraction and pellets were washed twice with 100µl high salt buffer with 1% TritonX100 before next buffer was applied. Pellets were dissolved in 50µl RIPA buffer and subjected to ultracentrifugation at 100000×g, 4°C for 38min before supernatants were collected as RIPA buffer fraction and 2×washing steps 50µl RIPA buffer were performed. Next, 25µl RIPA with 2% SDS was used to dissolve the RiPA pellets and samples were again centrifuged at 100000×g for 38min at 4°C. RIPA/2%SDS supernatant was collected and 2×washing steps 25µl RIPA/2%SDS buffer were performed. Finally, RIPA/2%SDS pellets were extracted in 70% formic acid, evaporated and dissolved in 25µl Tris buffer pH9. To compare different genotypes, equal volumes of different fractions (10µl of high salt and high salt/TX100 fractions, 20µl of RIPA and RIPA/SDS fractions, 25µl of formic acid fraction) were used in SDS-PAGE and Western blotting after adding 4×Lämmli buffer and boiling for 5min, 750rpm at 95°C.

5.2.2 Cellbiological methods

5.2.2.1 HeLa cell culture and transfection

Human cervical carcinoma cells (HeLa) were cultured in Dulbecco's modified Eagle's medium (DMEM) with Glutamax supplemented with 10% fetal calf serum (FCS) and 1% penicillin/streptomycin at 37°C and 5% CO_2. For transfections cells were seeded in 12 well cell culture dishes and transfected by inverse transfection. Per well, 2µl Lipofectamin 2000 incubated with 125µl OptiMEM for 5min was combined with 0.8µg of DNA mixed with 125µl OptiMEM. The DNA/lipofectamin transfection mix was placed into wells of the 12 well plate prior to plating 150000 cell in 500µl per well. Cells were incubated in transfection mix o/n and media was exchanged by DMEM/Glutamax/FCS/penicillin/streptomycin the next day. Cells were cultured until harvesting 48h after

transfection.

5.2.2.2 Harvesting of HeLa cells and cell lysis

Cells were washed 2×in PBS and detached from the dish using a cell culture spatula and ice cold PBS before centrifugation at 3500×g to pellet cells and lysis in 250µl ice-cold RIPA lysis buffer containing 1×Proteinase and Phosphatase Inhibitor by incubating on ice for 10min. Next, DNA was sheared by sonification and remaining debris were pelleted by centrifugation of the samples for 15 min at 13000 rpm and 4°C. Supernatant were collected in new microcentrifuge tubes and subjected to BCA assay measurements to determine protein concentrations. 4×Lämmli sample buffer was added to the cell lysates, and samples were boiled at 95°C, 750rpm for 5-10min and centrifuged for 1min at 13000rpm. Until being used for immunoblotting, samples were stored at -20°C.

5.2.2.3 Preparation and cultivation of primary neurons

Primary rat cortical neurons were obtained from Sprague-Dawly rat embryos at embryonic day 18 or 19 (E18 or E19). Embryos were removed from the uterus, decapitated and cortices dissected from the skull. Tissues were washed 4×in ice cold HBSS buffer prior to dissociation of neurons via incubation in 5mm HBSS containing 300µl 2.5% trypsin and 500µl DNAse treatment (200 units per mg) for 20min and another 4×washing steps with warm HBSS buffer before pipetting up and down several times. 400000 dissociated cortical neurons were plated on cover slips, beforehand subjected to 65% nitric acid treatment, sterilization, coating in 0.1M borate buffer containing 1.5% PDL and 0.625% laminin and equilibration in neurobasal media.
Primary rat cortical neurons were cultivated in neurobasal media supplemented with 2% B27, 1% Penicillin/Streptomycin and 0.25% glutamine.

5.2.2.4 Transfection of primary neurons

Primary rat cortical neurons were transfected with GFP-tagged $Fus^{mde1500}$ or $Fus^{wildtype}$ constructs under control of the CMV promotor on day *in vitro* (DIV) 6. 3.2µl Lipofectamin 2000 incubated with 100µl OptiMEM for 5min was combined with 1.8µg of DNA mixed with 100µl OptiMEM. DNA/Lipofectamin transfection mix was added to in prewarmed neurobasal media rinsed coverslips in a dropwise manner. After 45min transfection mix was removed by 2×rinsing of coverslips in neurobasal media and cover slips were transferred back to original media and incubated until fixation 4 days after transfection DIV6+4 in 4% PFA for 15min at RT after washing in PBS.

5.2.2.5 Immunofluorescence stainings in primary neurons

After fixation cover slips were treated with 3ml 50mM Ammonium Chloride containing 0.2% TritonX100 for 5min at RT prior to being washed 3×in PBS. Next, coverslips were blocked with 100µl of blocking solution (2%FCS, 2%BSA, 0.2% fish gelatin in 1×PBS) for 1h in a wet chamber to avoid drying. Next, blocking solution was aspirated and replaced by 100µl primary antibody diluted in 10% blocking solution (mouse α-GFP antibody diluted 1:500). Coverslips were incubated in primary antibody solution for 1h before 4×washing steps in PBS were performed. Secondary antibody was diluted in 10% blocking solution (Alexa α-mouse 488 diluted 1:500), added to coverslips and incubated at RT for 45min in darkness. After 2×washing with PBS, DAPI staining (dilution 1:5000 in PBS, incubation for 15min) was performed to visualize nuclei. After 2×washing steps in PBS, cover slips were mounted on glass slides using Vectashield H-1000 mounting media and analyzed by confocal microscopy.

5.2.3 Zebrafish specific methods

5.2.3.1 Zebrafish husbandry and handling of embryos

Husbandry, breeding, and mating of wildtype and mutant zebrafish was performed according to standard methods [164]. Embryos and larvae were kept at 28.5°C in E3 medium containing methylene blue until 5 dpf prior to being transferred to tanks. Developmental stages were determined according to [165]. Zebrafish embryos and larvae used for *in vivo* imaging or whole mount immunofluorescence (IF) stainings were treated with 1×PTU starting at 1 dpf to avoid pigmentation [166]. For embryonic stages analyzed earlier than 3 dpf, chorions were removed by adding 10µl pronase to embryos containing petri-dishes starting at 1 dpf. For very early stages (before 1 dpf) chorions were removed manually using forceps.

5.2.3.2 Mating of adult zebrafish

Pairs of adult zebrafish was transferred from tanks to mating boxes equiped with dividers to separate males and females o/n. Next morning, parallel removal of dividers allowed simultaneous spawning of several pairs, yielding age matched zebrafish embryos. Fertilized eggs were separated from unfertilized ones, transferred to petri-dishes and kept at 28.5°C in E3 medium containing methylene blue until further analysis or raising.

5.2.3.3 Microinjection into zebrafish eggs

Microinjections into zebrafish fertilized eggs were performed at one cell stage (zygotes). Before injections, injection needles and injection agar plates were prepared. Injection needles were generated with a needle puller device using the programme P(A)60. Microinjection molds were placed into a petri dish containing 1.5% agarose in E3 to generate injection agar plates. Most of the freshly spawned eggs were sorted into the cavities, created by the molds of the injection plates. The rest of spawned eggs was held back and served as a control for proper development. 2-4 pl of 0.4 µg/µl of the *fus* ZFN mRNAs or 1 mM of *fus* targeting gripNAs (dissolved in DEPC H_2O) were injected into the yolk. Fertilized embryos were kept at 28°C after eliminating unfertilized eggs. Phenotypes were briefly checked at 1 dpf prior to fixation for further analysis or raising to adulthood.

5.2.3.4 Knockdown of genes in zebrafish embryos using gripNAs

gripNAs targeting either the ATG start codon or the intron13-exon14 splice site of the *fus* mRNA were obtained from Gene Tools. 1 mM stocks were prepared by solubilizing the lyophilized solid in sterile dH_2O and 3µl aliquots stored at -20°C until injection. 1 mM concentrations were injected into one-cell-stage AB or mutant $Fus^{mde1500}$ embryos as described in subsubsection 5.2.3.3. The injected embryos were phenotypically analyzed, and knockdown efficiency of *fus* evaluated on Fus protein level by immunoblotting.

5.2.3.5 Bleaching of fertilized zebrafish eggs

Fertilized zebrafish eggs were bleached prior to being raised to prevent contamination of other fish with pathogens. This procedure is not harmful after epiboly is finished, until approx. 1.5dpf. Fertilized eggs placed in a tea net were exposed to bleaching solution for 5 min prior to being rinsed in tap water for 5 min. After repeating this procedure, embryos were transferred to fresh petri dishes filled with E3 medium without methylene blue containing 10 µl of Pronase stock solution to facilitate hatching of embryos from denaturated chorions at 3 dpf.

5.2.3.6 Fin biopsies from adult zebrafish

Determination of the genotype of a single zebrafish was performed with tail fin biopsies derived genomic DNA. To do so, zebrafish were anesthetized in 5-10% Tricaine solution.

Fin tissue from the periphery of the tail fin was cut on a cutting board and fixated in 100% methanol. Immediately after biopsy fish were transferred to a single box containing fresh fish water to recover.

5.2.3.7 Tissue harvesting from adult zebrafish

Tissues from adult zebrafish were isolated as described previously [167].

5.2.3.8 Fixation and storage of zebrafish samples

For protein analysis or mRNA isolation embryos, larvae and dissected tissue were snap frozen in microcentrifuge tubes using liq. N_2 after complete removal of all liquid. Snap frozen samples were stored at -80°C until usage.
Embryos and dissected brains for whole-mount IF stainings and immunohistochemistry were transferred to microcentrifuge tubes containing 4% PFA and samples were fixated o/n at 4°C. PFA solution was removed and samples were rinsed once with PBST, then washed three times for 5 min with PBST at room temperature (RT). Samples for immunohistochemistry were subjected to a dehydration series and embedded in paraffin (see subsubsection 5.2.3.16). Samples for whole mount immunofluorescence stainings were subjected to a series of methanol washes (25% methanol in PBST, 50% methanol in PBST, 75% methanol in PBST, 100% methanol) prior to being stored in 100% methanol at -20°C until usage.
For genotyping of individual zebrafish, embryos, larvae and biopsied fin tissue were stored in 100% methanol in individual microcentrifuge tubes until usage.

5.2.3.9 Whole mount *in situ* hybridizations

In 4% PFA fixed samples were rehydrated by a series of 5 min washing steps with decreasing methanol concentrations (75% methanol in PBST, 50% methanol in PBST, 25% methanol in PBST, 100% PBST) prior to a 3×5 min PBST washing cycle and permeabilization using 10µg/ml PK in PBST as indicated below.

24hpf	7min
48hpf	20min
72hpf	30min

After 2 washing steps with PBST samples were re-fixated by 20 min treatment with 4% PFA prior to another round of washing in PBST (3×5 min). Next, samples were incubated with hybridization buffer plus (HYB+) at 65°C for 20 h prior to incubation

with either 250 ng antisense probe or 250 ng sense probe containing HYB+ at 65°C o/n. Antisense and sense probe were generated in parallel to sample preparation (see subsubsection 5.2.1.14).
Next day, probes were removed and samples washed in 2xSSCT/50% formamide at 65°C 2×30 min, prior to 1×15 min washing in 2×SSCT followed by 2×30 min washing in 0.2×SSCT. Samples were then blocked with NCST for 2 h before being incubated with the alkaline phosphatase conjugated α-digoxygenin fragment antigen binding (Fab) antibody in NCST (dilution 1:4000) o/n, thereby detecting Digoxygenin labeled antisense and sense probes.
Next day, samples were washed 4×25 min in NCST to remove the antibody, before being washed in NTMTL for 3×5 min. Next, samples were stained with staining buffer containing the chromogenic substrates 5-bromo-4-chloro-3-indolyl phosphate (BCIP) and nitro blue tetrazolium chloride (NBT) in 12 well microtiter plates, and colorimetric detection of alkaline phosphatase activity due to catalysis of BCIP and NBT was stopped with 2×5 min PBST washing steps. Samples were imaged and stored in 100% glycerol at 4°C.

5.2.3.10 Whole mount immunofluorescence stainings

For whole mount IF stainings PFA fixated, methanol stored embryos and larvae were used. Samples were rehydrated in a stepwise manner using a methanol series (75% methanol in PBST, 50% methanol in PBST, 25% methanol in PBST, 100% PBST). After the 5 min lasting rehydration steps on a shaker at RT, the samples were washed 3×5 min in PBST at RT.
Depending on the age of examined embryos, different permeabilization strategies were performed. 24 hpf embryos injected with GFP-Fus^{wildtype} or GFP-Fus^{mde1500} constructs were counter-stained with GFP antibodies. To permeabilize, these embryos were subjected to a 10 min treatment with 10 µg/ml Proteinase K in PBST. 28 hpf embryos for CaP motor neuron staining using Zn1/Znp1 antibodies were treated for 10 min with 10 µg/ml Proteinase K in PBST. 48 hpf embryos for staining of vessels using ZE-5 4D1 antibody were subjected to a 20 min treatment with 10 µg/ml Proteinase K in PBST. 48 hpf embryos for staining of muscles using F59 myosin or α-actinin antibodies were treated with 10 µg/ml Proteinase K in PBST for 20 min.
After removal of Proteinase K by washing, the remaining proteases were inactivated by re-fixating the embryos for 20 min in 4% PFA on a shaker at RT. After removing the PFA, samples were washed for 3×5 min in PBST. Blocking was performed for 1h in

NCST on a shaker at RT. Then primary antibodies were added in NCST, 0.05% NaN_3 and samples were incubated on a shaker at 4°C o/n. The next day primary antibodies were removed and kept for further use at 4°C. Afterwards, the samples were rinsed with PBST and washed 3×15 min in PBST on a shaker at RT. Next, they were blocked 2×for 30 min in NCST. The secondary antibody was applied in NCST on a shaker at 4°C o/n. After removal of the secondary antibody samples were rinsed with PBST and washed 3×to 5×15 min in PBST depending on the strength of the fluorescence signal. After DAPI staining (diluted 1:1000 in PBST, incubation 30 min, remove DAPI solution and wash 2×with PBST) to visualize nuclei, samples were imaged as soon as possible.

5.2.3.11 Heat shock treatment

Zebrafish embryos were kept in petri dishes at until 3 dpf. Then larvae were transferred to 38°C for 20 h, whereas control larvae stayed at 28.5°C prior to fixation at 4 dpf and TUNEL staining (see subsubsection 5.2.3.13).

5.2.3.12 Pentylenetetrazole treatment

Pentylenetetrazole (PTZ) is an agent known to induce seizures in zebrafish [168]. Zebrafish embryos were treated in E3 containing 5 mM PTZ in 1%DMSO for 72h starting at 1 dpf. Control embryos were incubated in E3 containing 1%DMSO for 72 h starting at 1 dpf. Both groups were kept at 28.5°C, fixated at 4 dpf and subjected to TUNEL staining (see subsubsection 5.2.3.13).

5.2.3.13 TUNEL staining in zebrafish

Similar to whole mount immunofluorescence stainings, PFA fixated, methanol stored larvae were used. After samples were rehydrated in a stepwise manner using a methanol series (75% methanol in PBST, 50% methanol in PBST, 25% methanol in PBST, 100% PBST) for 5 min each, 2×5 min washing in PBST followed. Samples were permeabilized using 10µg/ml Proteinase K treatment in PBST for 45 min followed by 2×5 min washing in PBST. TUNEL reagent was applied according to the manufacturer's protocol. After 2×5 min washing in PBST, DAPI staining was performed (diluted 1:1000 in PBST, incubation 30 min, remove DAPI solution and wash 2×with PBST) to visualize nuclei and samples were imaged.

5.2.3.14 Motor neuron analysis

Spinal motor neuron axons were analyzed after whole mount immunofluorescence stainings with zn1/znp1 antibodies specifically staining caudal primary (CaP) motor neurons (see subsubsection 5.2.3.10). After immunofluorecent staining of motor neurons in 28hpf old embryos, heads were biopsied, collected in individual microcentrifuge tubes and lysed in TE/Proteinase K lysis buffer prior to being subjected to genotyping procedure using allele specific primers (see subsubsection 5.2.1.3). Immunostained tails of the embryos were stored 24 well plates in PBST to be able to correlate the genotyped sample with the respective tail until genotyping process was completed. 10 embryos per genotype in 3 different clutches were imaged and motor neuron axons were analyzed for morphology and length alterations.

5.2.3.15 Locomotion analysis

Locomotion analysis was performed at 4 dpf. Larvae were raised in petri dishes until 4 dpf and then transferred to 24 well plates with one larvae per well in 1ml E3 medium. To test whether the swimming response is changed upon a stimulus (darkness) in mutants compared to wildtype a high sensitivity digital camera (30 frames/s) in combination with the ZebraLab tracking software was used. After an adaptation phase of 60 min in 100% light, spontaneous movements were recorded during a 60 min 100% light baseline phase, before movement was traced during alternating cycles of 15 min 100% darkness, 15 min 100% light, 15 min 100% darkness, 15 min 100% light and analyzed via Viewpoint ZebraLab software and MS Excel.

5.2.3.16 Immunohistochemistry

For immunohistochemical experiments, zebrafish embryos, larvae, adult brains and whole adult truncs were fixated in 4% PFA for 48 h. Next, samples were dehydrated via a series of increasing ethanol concentrations (70% ethanol for 1 h, 96% ethanol for 1 h, 4×absolute ethanol for 1 h) before being cleared in 2×100% Xylene steps for 1 h each and infiltration of samples by paraffin for 2×1 h at 58°C. While paraffin is liquid at 58°C, paraffin samples can be embedded in molds covered in paraffin, yielding solid paraffin blocks once cooled down to RT. Molds were removed and sections of 2-5 µm are sliced off the paraffin block using a microtome before placing them on glass slides and drying o/n at 65°C.
Next day, glass slides with tissue sections were subjected to a 20 min 100% Xylene washing step and a 100% Xylene rinsing step followed by a series of decreasing ethanol

concentrations (2×absolute ethanol for 5 min each, 96% ethanol rinse, 2×70% ethanol rinse, 100% dH_2O for 5 min) to deparaffinate and rehydrate samples. To retrieve the antigen, slides were boiled in citrate buffer containing 100 mM citric acid and 100 mM sodium citrate for 4×5 min in a microwave at 750 W. After boiling, slides stayed in citrate buffer and were incubated at RT for 30 min to allow a slow cool down. Next, slides were rinsed in dH_2O prior to blocking in inhibiting endogenous peroxidase by incubating slides in 5% dH_2O_2 in 100% methanol for 20 min. Slides were rinsed in tap water for 10 min prior to a quick rinse in dH_2O followed by 2×5 min washing steps in PBS/0.05% Brij. Blocking of unspecific antibody binding sites was achieved with 2×5 min incubation steps in PBS/2% fetal calf serum (FCS). Per slide, 100 µl of antibody diluted in PBS/2% FCS was used. Slides were covered with cover slips and incubated in 4°C o/n.
Next day, primary antibodies were washed 2×5 min in PBS/0.05% Brij. 100 µl of DCS SuperVision 2 Polymer-Enhancer solution was applied, slices were covered with coverslips and incubated at RT for 20 min. Enhancer solution was removed by 2×5 min washing steps in PBS/0.05% Brij and 100 µl DCS Supervision 2 Polymer-Reagent was applied. Slides covered with coverslips were incubated at RT for 30 min. Polymer reagent was removed in 2×5 min washing steps in PBS/0.05% Brij. DCS Supervision 2 DAB concentrate is diluted in DAB substrate buffer (37 µl in 1 ml) and 100 µl of diluted DAB were applied on slides. Slides with different genotypes derived tissue were treated in parallel and DAB reaction was stopped simultaneously by rinsing in dH_2O. To visualize nuclei, haematoxylin staining was performed after DAB reaction was completed. Slides were incubated in haematoxylin for 30 s prior to rinsing with tap water for 10 min. Next, slides were sequentially dehydrated in a series of increasing ethanol concentrations (2×rinse in 70% ethanol, 1×rinse in 96% ethanol, 2×rinse in absolute ethanol followed by 5 min incubation in absolute ethanol) followed by clearing in 2×5 min incubations in Xylene and mounting using mounting media and coverslips. Stained sections were analyzed by microscopy.

5.2.3.17 Lysis of zebrafish samples

For the isolation of proteins RIPA lysis was used. Microcentrifuge tubes containing shock frozen embryos, larvae, or adult tissue were kept on dry ice. RIPA buffer containing 1×Proteinase and Phosphatase Inhibitor was added to samples and tissues were immediately and completely homogenized using a tissue homogenizer. Next, DNA was sheared by sonication and remaining debris pelleted by centrifugation of the samples

for 15 min at 13000 rpm and 4°C. The supernatant was used in BCA assays to determine protein concentration prior to adding a third of sample volume of 4×Lämmli buffer, boiling for 5 min, 750 rpm at 95°C and centrifuging 15 min at 13000 rpm to pellet debris. According to the BCA analysis, 5-20 mg of the samples were used for SDS-PAGE. Samples were stored at -20°C and reused after boiling for 5 min, 750 rpm at 95°C and centrifuging 1 min at 13000 rpm.

5.2.3.18 Generation of zebrafish Fus specific antibodies

Zebrafish specific peptide antibodies detecting Fus protein were generated by the service unit monoclonal antibodies at the Core Facility Monoclonal Antibodies, Institute for Molecular Immunology, Helmholtz Center Munich. Peptides for immunization of mice were synthesized and conjugated N- or C-terminally with ovalbumin (OVA) by Peptide Specialty Laboratories GmbH. After immunization of mice with the zebrafish Fus peptides antibodies producing lymphocytes were isolated from immunized animals to be fused with myeloma cells, yielding hybridomas. Hybridoma cells were cultured and polyclonal supernatant was tested for epitope specificity, prior to isolating single hybridoma cell clones, yielding monoclonal supernatants. Testing of polyclonal and monoclonal supernatants for specificity is described in the results chapter.

5.2.4 General methods

5.2.4.1 Databases used for primer design and cloning strategy

Genomic and transcript sequences were downloaded from Ensembl Genome Browser (http://www.ensembl.org/index.html) or NCBI (http://www.ncbi.nlm.nih.gov/). For sequence alignements, assemblies, and analysis including restriction enzyme mapping and construction of plasmid maps CLC Main Workbench was used. For design of primers, Primer3 (http://primer3.ut.ee/) was employed and specificity of primer pairs tested by Primer-BLAST (http://www.ncbi.nlm.nih.gov/tools/primer-blast/). Other BLAST searches were performed on the Ensembl (http://www.ensembl.org/Multi/blastview) and NCBI (http://blast.ncbi.nlm.nih.gov/Blast.cgi) web pages.

5.2.4.2 Image acquisition and processing

Images were acquired using Zeiss spinning disc cell observer microscope, Zeiss LSM 710 confocal microscope and Zeiss Axioplan 2 imaging microscope. Zebrafish embryos and larvae were embedded in 1,5% low melting agarose in PBST and imaged on glass bottom

microscope dishes. Rat primary neurons were imaged on cover slips. Histological sections were imaged after mounting of cover slips.
Images were processed using ZEN blue, ZEN black, AxioVision, or Adobe Photoshop to linearly adjust brightness and contrast as well as image size. For quantitative Western blots, band intensities were detected using LAS 4000 image reader and evaluated by Multi Gauge V3.0 software.

5.2.4.3 Statistics

Means and standard error of the mean (mean + SEM) were calculated using Graph Pad Prism. Graphs shown in this thesis were generated with the Graph Pad Prism software. The statistical analysis and tests used are indicated in the respective figure legend. In the respective graphs, the level of significance is indicated by asterisks: $*p < 0.05$; $**p < 0.01$; $***p < 0.001$. If there is no significant difference, the abbreviation ns is used.

6 Results

6.1 Characterization of Fus in zebrafish

6.1.1 *FUS* orthologue in zebrafish

Despite a genome duplication in the teleost lineage, only one orthologue of the human *FUS* gene exists in zebrafish. The zebrafish *fus* gene is located on chromosome 3 of the zebrafish genome encoding the 541 amino acids long Fus protein, which is 60% identical to the human FUS protein. Moreover, all amino acids altered in severe ALS causing mutations clustered in the very C-teminus of the protein are evolutionary conserved between human and zebrafish (see Figure 6.1).

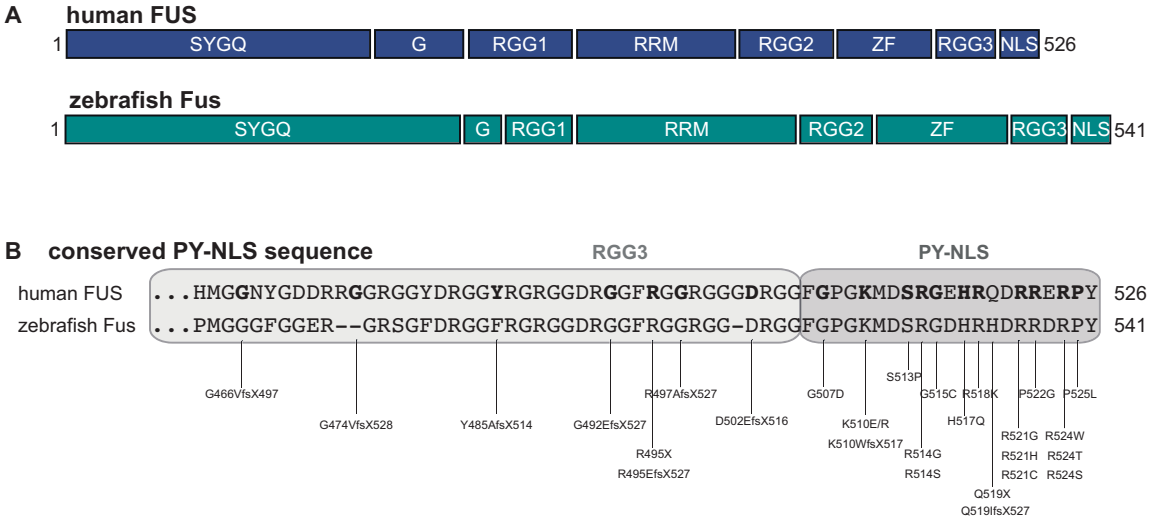

Figure 6.1: Schematic overview of the FUS protein. A Graphic illustration of the different protein domains in human FUS (blue) and zebrafish Fus (turquoise). **B** Conservation of the RGG3 and the PY-NLS domains. ALS relevant mutations are highlighted in bold.

6.1.2 Expression profile of Fus

To analyze expression profile of *fus* gene on transcript and protein level during zebrafish development, I performed in situ hybridization (ISH) and Western blot analysis. ISH

experiments showed *fus* expression in embryos already at 8 cell stage prior to zygotic transcription, indicating maternal *fus* RNA deposition into the oocyte. Stages analyzed were 8 cell stage at 1.5 hours post fertilization (hpf), shield at 6 hpf, 14 somites, 24 hpf, 2 days post fertilization (dpf), 3 dpf, and 4 dpf. Interestingly, *fus* expression is ubiquitous in early stages of development and gets restricted to the brain after 2 dpf.

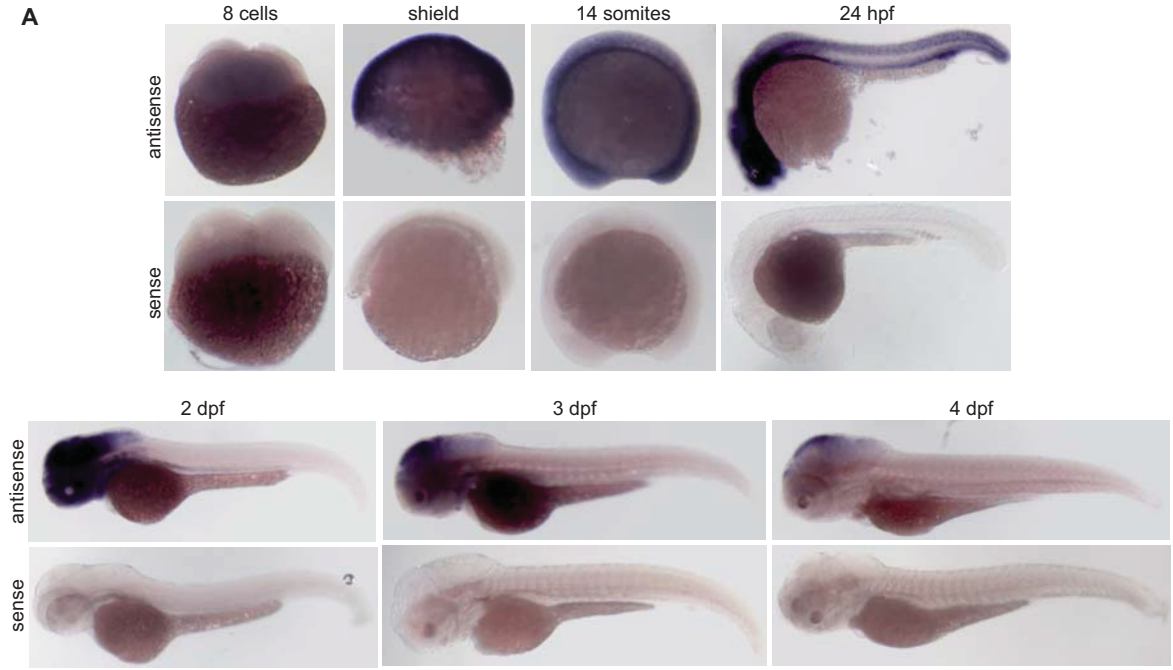

Figure 6.2: *fus* expression in zebrafish. A ISH. *fus* mRNA is detected via a digoxygenin labeled antisense probe, a sense probe serves as negative control. Zebrafish were fixated, stained and analyzed at different stages during development (8 cell, shield, 14 somites, 24 hpf, 2 dpf, 3 dpf, 4 dpf).

To determine Fus protein expression in zebrafish, Western blot using zebrafish Fus specific antibodies was performed.

I tested the specificity of in total 44 commercially available and custom made antibodies raised against different Fus antigens. To determine the antibody specificity I included several controls. Firstly, I cloned the coding sequence of zebrafish wildtype *fus* and fused it to the coding sequence of green fluorescent protein (GFP) and expressed it in HeLa cells as well as zebrafish embryos as positive control. Secondly, I injected two different *fus* RNA targeting gripNAs into zebrafish embryos and sacrificed them at 2 dpf together with buffer injected wildtype embryos as negative control. To determine immunoreactivity of the antibodies in adult tissues, adult brain derived samples were loaded additionally. Only one antibody, Santa Cruz human FUS antibody 4H11 (sc47711), detects the zebrafish Fus protein in embryonic, larval and adult stages. Western blotting using this antibody showed immunoreactive bands at 75 kDa

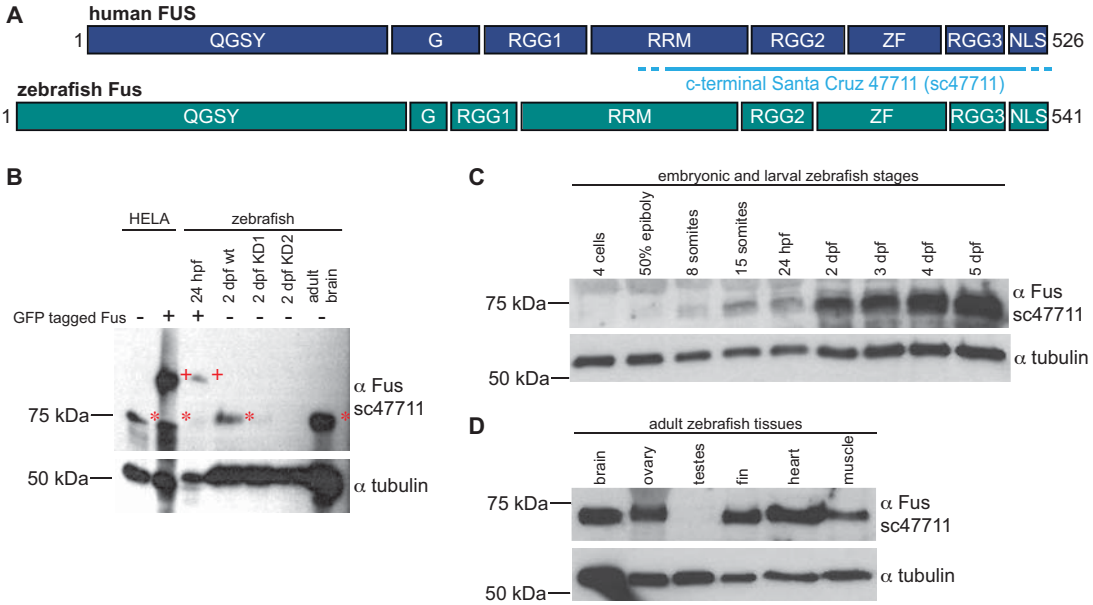

Figure 6.3: Fus expression in zebrafish. A Schematic depiction of human FUS and zebrafish Fus. The estimated C-terminal epitope of the Santa Cruz human FUS antibody 4H11 (sc47711) is indicated in light blue. **B** Antibody sc47711 was tested for cross-reactivity in zebrafish with samples generated from GFP-tagged zebrafish Fus expressed in HeLa cells and in 24 hpf old zebrafish as well as in two different gripNA mediated knockdown samples with wildtype controls derived from 2 dpf old fish and in adult brain tissue. Red crosses display GFP-tagged Fus, whereas red asterisks depict endogenous Fus protein. **C** Fus expression during embryonic and larval development. Nine developmental stages were analyzed, including 4 cell stage, 50% epiboly stage, 8 somites stage, 15 somites stage, 24 hpf, 2 dpf, 3 dpf, 4 dpf and 5 dpf. Fus protein expression levels are below detection limit before 15 somites - 24 dpf. **D** Fus expression in adult tissues. Fus is expressed in all tissues examined, except for testes tissue as visualized by the Fus immunoreactive 75 kDa band. α-tubulin serves as loading control in all blots depicted here.

and approximately 100 kDa, reflecting the endogenous and the GFP-tagged Fus protein, respectively which were absent in the two independent knockdown samples and enriched in transfected HeLa cells, indicating specificity (see Figure 6.3A-B).

After identification of a zebrafish Fus protein detecting antibody, Fus protein expression pattern was examined. I analyzed different embryonic and larval stages during development (see Figure 6.3C) as well as different tissues within adult fish (see Figure 6.3D). Zebrafish Fus protein expression is first detectable around 5 somites - 24 hpf and increases over the course of development. In adult fish, all tested tissues showed Fus expression including brain, ovary, fin, heart and muscle tissue except for testes.

6.1.3 Transient *fus* knockdown

The analysis of primary spinal motor neuron morphology has been a popular tool to study neuronal dysfunction. The caudal primary (CaP) spinal motor neuron is the first neuron that projects laterally from the spinal cord to the muscles and is especially well

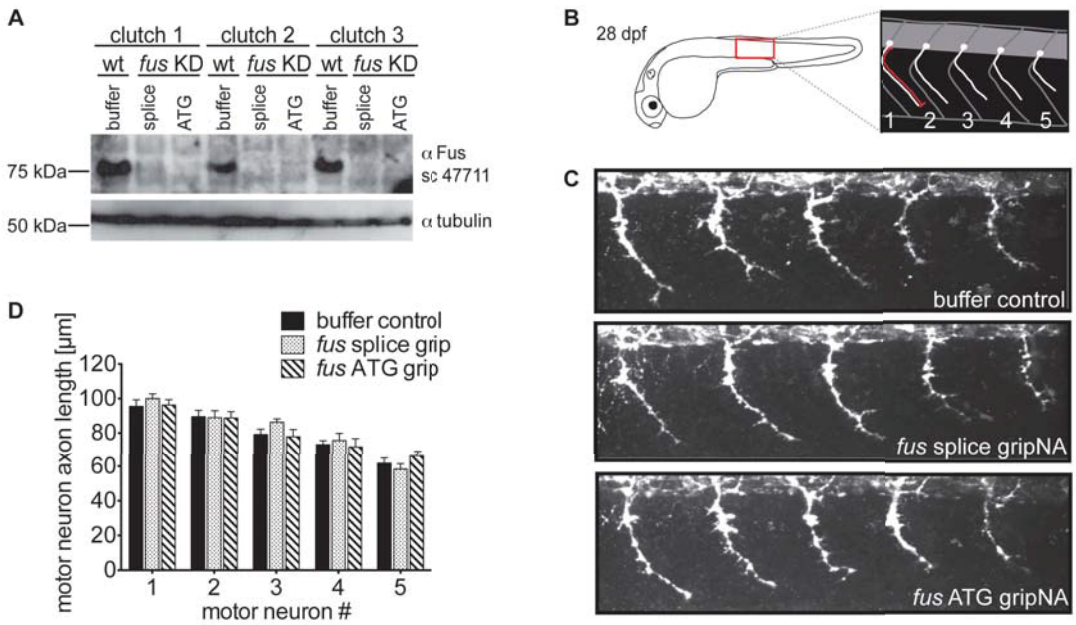

Figure 6.4: *fus* knockdown effects on motor neuron morphology. A Confirmation of knockdown efficiency via Western Blot. Fertilized eggs derived from one clutch were injected with either buffer, 1 mM *fus* splice gripNA or 1 mM *fus* ATG gripNA. At 28 hpf some embryos were separated for Western blot analysis, whereas most siblings were stained for primary motor neurons using zn1/znp1 antibodies. **B** Schematic illustration of analyzed motor neurons. The five most caudal motor neuron axons above the yolk sac extension were imaged and examined. **C** Representative images of analyzed motor neuron axons in buffer control, *fus* splice gripNA and *fus* ATG gripNA injected embryos. No changes in morphology were obtained upon *fus* knockdown. **D** Length of primary motor neuron axons was examined and plotted. No significant change in length was observed upon *fus* knockdown. Triplicates of $n = 10$ fish per condition were analyzed. Mean + SEM. Statistical test used: Kruskal-Wallis test followed by Dunn's test to correct for multiple comparisons. No statistical significance was obtained (ns).

suited for morphological examination due to its exposed position. Published data describe CaP axonal length and outgrowths deficits in motor neurons upon *fus* morpholino (MO) mediated transient knockdown in zebrafish [110], indicating a crucial role of Fus in motor neuron function. To study effects of Fus in motor neurons and to recapitulate published phenotypes, I silenced the *fus* gene using gripNAs transient knockdown technology in zebrafish. gripNAs are commonly used as antisense nucleotide reagents in zebrafish similar to MOs but consist of a negatively charged peptide based backbone instead of the organic chemical compound morpholine containing backbone in MOs. Two different gripNAs, *fus* ATG gripNA and *fus* splice gripNA were injected, directed against the ATG codon and the intron 13/exon 14 splice site of *fus*, respectively. *fus* ATG gripNA is intended to block transcription, whereas *fus* splice gripNA is designed to block the splice site between intron 13 and exon 14, resulting in skipping of exon 14 and a frameshift mediated RNA degradation via nonsense mediated RNA decay. After injection of gripNAs and confirming successful knockdown on protein level via

Western blot, zebrafish were analyzed for motor neuron axon branching morphology and outgrowth length (see Figure 6.4). Interestingly, no changes in axonal morphology or length of CaP motor neuron axons was observed upon *fus* knockdown contradicting published studies [110].

6.2 Generation of genetic *fus* mutants

In humans, neurodegeneration usually occurs during adulthood. To be able to analyze *fus* function in adult and aged brains and to investigate whether loss of *fus* directly contributes to ALS or FTLD pathology, stable knockout instead of transient knockdown techniques were applied to generate *fus* loss of function zebrafish. In contrast to transient knockdown of gene function, sequence specific editing of the genome allows to generate heritable knockout alleles. Moreover, genome editing is less prone to off-site target effects, that might lead to unspecific toxicity [169]. In addition, a genetic approach can resolve the controversy of different phenotypes upon knockdown utilizing either MO or gripNA mediated transient silencing of *fus*.
To mimic the patients situation in the best possible way and thereby recapitulate molecular requirements of pathology I aimed at the generation of not only complete loss of *fus* zebrafish but also zebrafish harboring ALS linked mutations. Hence, genome edited fish were screened not only for frameshift mutations leading to RNA decay but also for inframe premature stop mutations resulting in truncated Fus protein similar to reported ALS causing stop mutations in the human *FUS* gene.

6.2.1 Editing the *fus* locus using ZFNs

I used the ZFN technology to target the zebrafish *fus* locus (see Figure 6.5A). One set of CompoZr Custom ZFNs targeting exon 14, the second last exon of the *fus* gene was designed and cloned by Sigma-Aldrich, St. Louis, MO, USA. *fus*' exon 14 was chosen since it encodes the RGG3 domain and parts of the PY-NLS domain of the Fus protein. Hence, mutagenizing this region on genome level allows not only to induce frameshift mutations leading to RNA decay resulting in complete loss of function but also the occurrence of premature stop codons, resembling ALS patient mutations. I injected the *in vitro* transcribed set of ZFN mRNA into zebrafish zygotes. A Flag-tag on each of the two ZFNs allows to control *in vivo* translation of the ZFN proteins, each being 50kDa. By Western blot analysis of two injected clutches, I confirmed that the ZFN mRNAs were translated into proteins (see Figure 6.5B), the first prerequisite for

successful genome editing.

The second prerequisite is the ability of the ZFN proteins to induce DNA double-strand breaks (DSBs). To test this prior to raising injected P0 fish, I sacrificed injected siblings and performed screening assays to detect mutations induced during the NHEJ DNA repair process (see Figure 6.5C). Genomic DNA was extracted from zebrafish embryos and the *fus* target site containing DNA fragment was amplified by PCR, followed by a restriction digest with the BseDI restriction enzyme. This enzyme's recognition site is part of the ZFN target site and can be used to screen for lost of this restriction site as indicator for a frameshift mutation. PCR and restriction digest products were analyzed by agarose gel electrophoresis resulting polymorphic restriction fragment length (Restriction fragment length polymorphism, RFLP). In contrast to injected embryos, uninjected embryos show a complete digest of the PCR product. Hence, incomplete digestion can be excluded and undigested bands indicate successfully introduced mutations in the injected embryos.
After confirmation of the ZFNs functionality and mutagenesis in injected zebrafish, P0 generation fish were raised to adulthood. P0 generation fish are mosaic, since the mutagenesis events happen at a multicellular developmental stage and every affected cell resolves the DNA double stand break in a different manner, resulting a variety of different mutations within one fish. To identify germline borne mutations, P0 generation fish need to be mated with wildtype fish, allowing the analysis of single mutations in heterozygous F1 generation fish. Identification of desired mutations was performed via fin biopsy and genotyping of adult F1 generation fish. Prior to raising the F1 generation, some F1 generation embryos have been sacrificed and analyzed for induced mutations by PCR and RFLP (see Figure 6.5D). Clutches with undigested PCR fragments were selected to be raised. Once these promising F1 generation fish reach adulthood, fin biopsy was performed. Next, genomic DNA was extracted and *fus* target site containing DNA fragment were amplified by PCR, followed by restriction digestion and gelelectrophoresis to separate the mutant allele from the wildtype allele. The mutant DNA was extracted from the agarose gel and the mutation was identified via Sanger sequencing. In case of a desired mutation, e.g. frameshift mutation or in-frame premature stop codons, F1 generation fish were breed to homozygosity and F2 generation zebrafish were analyzed.
Besides RFLP, I established high resolution melting (HRM) analysis as an alternative genotyping technique to cost and time efficiently screen for mutation carriers in the F1 generation. HRM is based on identifying variations in nucleic acid sequences by

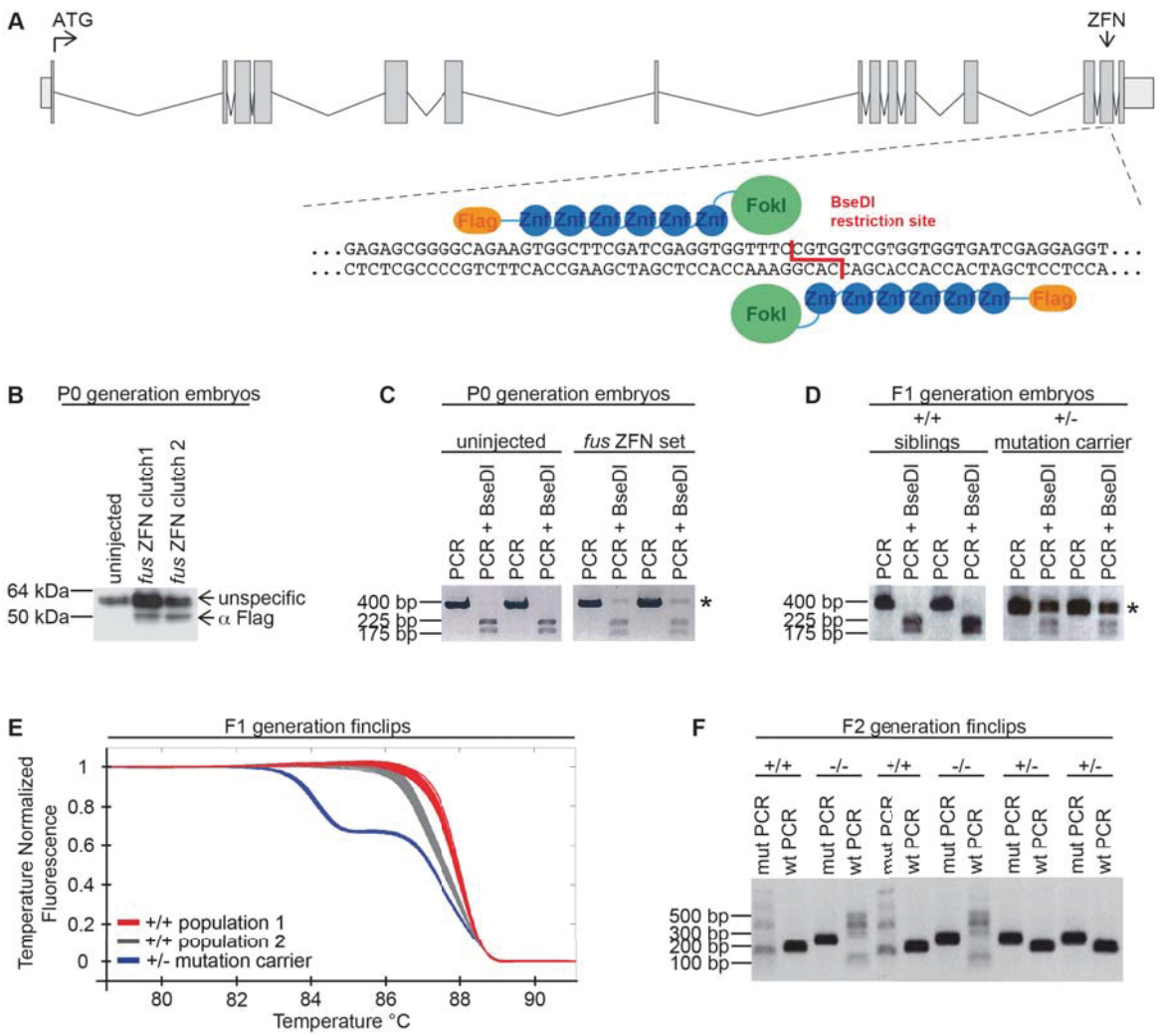

Figure 6.5: ZFN targeting of the zebrafish *fus* locus. A Schematic overview of forward and reverse ZFN arm targeting the *fus* locus. ZFN target site is localized in exon 14, which encodes the RGG3 domain and the PY-NLS of the Fus protein, where most of fALS mutations are clustered. Each ZFN arm consists of a FokI nuclease subunit (green) and several Znf motifs (blue). In addition, ZFNs are fused to a Flag-tag (orange). The restriction endonulease BseDI (red) binds and cuts within the ZFN binding and restriction site, thereby allowing to screen for potential loss of restriction site via RFLP analysis. **B** Confirmation of ZFN expression. Western blotting shows Flag-tagged ZFNs are being expressed in two ZFN-mRNA injected clutches indicated by the Flag immunoreactive band at 50kDa. The unspecific band serves as loading control. **C** Confirmation of ZFN mutagenicity. Amplification of *fus* ZFN target site containing fragment by PCR followed by RFLP analysis using BseDI restriction enzyme was performed to detect mosaic mutations in injected P0 generation embryos. **D** Genotyping of F1 generation embryos using PCR reactions to obtain *fus* ZFN target site amplicons prior to RFLP analysis. After back-crossing of mosaic P0 generation fish to wildtype fish approximately 50% heterozygous mutation carriers were obtained in F1 generation, as expected. **E** HRM analysis as an alternative genotyping technique in the F1 generation. Mutant alleles are distinguished from wildtype alleles via distinct melting curves. The shift in melting curves generated by a HRM software is detected by loss of incorporation of a DNA double-strand intercalating fluorescent dye by a real-time PCR device. **F** Mutation specific PCR analysis as alternative genotyping technique in the F2 generation. To discriminate homozygous and heterozygous carriers of a specific preselected mutation from wildtype fish, specific primers either recognizing the mutant or wildtype allele were utilized. For each sample, two PCR reactions were performed and separated by agarose gel electrophoresis. Only in heterozygous samples, both PCR reactions result in products, whereas in homozygous mutation carriers or wildtypes only the mutation or wildtype specific PCR reaction yield amplicons, respectively. Asterisks indicate undigested PCR products due to mutations.

detecting small differences in PCR fragment melting curves. DNA fragments of *fus* containing the ZFN target site were amplified from genomic DNA via PCR. A special dye, LC Green Plus, that is fluorescent when intercalating in double-stranded DNA molecules was added to the PCR reaction. Once the double-strand structure is gradually melted into single strands upon increasing temperature, LC Green Plus can no longer intercalate and fluorescence signal decreases. The dissociation temperature of double-stranded DNA molecules depends on forces resulting from sequence specific hydrogen bonds and amplicon length. Hence, the shape of the resulting melting curve varies between different DNA sequences, allowing to distinguish amplicons that differ by as little as a single base pair. After PCR, a real-time PCR instrument measures the decrease in fluorescence signal, and a HRM software plots fluorescence signal over temperature, resulting in distinct high resolution melting curves for different genetic variants analyzed (see Figure 6.5E).
Once desired mutations were identified and homozygosity was reached in the F2 generation, I further optimized genotyping procedures. Since HRM analysis is not well suited to reliably distinguish homozygous mutation carriers from wildtype fish in F2 generation, I designed mutation and wildtype specific primers to perform genotyping in two consecutive PCR reactions. With each genomic DNA containing embryo or fin biopsy derived sample two PCRs were performed, one using the mutation specific and one using the wildtype specific primers. PCR products were separated by agarose electrophoresis and analyzed for mutant and/or wildtype alleles (see Figure 6.5F).

6.2.2 Screening for *fus* mutations

Once mosaic P0 generation fish were mated with wildtype fish, mutant alleles were sequenced and analyzed in the heterozygous F1 generation. Strikingly, no frameshift mutations were identified in F1 generation after targeting the *fus* locus, only inframe substitutions or deletions of up to 16 codons, resulting in deletions of amino acids within the RGG3 domain of the Fus protein (see Figure 6.6A) were identified. One of these mutations is of particular interest, since deletions of three individual basepairs generates an inframe premature stop codon ($Fus^{mde1500}$) while the original reading frame 5' of the mutation is preserved. Assuming this new codon sequence is transcribed and translated, it would result in a truncated Fus protein with a completely deleted PY-NLS and a C-terminally shortened RGG3 domain. F1 generation fish carrying this promising allele were raised and mated to wildtype fish to expand the line on the one hand and in-crossed to siblings being heterozygous for the same allele to generate ho-

A **Identified *fus* alleles in F_1**

```
                                                RGG3                                   PY-NLS
Fus wt                          ...MGGGFGGERGRSGFDRGGFRGRGGDRGGFRGGRGGDRGGFGPGKMDSRGDHRHDRRDRPY*
Fus Δ(1498-1506)                ...MGGGFGGERGRSGFDRG---GRGGDRGGFRGGRGGDRGGFGPGKMDSRGDHRHDRRDRPY*
Fus Δ(1499-1501)                ...MGGGFGGERGRSGFDRGG-RGRGGDRGGFRGGRGGDRGGFGPGKMDSRGDHRHDRRDRPY*
Fus Δ(1482-1511)                ...MGGGFGGERGRS----------GGDRGGFRGGRGGDRGGFGPGKMDSRGDHRHDRRDRPY*
Fus Δ(1478-1507)                ...MGGGFGGERGR----------RGGDRGGFRGGRGGDRGGFGPGKMDSRGDHRHDRRDRPY*
Fus Δ(1503-1520)                ...MGGGFGGERGRSGFDRGGFR-----RGGFRGGRGGDRGGFGPGKMDSRGDHRHDRRDRPY*
Fus Δ(1503-1532)                ...MGGGFGGERGRSGFDRGGF----------RGGRGGDRGGFGPGKMDSRGDHRHDRRDRPY*
Fus Δ(1498-1515)                ...MGGGFGGERGRSGFDRGG------DRGGFRGGRGGDRGGFGPGKMDSRGDHRHDRRDRPY*
Fus Δ(1487-1504)                ...MGGGFGGERGRSGF------GRGGDRGGFRGGRGGDRGGFGPGKMDSRGDHRHDRRDRPY*
Fus Δ(1491-1502)                ...MGGGFGGERGRSGFD----RGRGGDRGGFRGGRGGDRGGFGPGKMDSRGDHRHDRRDRPY*
Fus Δ(1501-1530)                ...MGGGFGGERGRSGFDRGG----------FRGGRGGDRGGFGPGKMDSRGDHRHDRRDRPY*
Fus Δ(1486-1515)                ...MGGGFGGERGRSGF----------DRGGFRGGRGGDRGGFGPGKMDSRGDHRHDRRDRPY*
Fus Δ(1456-1503)                ...MGGG----------GRGGDRGGFRGGRGGDRGGFGPGKMDSRGDHRHDRRDRPY*
Fus Δ(1454-1501)                ...MGG----------RGRGGDRGGFRGGRGGDRGGFGPGKMDSRGDHRHDRRDRPY*
Fus Δ(1498-1503)                ...MGGGFGGERGRSGFDRGG--GRGGDRGGFRGGRGGDRGGFGPGKMDSRGDHRHDRRDRPY*
Fus Δ(1495-1506)                ...MGGGFGGERGRSGFDRG----RGGDRGGFRGGRGGDRGGFGPGKMDSRGDHRHDRRDRPY*
Fus Δ(1498-99;1501-02;1504-05)  ...MGGGFGGERGRSGFDRGG--LRGGDRGGFRGGRGGDRGGFGPGKMDSRGDHRHDRRDRPY*
Fus Δ(1492-1503)                ...MGGGFGGERGRSGFDR----GRGGDRGGFRGGRGGDRGGFGPGKMDSRGDHRHDRRDRPY*
Fus Δ(1498-1500)                ...MGGGFGGERGRSGFDRGG-RGRGGDRGGFRGGRGGDRGGFGPGKMDSRGDHRHDRRDRPY*
Fus Δ(1495-1500)                ...MGGGFGGERGRSGFDRG--RGRGGDRGGFRGGRGGDRGGFGPGKMDSRGDHRHDRRDRPY*
Fus ins(1498-1500;T1498C;C1500T) ...MGGGFGGERGRSGFDRGGRGRGRGGDRGGFRGGRGGDRGGFGPGKMDSRGDHRHDRRDRPY*
Fus Δ(1499-1507)                ...MGGGFGGERGRSGFDRGG---RGGDRGGFRGGRGGDRGGFGPGKMDSRGDHRHDRRDRPY*
Fus Δ(1495-1524)                ...MGGGFGGERGRSGFDRG---------GGFRGGRGGDRGGFGPGKMDSRGDHRHDRRDRPY*
Fus Δ(1498-1512)                ...MGGGFGGERGRSGFDRGG-----GDRGGFRGGRGGDRGGFGPGKMDSRGDHRHDRRDRPY*
Fus^mde1500                     ...MGGGFGGERGRSGFDRGG-*
```

B **Identified *fus* alleles in P_0**

```
Fus Δ(1498-1515)                ...MGGGFGGERGRSGFDRGG------DRGGFRGGRGGDRGGFGPGKMDSRGDHRHDRRDRPY*
Fus Δ(1498-1506)                ...MGGGFGGERGRSGFDRG---GRGGDRGGFRGGRGGDRGGFGPGKMDSRGDHRHDRRDRPY*
Fus Δ(1498-1512)                ...MGGGFGGERGRSGFDRGG-----GDRGGFRGGRGGDRGGFGPGKMDSRGDHRHDRRDRPY*
Fus Δ(1495-1524)                ...MGGGFGGERGRSGFDRG---------GGFRGGRGGDRGGFGPGKMDSRGDHRHDRRDRPY*
Fus Δ(1500-1508)                ...MGGGFGGERGRSGFDRGGF---GGDRGGFRGGRGGDRGGFGPGKMDSRGDHRHDRRDRPY*
Fus Δ(1494-1500)                ...MGGGFGGERGRSGFDRGVVVVVIEEVSEEEEEEIVEDLDLERWTRGVTTDMTAETALTNISFV*
Fus Δ(1494-1586+46 bps intron14) ...MGGGFGGERGRSGFDRGVFLNIYH*
```

C ***fus* allele summary**

generation	# tested for mutation	# positive for mutation	% positive for mutation	% inframe alleles	% frameshift alleles
P0	87	25	28.7%	77.8%	22.2%
F1	1514	400	26.4%	100%	0%

Figure 6.6: Identified alleles after *fus* locus targeting. A Amino acid sequences of identified alleles in F1 generation. Sequences are aligned to the wildtype Fus sequence and RGG3 (light grey) and PY-NLS (dark grey) domains are depicted. Only inframe alleles were obtained. The $Fus^{mde1500}$ allele harbors a premature stop codon due to the deletion of three individual basepairs, maintaining the correct reading frame upstream of the mutation. **B** Amino acid sequences of identified alleles in P0. In contrast to F1 generation alleles, *fus* frameshift mutations were identified in P0 generation fin biopsy derived genomic DNA. **C** Table summarizing allele frequencies. Interestingly, less frameshift alleles than expected (2/3) were identified in P0 and F1 generations. Deletion or substitution of codons is indicated by red hyphens or letters, respectively. Premature stop codons are indicated by red asterisks, whereas black asterisks display endogenous stop codons.

mozygous carriers on the other hand.
Since no frameshift mutations were identified in the F1 generation, I analyzed the mosaic P0 generation to determine whether frameshift alleles would not occur upon DNA double-strand break within the *fus* locus at all or whether they fail to being transmitted trough the germline. I fin-biopsied P0 generation fish and amplified the *fus* ZFN targeting site from extracted genomic DNA prior to subcloning and sequencing of isloated alleles. Interestingly, besides inframe mutations frameshift mutations resulting in addition of amino acids prior to the premature stop codon occurred in P0 generation fin tissue (see Figure 6.6B). Thus, frameshift mutations are induced in the P0 generation but are not transmitted through the germline into the F1 generation.
In summary, the efficiency of the *fus* targeting ZFNs to induce germline transmittable mutations was 22% (10/46 P0 fish). Of the 1514 F1 generation fish analyzed for mutations, 400 were heterozygous mutation carriers (26.4 %). Similarly, of 87 analyzed P0 generation fish, 25 carried mutations (28.7 %). Of these mutant alleles, 100 % were inframe alleles in the F1 generation versus 77.8 % inframe mutations in the P0 generation. 0 % of frameshift alleles in F1 and only 22.2 % in P0 are surprisingly low rates, considering an expected probability of 2/3 for a frameshift event to happen during indel formation DNA repair, given that a codon consists of three basepairs with a probability of only 1/3 to yield the correct reading frame. Interestingly, neither male nor female P0 generation fish did transmit frameshift mutations through the germline, indicating no gender bias.

6.3 Basic characterization of genetic *fus* mutants

6.3.1 $Fus^{mde1500}$ allele characterization

No frameshift mutations allele were identified upon ZFN mediated genome editing, suggesting that potential loss of function mutations are not germline transmittable. The $Fus^{mde1500}$ inframe allele is very interesting, since it is the only identified allele with a premature stop codon within the RGG3 domain, hypothetically deleting the entire PY-NLS of the Fus protein (see Figure 6.7A). Strikingly, the exact location of the stop mutation in the zebrafish $Fus^{mde1500}$ allele is very similar to two severe ALS causing mutations in human FUS (see Figure 6.7B). Both mutations, G466Vfs497X and R495X, lead to a premature stop codon within the RGG3 domain, thereby potentially deleting the entire PY-NLS and parts of the RGG3 domain. Interestingly, these truncation mutations show a more severe cause of disease than point mutations within the PY-

NLS including earlier age of onset and faster progression of symptoms.

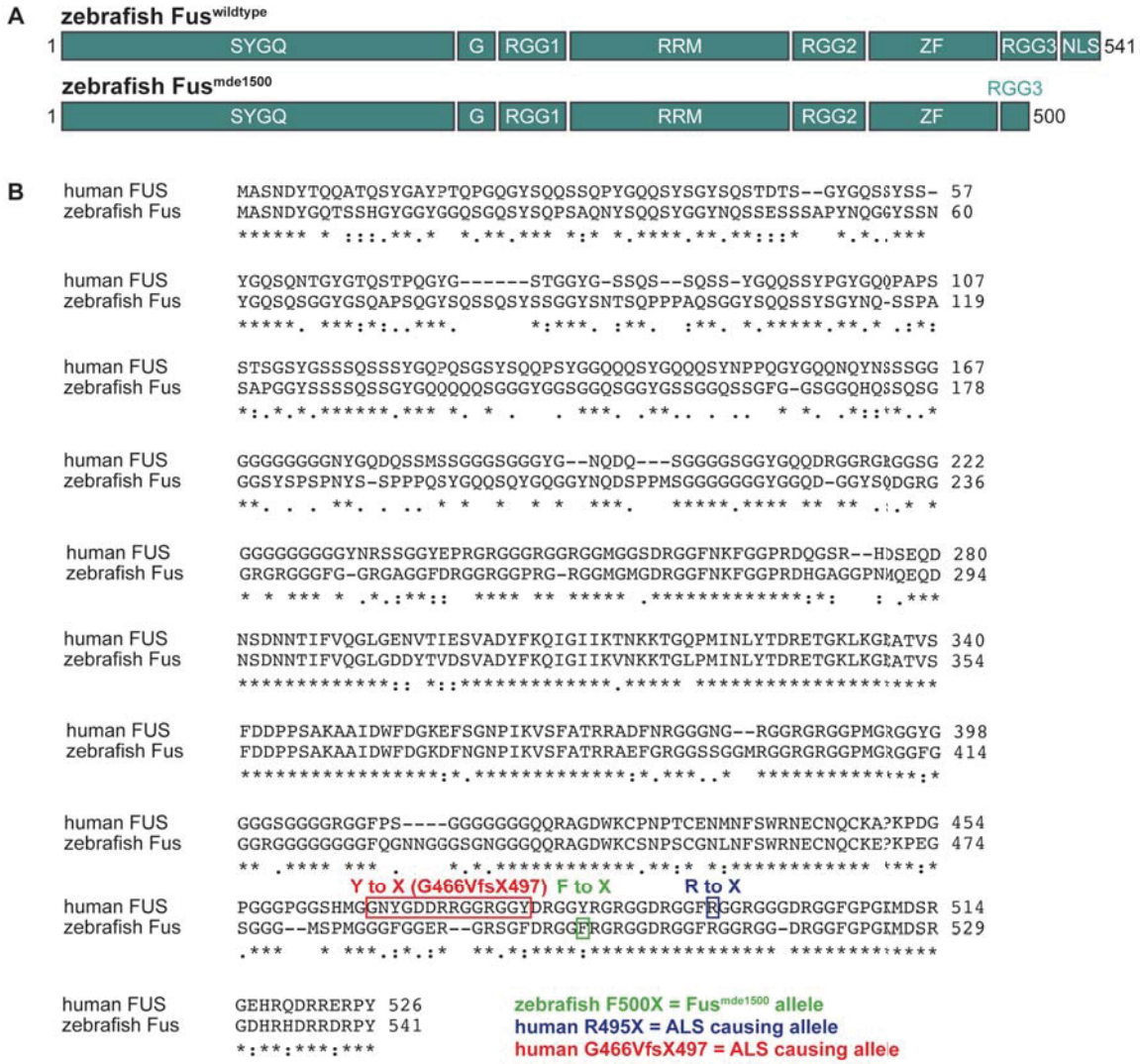

Figure 6.7: Fus^{mde1500} allele. A Schematic representation of the hypothetically truncated Fus^{mde1500} protein in comparison to the wildtype Fus protein. The entire PY-NLS and the C-terminal half of the RGG3 domain is deleted. **B** Amino acid sequences of human FUS and zebrafish Fus are aligned and positions of two representative ALS causing mutations are depicted in blue and red, whereas green indicates the position of the premature stop codon leading to the truncated Fus^{mde1500} protein.

Due to the genetic similarities between the zebrafish Fus^{mde1500} allele and the two ALS patients mutation displayed here, the Fus^{mde1500} allele serves as perfect model to investigate physiological and pathological functions of the PY-NLS domain of zebrafish Fus and human FUS. Furthermore, this patient like Fus mutation allows to study mechanisms of disease onset and pathology *in vivo*. Hence, heterozygous F1 generation fish were breed to homozygousity to further examine the Fus^{mde1500} protein.

6.3.2 Fus^{mde1500} protein characterization

To analyze Fus^{mde1500} protein in zebrafish, adequate antibodies had to be identified. The previously used Santa Cruz human FUS 4H11 (sc47711) antibody recognizes a non-specified C-terminal epitope, which might be deleted in Fus^{mde1500} protein. To test the suitablility of sc47711 antibody to detect Fus^{mde1500} protein, I cloned two reporter constructs fusing Fus^{wildtype} or Fus^{mde1500} protein to a GFP tag under the control of the cytomegalovirus (CMV) promotor (see Figure 6.8A). Next, HeLa cells were transfected with these constructs and cells were harvested, blotted and probed against either GFP or the sc47711 antibody. Both antibodies show similarly strong immunoreactivities with both Fus^{wildtype} or Fus^{mde1500} proteins, indicating that the antibody is still capable to detect Fus^{mde1500} protein (see Figure 6.8B). Thus, the epitope is not deleted due to the stop mutation and the antibody is suitable for detection of the truncated Fus^{mde1500} protein.

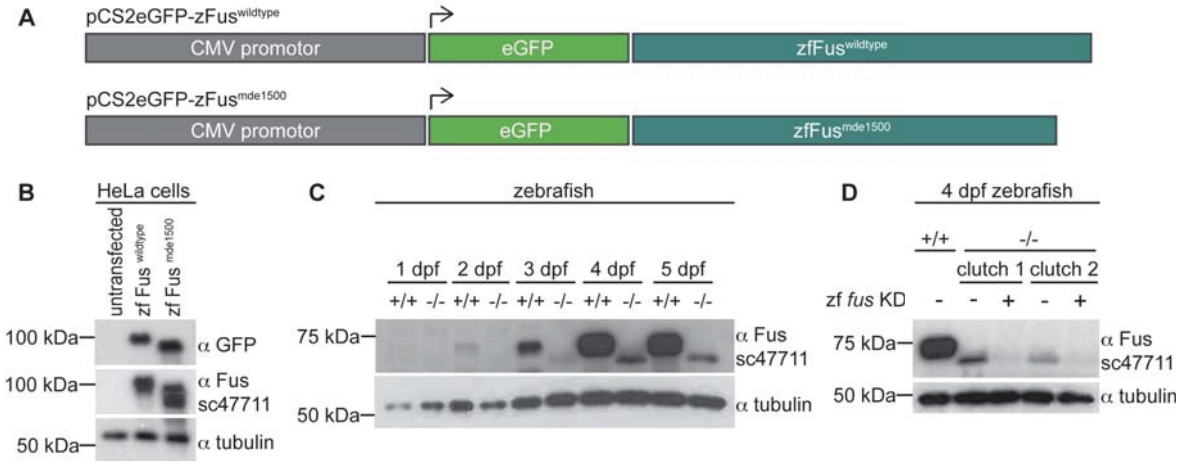

Figure 6.8: Fus^{mde1500} protein expression. **A** Schematic depiction of transgenic Fus constructs. Fus^{wildtype} and Fus^{mde1500} coding sequences (dark green) were cloned from mRNA derived cDNA pools of either wildtype or mutant fish and fused to GFP (light green). Expression in cell culture is driven by cytomegalovirus (CMV) promotors (grey). **B** Expression of transgenic Fus constructs in HeLa cells. Fus^{wildtype} and Fus^{mde1500} transfected HeLa cells derived samples were probed with GFP antibody and the zebrafish Fus specific sc47711 antibody. Both antibodies generate similar band intensities in Fus^{wildtype} and Fus^{mde1500} overexpressed samples. Due to the GFP-tag, Fus' molecular weight shifts from 75 kDa to approximately 100 kDa. **C** Fus^{mde1500} protein expression during development. Fus^{mde1500} protein is detectable in homozygous mutation carriers starting between 3 dpf and 4 dpf, whereas wildtype fish express Fus already from 2 dpf onwards. Note that Fus^{mde1500} protein runs below Fus^{wildtype} protein in the gel, thus is of smaller size. Moreover, wildtype bands appear much stronger than mutant bands, indicating different expression levels. **D** Confirmation of the Fus^{mde1500} protein band specificity via knockdown. Fus^{mde1500} protein expression was silenced in two independent clutches using *fus* ATG gripNA to confirm identity of the truncated immunoreactive band as the Fus^{mde1500} protein. Tubulin served as loading control in all blots depicted here. +/+ = wildtype, -/- = homozygous mutation carrier.

I tested Fus^{mde1500} protein expression at several stages during development including

1 dpf, 2 dpf, 3 dpf, 4 dpf, and 5 dpf in homozygous Fus^{mde1500} mutants. Fus^{mde1500} protein expression is detectable from 3 dpf on, whereas in wildtype siblings, Fus expression is evident already at 2 dpf (see Figure 6.8C). Moreover, mutant Fus^{mde1500} protein is expressed at lower levels compared to wildtype Fus protein. To confirm the identity of the immunoreative band in Fus^{mde1500} carriers to be the truncated mutant Fus protein, I further performed knockdown experiments using the previously established *fus* ATG gripNA in homozygous Fus^{mde1500} mutants. I examined Fus expression in two individual clutches of homozygous Fus^{mde1500} mutation carriers with and without *fus* knockdown and blotted samples together with a non treated wildtype control. In knockdown samples but not in buffer injected control samples the Fus^{mde1500} protein band is absent (see Figure 6.8D). Thus, in Fus^{mde1500} allele carriers mutant Fus protein is made and truncated, lacking the PY-NLS and the C-terminal half of the RGG3 domain.

6.3.3 Fus^{mde1500} allele expression profile

Characterization of the mutant Fus protein in larval zebrafish revealed reduced expression levels of the mutant Fus protein in Fus^{mde1500} allele carriers compared to Fus expression levels in wildtype siblings. To further investigate Fus^{mde1500} expression levels in zebrafish larvae and adult stages, I performed quantitative Western blot analysis. Homozygous and heterozygous Fus^{mde1500} allele carriers were analyzed together with the equivalent wildtype siblings at 4 dpf larval stages and brains were dissected from adult fish (see Figure 6.9A&C). Experiments were performed in six replicates of each genotype containing either 4 dpf larvae pools of six different clutches or six individual fish derived adult brain samples. Quantitative results from Western blots show a significant decrease in protein levels in homozygous Fus^{mde1500} allele carriers versus heterozygous Fus^{mde1500} allele carriers and wildtype siblings in both 4 dpf larvae and adult brain samples (see Figure 6.9B&D). Moreover, total Fus protein levels in heterozygous Fus^{mde1500} allele carriers are also decreased compared to wildtype siblings in 4 dpf larvae and adult brain samples, but not as severely as in homozygous Fus^{mde1500} carriers.

To test whether Fus^{mde1500} expression is already reduced at transcript levels, I further conducted quantitative reverse transcription PCR (qRT-PCR) experiments with 4 dpf larvae and adult brain samples (see Figure 6.9E&F). All experiments were performed with six replicates of each genotype for every sample. Also on transcript level, mutant *fus* is expressed at lower levels in homozygous carriers compared to heterozygous carriers and wildtype fish. Again, heterozygous Fus^{mde1500} allele carriers show also re-

duced amounts of mRNA, however the reduction is not as severe as in the homozygous Fus^{mde1500} allele carriers.

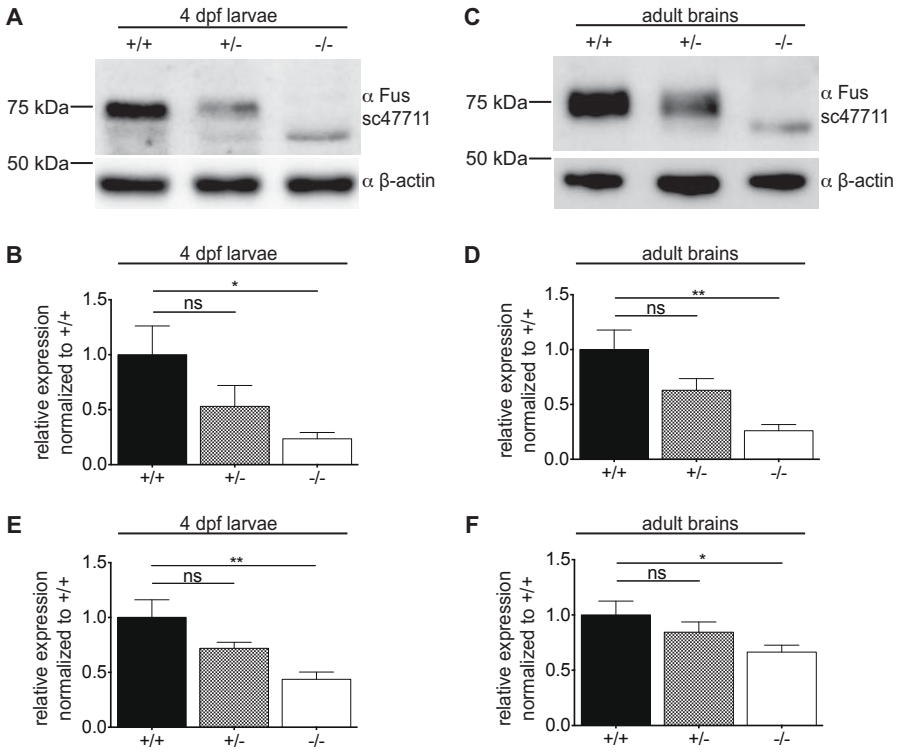

Figure 6.9: Fus^{mde1500}allele expression levels. A Western blot analysis of Fus^{mde1500} protein in 4 dpf larvae. sc47711 FUS antibody was used to analyze Fus^{mde1500} protein. Tubulin served as loading control. **B** Quantitative analysis of Western blots performed in 4 dpf larvae. **C** Western blot analysis of Fus^{mde1500} protein in adult brain samples. sc47711 FUS antibody was used to analyze Fus^{mde1500} protein, while tubulin served as loading control. **D** Quantitative analysis of Western blots performed with adult brain samples. **E** mRNA expression levels of the Fus^{mde1500} allele in 4 dpf larvae. **F** mRNA expression levels of the Fus^{mde1500} allele in adult brain samples. +/+ = wildtype, +/- = heterozygous mutation carrier, -/- = homozygous mutation carrier. n = 6. Mean + SEM. Statistical test used: Kruskal-Wallis test followed by Dunn's test to correct for multiple comparisons. * = 0.0304 in **B**, ** = 0.001 in **D**, ** = 0.0052 in **E**, * = 0.0491 in **F**. ns = not significant.

6.3.4 Fus^{mde1500} protein localization

To investigate whether lack of the PY-NLS and parts of the RGG3 domain influence nuclear import of the Fus protein, resulting in Fus protein redistribution to the cytosol, localization of the Fus^{mde1500} protein was analyzed *in situ*. Unfortunately, sc47711 antibody failed to specifically stain Fus protein in whole mount immunofluorescence experiments. Therefore, I cloned reporter constructs to express either Fus^{wildtype} or Fus^{mde1500} protein N-terminally fused to GFP under the control of the ubiquitin promotor. These constructs were injected into zebrafisch zygotes and immunoflurence stainings were performed at 1 dpf prior to analysis of protein expression and localization using confocal

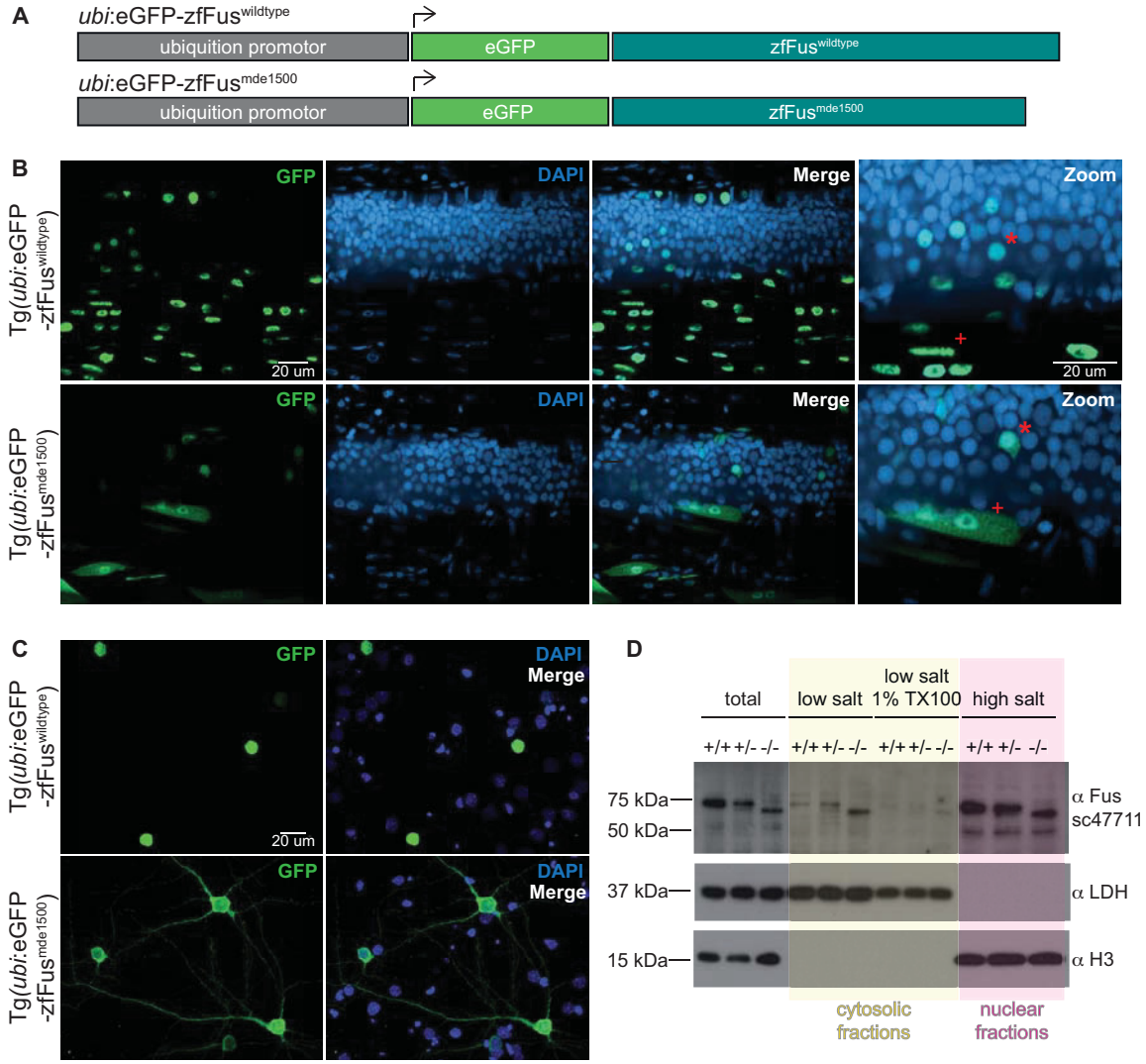

Figure 6.10: Fus^{mde1500} localization. **A** Schematic representation of Fus expression constructs. Fus coding sequences (dark green) are fused to GFP (light green) under the control of the ubiquitin promotor (grey). **B** Representative images of Fus^{wildtype} or Fus^{mde1500} protein expression in zebrafish. Fus proteins were re-stained using a GFP antibody against the N-terminal GFP-tag, DAPI staining allows visualization of nuclei. Areas of interest are additionally shown enlarged (Zoom). Red asterisks indicate neurons, red crosses indicate muscle cells. **C** Representative images of Fus^{wildtype} or Fus^{mde1500} protein expression in rat primary cortical neurons. Zebrafish Fus proteins were stained with a GFP antibody directed against the N-terminal GFP tag, DAPI served as nuclear marker. **D** Subcellular fractionation. Low salt buffer and low salt buffer with 1% TritonX100 (TX100) were used to extract cytoslic proteins, whereas high salt buffer was used to open up nuclei and extract nuclear proteins. Cytosolic and nuclear fractions are indicated in yellow and pink, respectively. LDH and H3 serves as reference markers for cytosolic and nuclear fractions, respectively. +/+ = wildtype, +/- = heterozygous mutation carrier, -/- = homozygous mutation carrier.

microscopy (see Figure 6.10A&B). Strikingly, mutant Fus protein is localized to nuclear and cytoplasmic cell compartments in spinal cord neurons and muscle cells, whereas wildtype Fus protein localization is restricted to nuclei (see Figure 6.10B). Similar experiments were performed in primary rat cortical neurons, resulting in strictly nuclear localization of wildtype zebrafish Fus protein, whereas mutant Fus protein is partially redistributed to the cytosol, thereby also staining soma and neurites (see Figure 6.10C). Thus, effects of the $Fus^{mde1500}$ mutation on Fus protein transport and localization is conserved between different species. To determine endogenous Fus protein localization, I analyzed homozygous and heterozygous $Fus^{mde1500}$ mutant zebrafish with the adequate wildtype controls in subcellular fractionation experiments. Samples were exposed to different salt concentrations and/or detergents containing buffers and proteins were extracted via ultracentrifugation prior to Western blotting of the different fractions. Fus protein distribution in the different fractions was examined using sc47711 antibody. Lactat dehydrogenase (LDH) and histone 3 (H3) were used to distinguish between cytosolic and nuclear fractions, respectively. Although general expression levels of the Fus protein in homozygous $Fus^{mde1500}$ carriers is already reduced within the total lysis sample prior to fractionation (total), more Fus protein is detected in cytosolic fractions derived from homozygous $Fus^{mde1500}$ carriers than in cytosolic fraction derived from heterozygous $Fus^{mde1500}$ carriers and wildtype fish. *Vice versa*, in nuclear fractions, less Fus protein is detected in homozygous $Fus^{mde1500}$ carriers derived samples compared to heterozygous $Fus^{mde1500}$ carriers and wildtype fish.
Thus, endogenously expressed mutant $Fus^{mde1500}$ protein as well as transgenic $Fus^{mde1500}$ protein shift from pure nuclear localization as seen in case of wildtype Fus to a more cytosolic localization.

6.3.5 $Fus^{mde1500}$ protein solubility properties

Biochemical analysis of the aggregated human FUS protein extracted from FTLD-FUS brain tissue revealed increased levels of insoluble FUS compared to healthy controls [38]. To biochemically characterize $Fus^{mde1500}$ protein in zebrafish, I performed sequential extraction from adult zebrafish brains, using buffers containing increasingly strong detergents or acids followed by Western blot analysis (see Figure 6.10A). Wildtype fish, homozygous and heterozygous $Fus^{mde1500}$ mutation carriers were sacrificed at $6, 9, 12, 15,$ and 24 months post fertilization (mpf) and Fus protein was sequentially extracted with high salt buffer, high salt buffer containing 1% of TritonX100 (TX100), radioimmunoprecipitation assay buffer (RIPA), RIPA containing 2% of sodiumdode-

cylsulfate (SDS) and formic acid (fractionation protocol adapted from [38]). Western blotting showed a strong mutant Fus protein band in the second fraction, containing low salt buffer with 1% of TritonX100 (TX100), that is also apparent in the heterozygous sample, although less intense. Remarkably, wildtype Fus is only detected in the first fraction, containing only high salt buffer without TX100. Thus, Fus^{mde1500} protein is less soluble than the wildtype Fus protein.

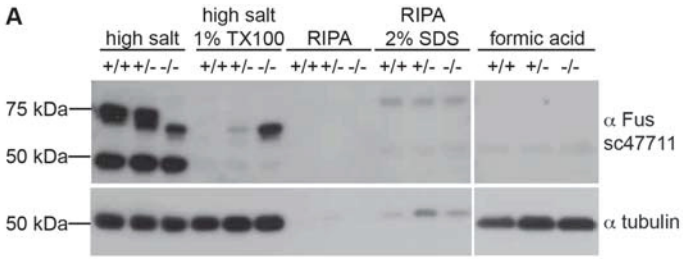

Figure 6.11: Differential fractionation of Fus^{mde1500} protein. A Representative blot of analyzed, 6 mpf old fish derived brains. 6, 9, 12, 15, and 24 mpf old adult brains of all three genotypes were examined. Solubility was determined via Western blotting of sequential fractionation with high salt buffer, high salt buffer containing 1% of TritonX100 (TX100), radioimmunoprecipitation assay buffer (RIPA), RIPA containing 2% of sodiumdodecylsulfate (SDS) and formic acid using sc47711 Fus antibody, whereas tubulin served as loading control. +/+ = wildtype, +/- = heterozygous mutation carrier, -/- = homozygous mutation carrier.

6.4 Consequences of Fus^{mde1500} mutation on Fus' function

6.4.1 Phenotypic analysis of Fus^{mde1500} mutant zebrafish

To analyze mutant Fus^{mde1500} zebrafish for ALS related deficits, I first examined morphological changes in ALS affected tissues, e.g. motor neurons, muscles and vessels. Due to the lateral projection of the caudal primary motor neuron axons from the spinal cord to innervated muscles in zebrafish, the analysis of motor neuron axon outgrowth and branching morphology has been used as readout for neuronal vulnerability [159], [110], [160], [170], [157] (besides others). Also muscle and vessel developmental phenotypes have been described in zebrafish [157]. Moreover, motor neurons degenerate in ALS and other motor neuron diseases leading to muscle atrophy [10]. Also dysfunctional circulation effects like hypoperfusion have been reported in some cases of ALS [171], [172]. Hence I analyzed CaP motor neuron axon outgrowth and branching morphology as well as muscle and vessel morphology in mutant Fus^{mde1500} embryos compared to wildtype fish (see Figure 6.12).

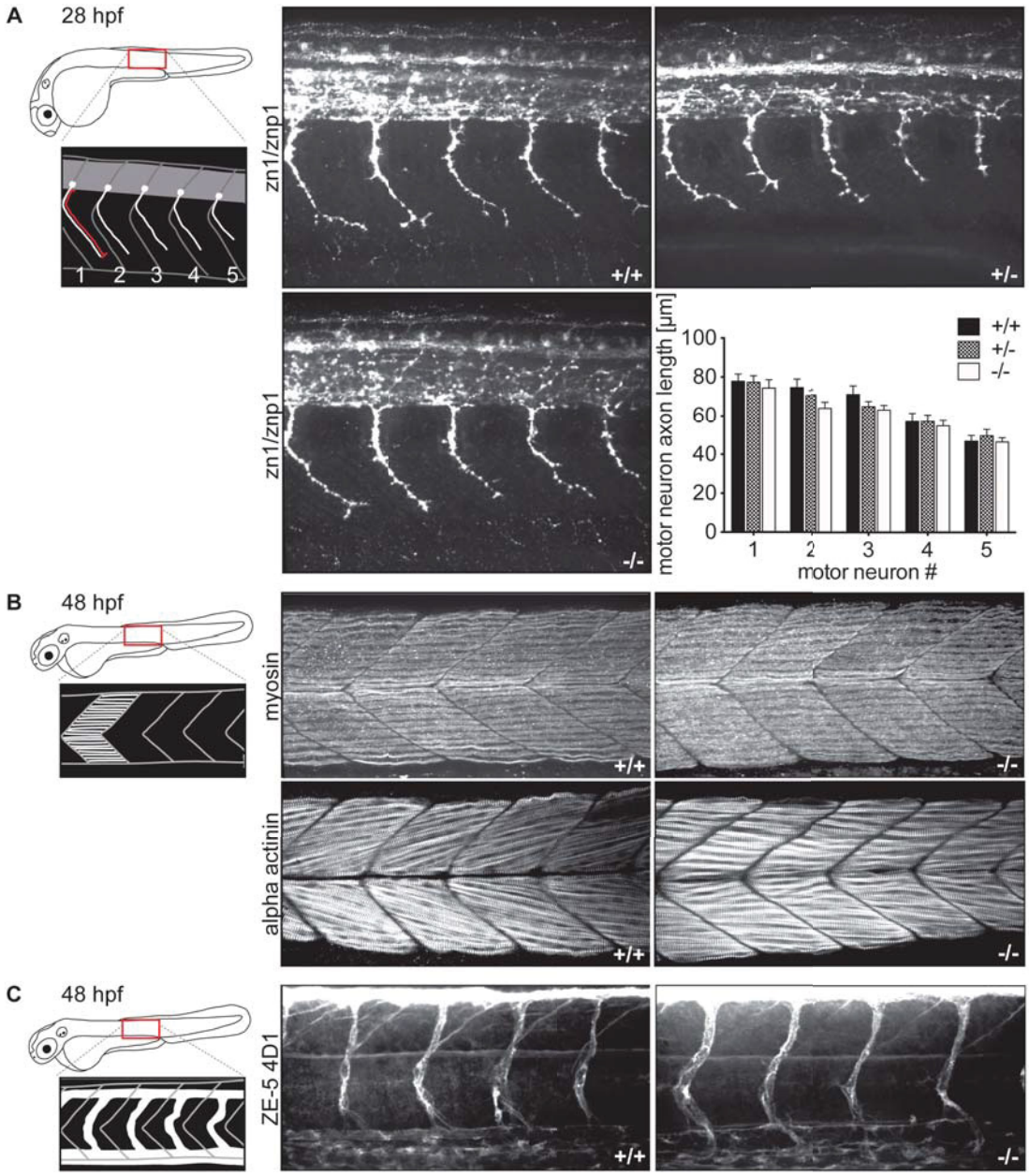

Figure 6.12: Phenotypical analysis of Fus^{mde1500} mutants. **A** Motor neuron axon outgrowth and length. Schematic illustration of assayed region, representative images of zn1/znp1 stained motor neurons and quantitative analysis of motor neuron axon length. The five most caudal motor neurons above the yolk sac extension were analyzed in all three genotypes at 28 dpf. n = 30 fish were analyzed per genotype derived from three different clutches. Mean + SEM. Statistical test used: Kruskal-Wallis test followed by Dunn's multiple comparisons test. No statistical significance was obtained (ns). **B** Schematic illustration of examined region and representative images of stained muscle tissue. Two different muscle marker were used: alpha actinin, staining Z-discs and myosin. **C** Schematic illustration of analyzed region and representative images of intersegmental vessels stained with the antibody ZE-5 4D1. +/+ = wildtype, +/- = heterozygous mutation carrier, -/- = homozygous mutation carrier.

Phenotypically, mutant Fus^{mde1500} embryos are indistinguishable from their wildtype siblings. Analysis of motor neuron axon outgrowth and morphology by immunofluorescent staining of primary spinal motor neurons using zn1/znp1 antibodies and measurements of axonal length yield no significant difference in axonal outgrowth and branching between homozygous and heterozygous Fus^{mde1500} mutant embryos and wildtype siblings (see Figure 6.12A).
Next, I tested for correct muscle and vessel development via immunofluorecent staining of specific muscle and vessel marker proteins and subsequent analysis of morphological features in homozygous mutant Fus^{mde1500} embryos compared to age-matched wildtype siblings. Interestingly, neither the complex development of muscle structures nor vessel patterning is affected by the Fus^{mde1500} mutation (see Figure 6.12B&C).

6.4.2 Motor function in Fus^{mde1500} mutant zebrafish

In ALS patients muscle atrophy due to motor neuron degeneration leads to motor dysfunction and paralysis or spasticity [10]. To test for potential motor deficits upon Fus^{mde1500} mutation, I analyzed swimming behavior of mutant versus wildtype larvae. Zebrafish embryos and larvae have been shown to respond to cycles of light/dark stimuli with changes in locomotion behavior, i.e. speed, duration and directionality of swimming [173], [174], [175]. Hence, I utilized the so called photo-motor response (PMR) as a readout for motor function in zebrafish. Briefly, 4 dpf larvae in 24 well plates were subjected to alternating light/dark cycles and motion was traced by a video tracking device, and subsequently analyzed for parameters of swimming behavior, in particular distance, duration and velocity (see Figure 6.13). To avoid inter-clutch variations in development, that might influence swimming behavior, only siblings from the same clutch were compared. 4 dpf larvae derived from incrossed heterozygous Fus^{mde1500} allele carriers resulting three genotypes, homozygous Fus^{mde1500} mutants, heterozygous Fus^{mde1500} mutants and wildtype fish. In total, three clutches were analyzed with at least 10 larvae per genotype per clutch. After a 60 min light adaptation phase, spontaneous movement was traced during baseline recordings and during alternating cycles of 15 min of darkness stimulus and 15 min of no stimulus light phase (see Figure 6.13A). Upon darkness stimuli, zebrafish movement is strongly increased in all three genotypes, but no significant differences were observed when distance, duration and velocity parameters were compared between homozygous Fus^{mde1500} mutants, heterozygous Fus^{mde1500} mutants and wildtypes (see Figure 6.13B-E).

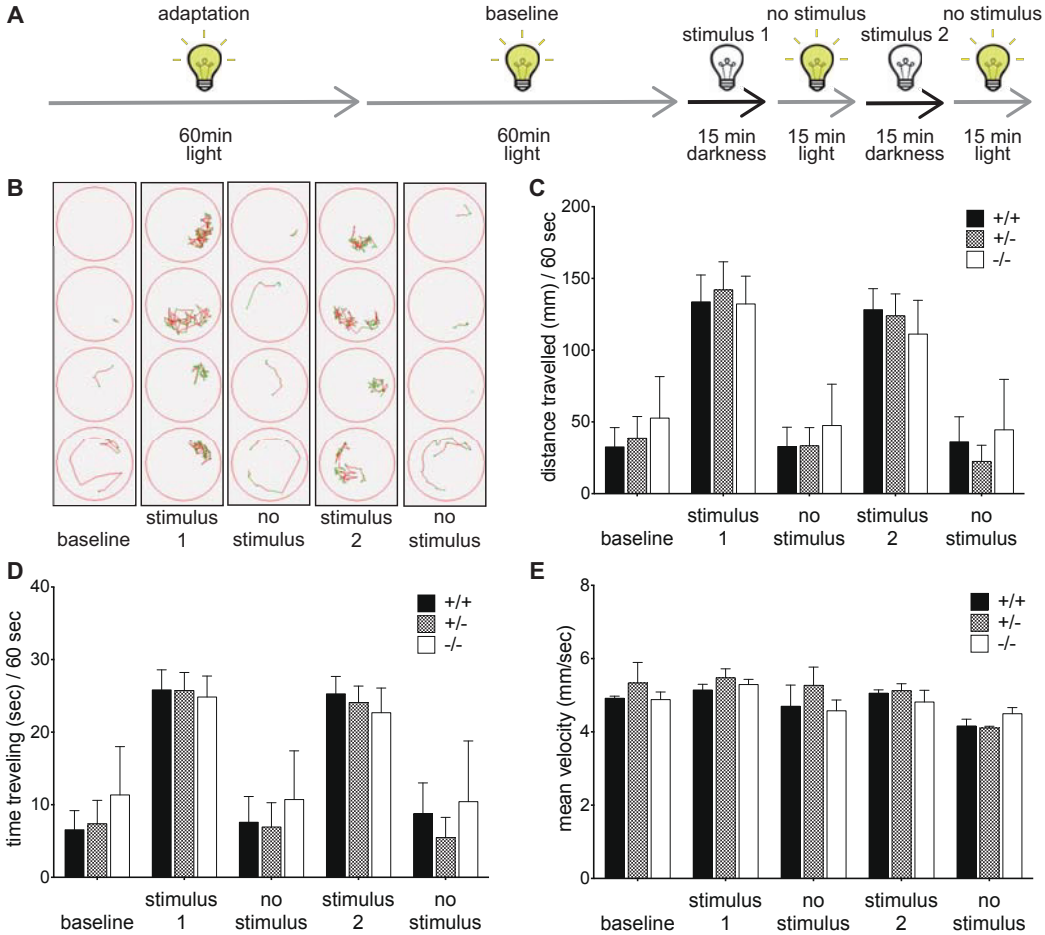

Figure 6.13: Photomotor response in Fus^{mde1500} mutants. A Schematic illustration of the experimental setup and alternating light/dark cycles. **B** Representative recordings of larval movement tracking. Fast swimming (> 8mm/sec) is depicted in red traces, slow swimming (2 - 8mm/sec) in green, swimming velocity of < 2 mm/sec is considered as resting. **C** Travelled distance per 60 sec plotted for all three genotypes. **D** Time spend with travelling per 60 sec plotted for all three genotypes. **E** Calculated mean velocity plotted for all three genotypes. +/+ = wildtype, +/- = heterozygous mutation carrier, -/- = homozygous mutation carrier. n = 3 independent experiments with 48 embryos each were performed. Mean + SEM. Statistical test used: 2way ANOVA test followed by Dunnett's multiple comparisons test. No statistical significance was obtained (ns).

6.4.3 Stress response in Fus^{mde1500} mutant zebrafish

Macroscopic analysis of Fus^{mde1500} mutant zebrafish revealed no obvious phenotype that would imply a deficit in Fus' function upon Fus^{mde1500} mutation. Potentially, the mutation in the *fus* gene as one event is not enough to impair Fus' function and to elicit a phenotype, indicating that a functional defect due to the mutation is only detectible upon additional challenges. This hypothesis is currently being discussed as potential pathomechanisms in ALS patients, with the mutation being the '1st hit' and a challenging condition, e.g. environmental or cellular stress being the '2nd hit' [73], [37]. To test whether stress can elicit ALS related phenotypes in Fus^{mde1500} mutant zebrafish, I

analyzed Fus^{mde1500} mutant zebrafish under different stress conditions.
Heat shock has successfully been used as a stressor to elicit stress response in cell culture, including stress granule formation as a potential requirement for pathologic inclusion formation [176]. I tested several heat shock conditions in zebrafish and used increased expression of heat shock protein (HSP) 70 and HSP 40 as a readout for successful heat shock (see Figure 6.14A). Incubation of 4 dpf larvae in 38°C for 20 h is the maximum length of tolerated stress and was chosen as heat shock condition in further experiments.
Glutamate mediated excitotoxicity caused by over-stimulation of the glutamate receptors is one pathological feature of ALS and thought to play a role in ALS pathogenesis [177]. To elicit excitotoxicity in zebrafish as an internal stressor I used pentylentetrazole (PTZ), shown in zebrafish to induce seizure-like convulsion behaviour, [168] caused by neuronal hyperactivity due to dishinhibition of excitatory neurons. I tested several concentrations and incubation periods of PTZ and established 5 mM PTZ treatment for 72 h as condition to induce convulsions (see Figure 6.14B).
After having established heat shock and excitotoxicity as stressors, response to these stressors was examined in Fus^{mde1500} mutation carriers. As a readout for increased susceptibility towards stress, apoptosis in the spinal cord was analyzed via TdT-mediated dUTP-biotin nick end labeling (TUNEL) staining of treated and fixated fish. TUNEL staining allows to identify apoptotic cells via labelling of fragmented DNA during apoptosis. TUNEL stained fish were imaged and apoptotic cells were counted in a defined spinal cord region above the yolk sac extension (see Figure 6.14C). For responses to heat shock 3 dpf larvae were treated with 38°C for 20h and fixated at 4 dpf. PTZ treated fish were incubated in 5 mM PTZ for 72h starting at 1 dpf and fixated at 4 dpf. Absolute numbers of apoptotic cells were plotted in both stress conditions (see Figure 6.14D). Moreover, ratios of stress induced apoptosis to baseline apoptosis levels were calculated for both stressors (see Figure 6.14E). In PTZ treated as well as in heat shocked fish no significant differences in numbers of apoptotic neurons were detected comparing Fus^{mde1500} mutation carriers to wildtype fish.
To explore the possibility that Fus^{mde1500} mutant zebrafish have an impaired stress response or show elevated stress levels already under baseline conditions, I examined molecular markers of stress response in Fus^{mde1500} mutant zebrafish. Eukaryotic translation initiation factor 2α (eiF2α) gets phosphorylated upon stress, thereby inhibiting translation and triggering stress granule formation [178]. I analyzed phosphorylated eiF2α levels in heat shocked Fus^{mde1500} mutant zebrafish and wildtype fish in comparison to non treated controls (see Figure 6.14E). Increased HSP70 and HSP90 expression

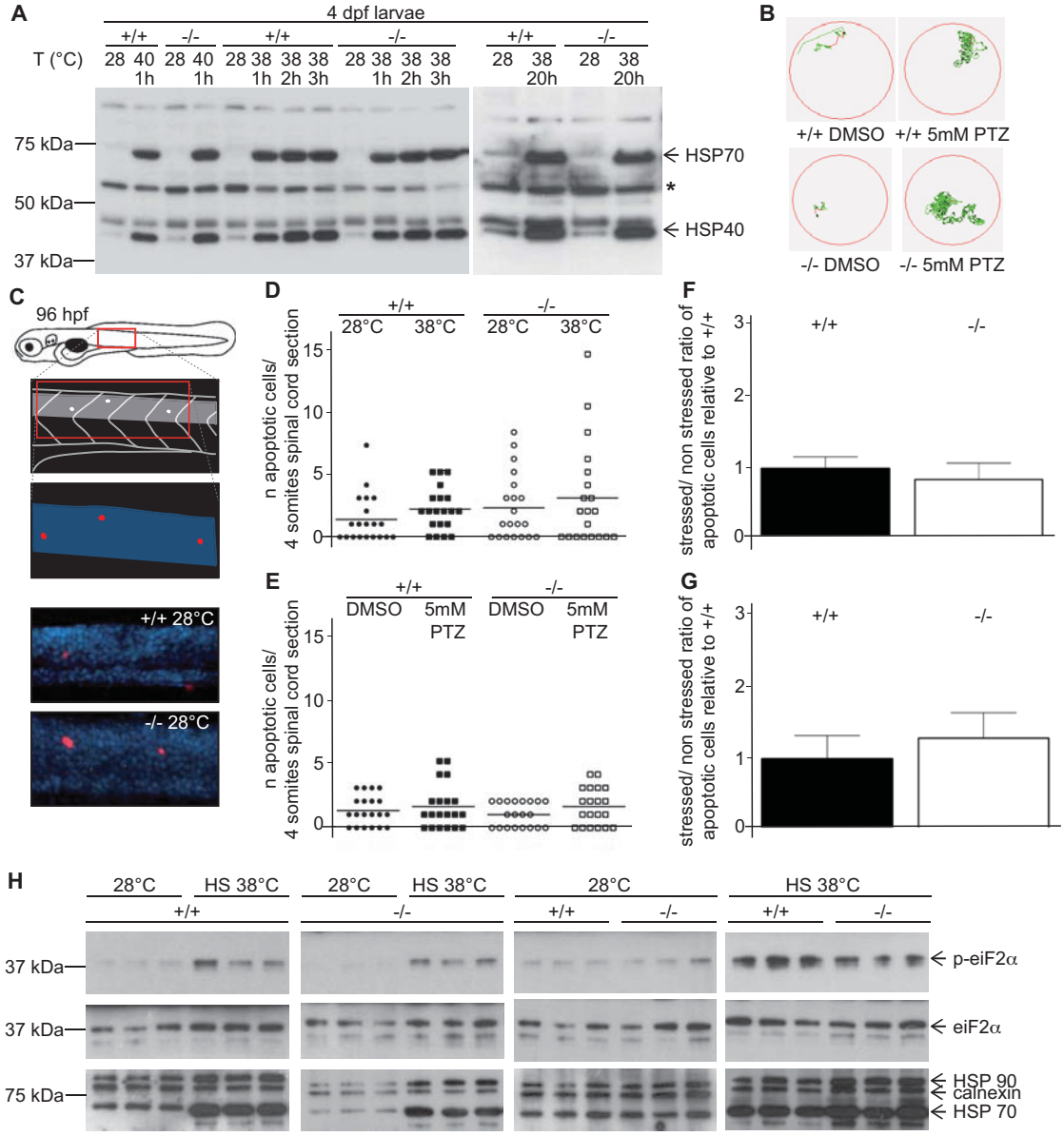

Figure 6.14: Examination of stress responses in Fus^{mde1500} mutants. **A** Establishing heat shock conditions. Several temperatures and incubation periods were tested in wildtypes and Fus^{mde1500} mutants. Elevated HSP70 and HSP40 expression levels served as readout. The unspecific band (asterisk) serves as internal loading control. **B** Establishing excitotoxicity conditions. With 5 mM PTZ for 72 h treated Fus^{mde1500} mutants and wildtypes were screened for seizure-like convulsions. **C** Schematic illustration of analyzed region. The four most caudal somites towards the yolk sac extension end were analyzed for apoptotic cell in the spinal cord, visualized by the high density of DAPI stained nuclei. **D** Absolute numbers of apoptotic cells for heat shock stress conditions. TUNEL positive nuclei were counted after staining and image aquisition. **E** Absolute numbers of apoptotic cells for excitotoxicity stress conditions. TUNEL positive nuclei were counted after staining and image aquisition. **F** Numbers of apoptotic cells after heat shock relative to spontaneous apoptosis during baseline. Ratio of stressed to non stressed number of apoptotic cells was calculated and plotted. **G** Numbers of apoptotic cells after excitotoxicity stress relative to spontaneous apoptosis during baseline. Ratio of stressed to non stressed number of apoptotic cells was calculated and plotted. **H** Molecular markers of stress response. Total eiF2α and phosphorylated eiF2α levels were analyzed by Western blotting using antibodies against phosphorylated eiF2α (p-eiF2α) in comparison to total eiF2α (eiF2α). Antibodies against HSP90 and HSP70 were used to confirm heat shock response, calnexin served as loading control. +/+ = wildtype, -/- = homozygous mutation carrier. n = 20 fish of each genotype and condition. Mean + SEM. Statistical test used: Kruskal-Wallis test followed by Dunn's multiple comparisons test in **D** and **E**, unpaired T-test in **F** and **G**. No statistical significance was obtained (ns).

levels upon heat shock indicate stress response in all samples examined. Also, increased phosphorylation levels of eiF2α were obtained in all samples upon heat shock, indicating that Fus^{mde1500} mutant and wildtype fish respond to stress in a similar manner. Similarly, total eiF2α levels were comparable in all samples. Interestingly, no changes in phosphorylated eiF2α levels were detectible under baseline conditions when comparing Fus^{mde1500} mutant and wildtype fish. Thus, Fus^{mde1500} mutant zebrafish show neither altered stress response upon heat shock and excitotoxic stress nor elevated stress levels under baseline conditions in comparison to wildtypes.

6.4.4 Fus^{mde1500} protein splicing function

To determine potential impacts of the Fus^{mde1500} mutation on Fus' function on a molecular level, I analyzed whether mutant Fus^{mde1500} protein maintains its splicing function. FUS protein is known to play a role in direct binding and splicing of various mRNA transcripts in mammals [94]. I analyzed splicing effects of the mutant Fus^{mde1500} pro-

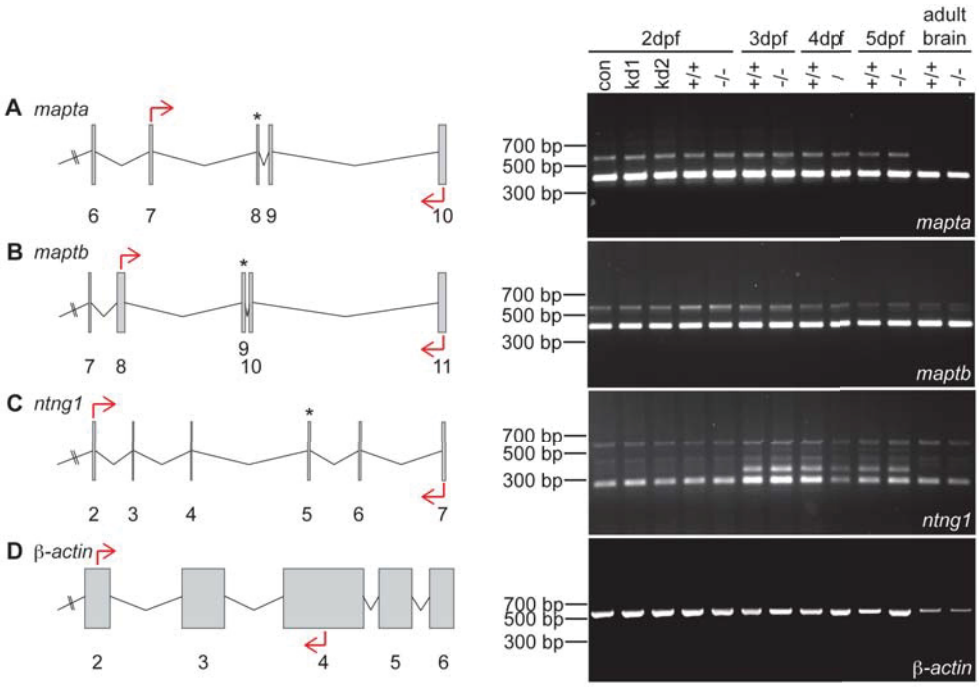

Figure 6.15: Splicing function of Fus^{mde1500} protein. **A** Splicing analysis of *mapta* transcript. **B** Splicing analysis of *maptb* transcript. **C** Splicing analysis of *ntng1* transcript. **D** Splicing analysis of β-*actin* transcript. Grey bars represent exons, asterisks display alternatively spliced exons in mice, and red arrows indicate position of PCR primers. con = buffer injected control for *fus* knockdowns, kd1 = *fus* knockdown using ATG gripNA, kd2 = *fus* knockdown using splice site gripNA, +/+ = wildtype, -/- = homozygous mutation carrier.

tein on *MAPT* and *Netrin G1 (Ntng1)*, two Fus target mRNAs that were found to be alternatively spliced upon silencing of murine *Fus*. Moreover, affected exons in these

target RNAs are conserved in zebrafish. Murine *Ntng1* has only one orthologue in zebrafish, *ntng1*, whereas two orthologues for *Mapt*, *mapta* and *maptb* exist. I analyzed all three potential target RNAs together with β-*actin* as a control transcript. I performed semi-quantitative reverse transcription PCR (RT-PCR) with homozygous Fus^{mde1500} mutants and wildtype control fish in comparison to gripNA mediated transient *fus* knockdown at several stages of development and analyzed PCR products via agarose gel electrophoresis (see Figure 6.15).
Interestingly, no alternatively spliced RNA molecules were detected in stable genetic mutants or upon transient silencing of *fus*, indicated by the lack of alternative PCR products after agarose gel electrophoresis in all candidate zebrafish Fus target mRNAs examined here. Thus, zebrafish *fus* splicing targets might differ from those identified in mouse or might be affected only in specific tissues or at specific time points.

6.4.5 Immunohistochemical examination in Fus^{mde1500} mutant zebrafish

After phenotypic, functional and molecular analysis of Fus^{mde1500} mutant zebrafish no defects indicating a compromised Fus function due to the Fus^{mde1500} mutation are evident. I next conducted immunhistochemistry (IHC) in Fus^{mde1500} mutant zebrafish to investigate protein mislocalization and inclusion formation. First, IHC-suitable antibodies had to be established. To test cross-reactivity and specificity of available antibodies targeting human or murine FUS, I used gripNA mediated *fus* knockdown. Briefly, I injected two different *fus* gripNAs, *fus* splice gripNA and *fus* ATG gripNA, into zebrafish zygotes prior to fixation of embryos with paraformaldehyde and embedding in paraffin at 2 dpf. 2-5 µm thin sections were sliced off the paraffin blocks using a microtome. Sections were then mounted on glass slides, dehydrated and cleared by xylene treatment followed by antigen retrieval and incubation with first and secondary antibodies. Antigen-antibody interaction is visualized by an indirect IHC reporter e.g. the herein used 3,3'-diaminobenzidine (DAB).
Unfortunately, none of the commercially available antibodies, including sc47711, specifically stained zebrafish Fus protein in IHC. Hence, zebrafish Fus specific antibodies were generated with the selected peptide derived epitopes localized to the N-terminal part of the Fus protein, thereby allowing the resulting antibody to detect both, wildtype and truncated mutant Fus protein (see Figure 6.16A). Antibodies were generated by immunization of mice with the zebrafish specific Fus peptides and antibodies producing lymphocytes were isolated from immunized animals and fused with myeloma cells,

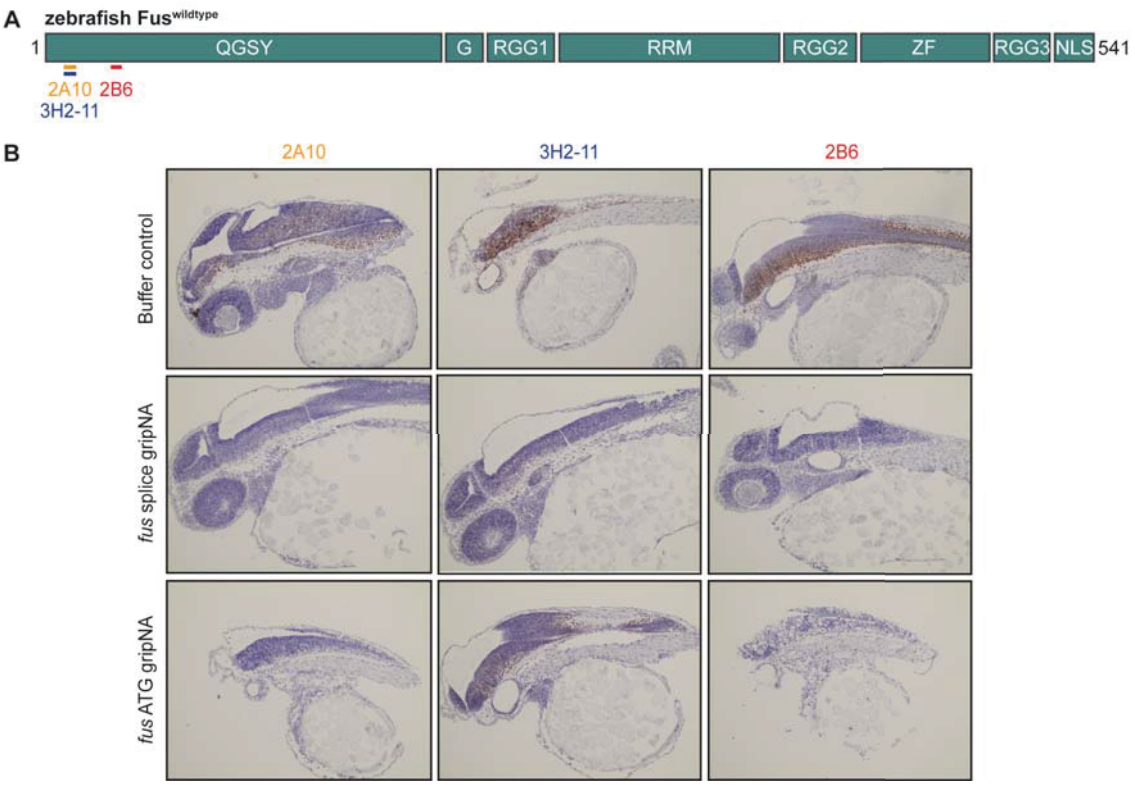

Figure 6.16: Identification of IHC suitable zebrafish Fus specific antibodies. A. Schematic illustration of epitopes of zebrafish Fus peptide antibodies. **B**. Specificity of zebrafish Fus peptide antibodies tested in IHC experiments. Reduction or lack of Fus immunoreactivity due to *fus* knockdown, indicated by DAB staining (brown) served as readout for antibody specificity. Haematoxylin staining (blue) allows for visualization of nuclei. Similar regions of the stained embryos including head and yolk were imaged and orientated with the rostral end to the left, caudal end to the right.

yielding hybridomas. Hybridoma cells were cultured and polyclonal supernatant was tested for epitope specificity, prior to isolating single hybridoma cell clones, yielding monoclonal supernatants. Generation of antibodies was outsourced to the Core Facility Monoclonal Antibodies, Institute for Molecular Immunology, Helmholtz Center Munich. I tested specificity of polyclonal pools and monoclonal supernatants in IHC and identified two pools, 2A10 and 2B6, and one monoclonal supernatant, 3H2-11 to show a positive IHC staining in buffer injected embryos but a reduced or no signal in gripNA mediated *fus* knockdown embryos (see Figure 6.16B).

After successfully establishing IHC-suitable Fus antibodies, I conducted IHC experiments to screen mutant Fus^{mde1500} zebrafish for pathological changes of Fus. Adult homozygous and heterozygous Fus^{mde1500} mutation carriers together with wildtype control fish were sacrificed, brains were dissected and subjected to IHC. All analyzed individuals were age matched siblings and stained with the three zebrafish specific Fus antibodies 3H2-11, 2B6 and 2A10 (see Figure 6.17A). To also include spinal cord tissue in IHC experiments, whole truncs of adult homozygous and heterozygous Fus^{mde1500}

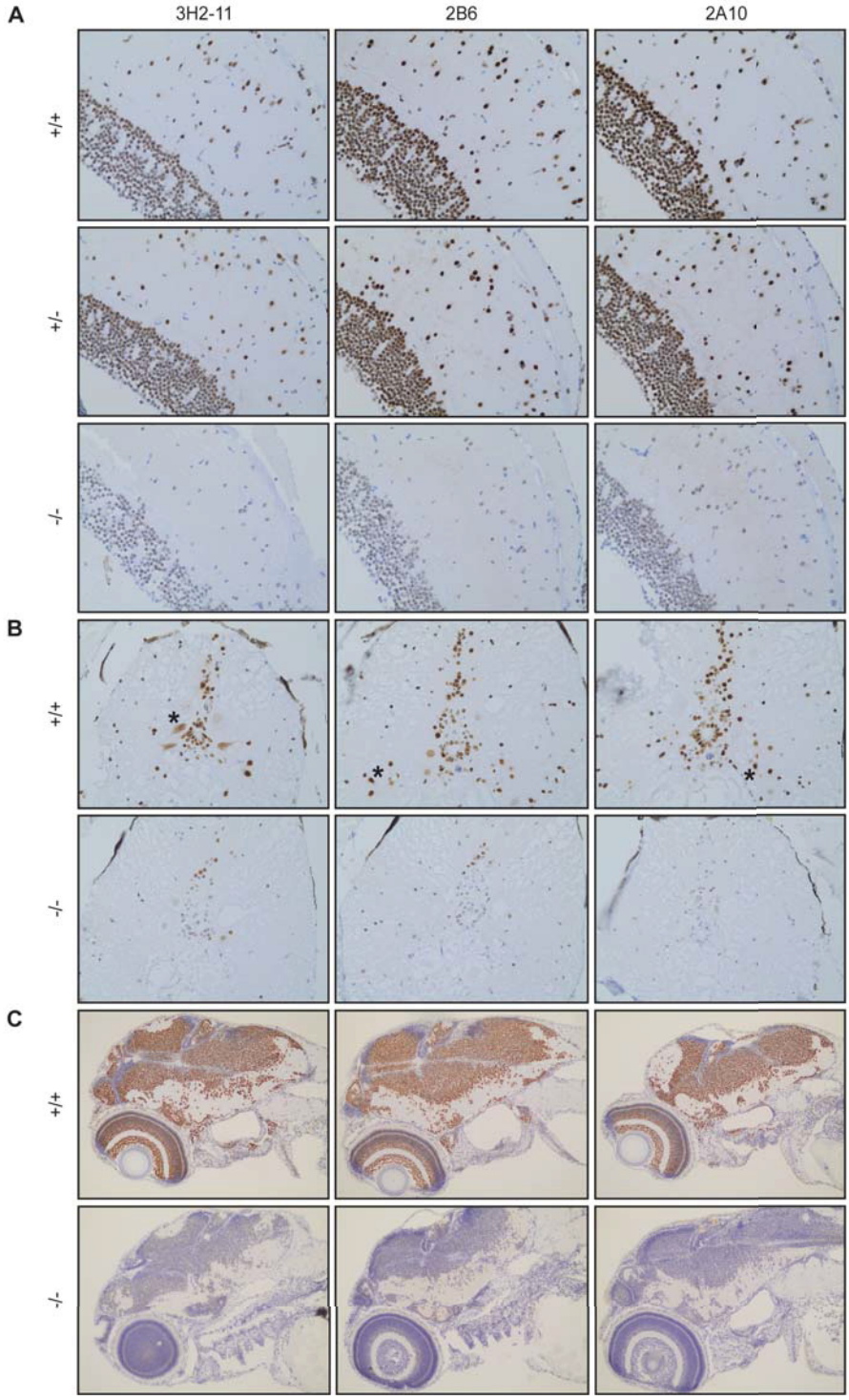

Figure 6.17: IHC in Fus^{mde1500} mutant zebrafish. **A** Immunohistochemical staining of adult brain sections. Representative pictures taken from the optical tectum. **B** Immunohistochemical staining of adult spinal cord sections. Neurons and glial cells were stained with all three zebrafish specific Fus antibodies, yielding some cells with a cytosolic staining (asterisks) besides the nuclear signal seen in all tissues. **C** Immunohistochemical staining of 4 dpf old larvae. Fus staining is strongly reduced in homozygous Fus^{mde1500} mutants. +/+ = wildtype, +/- = heterozygous mutation carrier, -/- = homozygous mutation carrier. Fus staining indicated by DAB reporter in brown, nuclear counterstaining with haematoxylin in blue.

mutation carriers together with wildtype control fish were fixated, embedded in paraffin and sectioned prior to staining with 3H2-11, 2B6 and 2A10 antibodies (see Figure 6.17B). Again only siblings were compared in these experiments. Additionally, 4 dpf old embryos were examined for pathological changes with 3H2-11, 2B6 and 2A10 antibodies (see Figure 6.17C).

Strikingly, Fus staining is mainly nuclear in wildtype as well as in Fus^{mde1500} mutant fish, although the staining intensity is weaker in homozygous than in heterozygous Fus^{mde1500} mutants and wildtype fish. This effect is observed with all of the three antibodies used and in all tissues (adult brains, adult spinal cords and whole larvae) analyzed. Interestingly, some cells show a cytosolic Fus staining in spinal cord sections, however, the effect is stronger in wildtype than in mutant fish, where a general reduction of Fus protein levels is more prominent than a shift of Fus protein to the cytosol. However, neuropil stainings in homozygous Fus^{mde1500} mutants show slight Fus positive signals, indicating a small fraction of Fus^{mde1500} protein in cytosolic compartments. Similar to adult brains, mutant Fus^{mde1500} protein is strongly reduced in 4 dpf old larvae, resulting in a weaker staining than in wildtype fish. Apart from this finding, no differences, e.g. inclusion formation of mutant Fus^{mde1500} protein was observed in all tissues examined. Thus, no complete redistribution of the Fus^{mde1500} protein was detected, despite lack of the PY-NLS and the C-terminal part of the RGG3 domain.

7 Discussion

7.1 Evolutionary conservation of *FUS* function

Comprehensive blast searches revealed one orthologue of the *FUS* gene in members of the vertebrate subphylum, including human *FUS*, rat *Fus*, mouse *Fus*, *Xenopus fus* and zebrafish *fus*, despite a genome duplication within the teleostei infraclass, resulting in approximately 2.28 zebrafish orthologues for each human gene [115]. Conservation of the human FUS protein ranges from 90% in rats to remarkable 60% in zebrafish. In contrast, the *Drosophila* orthologue Cabeza shows only 30% homology with the human FUS protein. Thus, the *FUS* gene is highly conserved through evolution, especially within the subphylum of vertebrates. Zebrafish Fus protein with 541 amino acids is similar to the 526 amino acid long human FUS protein and shares the same protein domains. Interestingly, the C-terminal half of the protein is highly homologous, harboring RNA/DNA-binding properties and protein interaction domains, indicating conserved functions. In particular the NLS and RGG3 domain show high levels of homology and most of the amino acids affected by fALS associated mutations in the NLS and RGG3 domain are conserved making the zebrafish an excellent model to study disease pathogenesis and effects of ALS causing mutations on *FUS*' function *in vivo*.
Moreover, FET protein family members beside FUS, namely EWS and TAF15 are conserved in vertebrates but not in invertebrates. In zebrafish human *EWS* and *TAF15* orthologues are encoded by the zebrafish genes *ewsr1a* and *ewsr1b* and *taf15*, respectively. Due to the similarities of FET family members regarding domain structure and protein function, e.g. DNA damage response, transcriptional regulation, and mRNA splicing [37], [179], potential redundant functions and compensation capacities cannot be ruled out.

7.2 Potential zebrafish *fus* functions during oogenesis

in situ hybridization (see subsection 6.1.2) revealed that *fus* mRNA can be detected as early as at 4 cell stage, indicating that *fus* mRNA is maternally deposited in the

oocyte, since embryonic transcription is absent until completion of maternal to zygotic transition (MZT). MZT is a phase in embryonic development during which developmental control is successively shifted from the maternal to the zygotic transcriptome at approximately 4.3 hpf prior to gastrulation [180]. Interestingly, spatiotemporal control of mRNA localization during oogenesis and early embryogenesis are known to mediate cell polarity and embryonic organization and patterning [181], [182], thus determining cell fate [183]. Importantly, other polarized cell types like neurons also depend on selective mRNA localization and translation [181], indicating that RNA localization represents a fundamental mechanism for spatial regulation of gene expression in a variety of tissues [181], [182].

Localization of RNAs is known to be mediated by RNA/protein structures comprised as ribonuclearprotein complexes (RNPs). Heterogeneous nuclear ribonucleoprotein complexes (hnRNPs) are predominantly nuclear RNP structures, consisting of heterogeneous nuclear RNAs and heterogeneous ribonuclear proteins [186] and important for various steps during RNA metabolism and maturation besides RNA stability, storage, and localization [185], [187]. FUS belongs to the family of hnRNP proteins and was initially referred to as hnRNP P2 protein [84]. Moreover, FUS protein is known to mediate local translation by transport of specific mRNAs to their site of action [190]. Together with FUS' RNA-binding properties and hnRNP protein characteristics, this suggest crucial functions of FUS in RNA metabolism [76], [60], [69], [100]. Interestingly, several hnRNP proteins have been identified to be associated with ALS through the identification of pathogenic mutations [188] and inclusion formation [189], indicating that RNA localization and metabolism is a central component in neurons in general and in motor neurons in particular.

Interestingly, hnRNP proteins in oocytes and spermatocytes mediate crucial functions during germ cell development [?], [?], [?], [?], [?], [?], [?], indicating that RNA localization in germ cells also depends on hnRNP complexes. Thus, the presence of zebrafish *fus* mRNA in oocytes suggests important Fus protein function during germ cell development.

Remarkably, *fus*' functions are not required during early embryonic development, since transient gripNA-mediated knockdown *fus* does not result in an obvious phenotype. In line with this finding, Fus protein levels are only detectable from 15 somites - 24 hpf on, although that does not rule out that Fus protein levels might be below detection level at earlier time points. Also in later stages of development, Fus protein is widely expressed, implying important RNA binding functions in several cell types and undermining the importance of an whole organism approach. In particular, high *fus*

mRNA and Fus protein abundancy in brain and spinal cord evidenced by ISH, IHC, and Western blot analysis indicate important functions in neuronal tissue. In line with this finding, mutations in the human *FUS* gene cause the neurodegenerative disease ALS.

7.3 ZFN-mediated genomic targeting of *fus*

To generate ALS reminiscent mutations within the *fus* locus, the second last exon (exon 14) was chosen as ZFN target site since this region encodes the C-terminal NLS and RGG3 domain, where most of the fALS mutations are clustered. Unfortunately, ZFN directed against early exons (exon 2 and 3) turned out be non-functional. After targeting the zebrafish *fus* locus with ZFNs and subsequent genotyping of induced alleles, only inframe and no frameshift mutations were identified in the F1 generation. In contrast, reading frame disrupting frameshift mutations do occur in mosaic P0 generation fish (see Figure 6.6), demonstrating that genomic editing leading to frame shift mutations is feasible at the zebrafish *fus* locus. However, frameshift mutations were not transmitted through the germline, indicating a selection against frameshift mutations. Identified inframe mutations result in loss of single amino acids or in case of $Fus^{mde1500}$ in deletion of the complete C-terminal NLS and parts of the RGG3 domain but maintain the original reading frame, whereas frameshift mutations lead to a reading frame shift, thereby generating additional amino acid sequences followed by a random stop codon. Usually these frameshift mutations are thought to mediate loss of function due to nonsense mediated RNA decay induced by the premature stop codon [191]. In case of the zebrafish *fus* locus, also a stabilization of the random sequences is plausible due to the location of the target site in the second last exon. After translation, the resulting aberrant amino acid sequence might act in a dominant-negativ manner and convey toxicity by aberrant interaction with crucial factors during germ cell development on RNA and/or protein level.

Potentially, depletion of *fus* via RNA decay or toxic gain of function might interfere with crucial *fus*' functions during DNA repair and genomic stability. Therefore *fus* frameshift mutations might not be compatible with proper germ cell development, especially during haploid stages of germ cell development with no wildtype *fus* allele to compensate. Thus, frameshift mutations in *fus* mediated by ZFN targeting of exon 14 are potentially toxic during germ cell development and only non-toxic mutations were selected for after crossing P0 generation fish and analysis of mutant alleles in the F1 generation. Interestingly, no gender specificity was observed when analyzing

germline transmittability of frameshift mutations in *fus*, indicating that *fus*' functions are essential in both oocytes and sperm cells. In line with this finding, defects in spermatogenesis have been reported upon depletion of murine *FUS* [79]. No zebrafish Fus protein was detectible in testes, which possibly is due to limited sensitivity of the antibody.
Disruption of the *Fus* gene in mice by gene entrapment has been reported to be feasible, and mutant alleles are transmitted through the germline [78], [79], even though ZFN induced mutagenesis targeting exon 14 of the *fus* locus yielded neither frameshift mutations nor complete loss of *fus* function. The genomic target side seems to be crucial for the efficiency of Fus depletion since targeting of exon 8 of the murine *Fus* yields a complete knockout [79], whereas targeting of exon 12 of the murine *Fus* results in low levels of truncated *Fus* RNA and FUS protein [78], similar to the RNA and protein expression levels of the mutant $\text{Fus}^{\text{mde1500}}$ allele. Potentially, a target site upstream of exon 14 in the zebrafish *fus* might also result in a more efficient disruption of *fus*, possibly resulting in germ line transmittable *fus* loss of function alleles.

7.4 Why do $\text{Fus}^{\text{mde1500}}$ mutant zebrafish reveal no motor neuron phenotype?

$\text{Fus}^{\text{mde1500}}$ mutant zebrafish show no motor neuron axon outgrowth defects evidenced by analysis of morphology and quantification of CaP motor neuron axon length (see subsection 6.4.1). Although expression levels are reduced, nuclear amounts of the mutant $\text{Fus}^{\text{mde1500}}$ protein might be sufficient to maintain *fus*' functions, thereby impeding manifestation of a phenotype. Published phenotypes upon Morpholino (MO)-mediated transient FUS knockdown in zebrafish describe motor neuron deficits, including shortened and hyperbranched primary spinal motor neuron axons [110]. However, in *fus* gripNA-mediated knockdown embryos completely depleted of Fus, I detected no defects in CaP motor neuron axon outgrowth abnormalities (see subsection 6.1.3), indicating that reduced levels of Fus are not sufficient to cause developmental motor neuron axon phenotypes. Moreover, assaying motility in $\text{Fus}^{\text{mde1500}}$ mutants (see subsection 6.4.2) revealed no compromised motor function concerning distance, duration and velocity of swimming, reflecting no motor neuron dysfunction consistent with intact motor neuron morphology. These findings indicate that *fus*' function is not necessary during embryonic motor neuron development since neither complete nor partial depletion of Fus via knockdown or $\text{Fus}^{\text{mde1500}}$ mutation affects motor neuron outgrowth. Interestingly, also

for other neurodegeneration related genes, contradictory motor neuron axon outgrowth phenotypes obtained from knockout and knockdown studies have been reported, e.g. *granulin (grn) a* and *grnb* [201], [160], [156], *tardbp* [157], [159], and *fragile X mental retardation 1 (fmr1)* [202], [203], indicating that MO-induced toxicity is possibly responsible for the phenotypic discrepancies.
Alternatively, discrepancies between knockdown and knockout studies might be explained by different consequences upon acute or chronic depletion of gene function regarding alternative stable upregulation of compensatory factors upon knockout and knockdown. Hence, FET family members might mediate putative compensation of loss of *fus*' function in gripNA-mediated *fus* knockdown and Fus^{mde1500} mutant zebrafish, thereby explaining lack of obvious phenotypes. Interestingly, FET protein family members EWS and TAF15 have been shown to coaggregate with FUS in inclusions found in FTLD-FUS [204],[43]. Moreover, all FET family members share structural and functional similarities, including DNA damage response, transcriptional regulation, and mRNA splicing [37]. However, NGS experiments in Fus^{mde1500} mutant zebrafish brains compared to wildtype controls revealed no upregulation of *ewsr1a*, *ewsr1b* or *taf15* gene expression (data not shown), indicating no compensatory mechanisms by FET family members in Fus^{mde1500} mutant zebrafish on mRNA levels. Protein levels have to be analyzed to exclude increased translation rates resulting in elevated Ewsr1a, Ewsr1b and Taf15 protein levels.
In addition, putative subtle phenotypes resulting from the Fus^{mde1500} mutation might be masked by the tremendous capacity of zebrafish to regenerate. However, neuronal vulnerability can be induced [157], [159], [160], [201], [213], [214], [215], [216], [217], [218], pointing to specific mechanisms of neuronal degeneration and regeneration in zebrafish.

7.5 One hit is not enough

The 'multiple hit' theory is currently being discussed as a potential pathomechanism in ALS pathogenesis, with mutations in ALS associated genes and redistribution of the encoded protein to the cytosol being the '1st hit' and challenging conditions, e.g. environmental or cellular stress, mediating accumulation and subsequent inclusion formation being the '2nd hit' [178], [37], [73]. Several stressors are currently being discussed as potential 2nd hits.
Work in cell culture has shown that heat shock is a sufficient stressor to elicit a cellular stress response, including the formation of stress granules (SGs) [176]. SG formation is

thought to be a crucial prerequisite for pathological formation of insoluble inclusions [178], [73], [37], possibly due to impaired disassembly of these dynamic structures. In line with this, several ALS and FTLD associated proteins, including FUS, TDP-43, and VCP, have been linked to altered assembly, disassembly, and clearance of SGs [**?**], [**?**], [**?**], indicating that maintenance of SG dynamics is important for neuronal survival. Another potent 2nd hit stressor is glutamate mediated excitotoxicity caused by over-stimulation of the glutamate receptors since it was found as a pathological feature of ALS and is thought to play a role in ALS pathogenesis [177].

Both stressors, heat shock stress and glutamate mediated excitotoxicity, are not capable to serve as '2nd hit' to induce neurodegeneration in Fus^{mde1500} mutants since Fus^{mde1500} mutant zebrafish show neither altered apoptosis levels upon heat shock and excitotoxic stress nor elevated stress levels under baseline conditions (see subsection 6.4.3). However, subtle pathological changes not detected by the methods used in this study, cannot be ruled out. SG formation has been observed *in vitro* and *in vivo* upon treatment with a variety of different stressors as well as overexpression of human ALS causing FUS mutations [176], [195], [196], [197], [74]. Hence, it will be interesting to determine whether SG formation can be triggered by heat shock stress and glutamate mediated excitotoxicity in Fus^{mde1500} mutant zebrafish. Alternatively, other stress conditions, combination of stressors, or even different stressors such as oxidative stress, neuroinflammation or proteasomal dysfunction might be required to induce ALS-like pathology.

In addition, aging might be a crucial regulator during manifestation of potential morphological and functional consequences of the Fus^{mde1500} mutation. Usually, clinical symptoms onset of ALS and FTLD ranges between 50 and 60 years of age [4], depending on the severity of the respective disease variant, reflecting the fact that aging is a major risk factor for the development of neurodegenerative diseases [198]. Moreover, lethality of Fus knockout mice differs depending on the genetic background [78], [79], implying that additional genetic and/or environmental factors affect the severity of phenotypical consequences upon genetic targeting. Thus, putative phenotypes might manifest in Fus^{mde1500} mutant zebrafish upon further aging and breeding to different backgrounds, increasing the probability of genetic and environmental factors [198] to interact with the Fus^{mde1500} mutation and elicit disease pathology.

7.6 Regulation of mutant Fus^{mde1500} allele expression

Gene expression levels can be controlled via regulation of transcription, at RNA level via increased RNA stability or enhanced RNA decay, or at protein levels via increased or reduced translation and degradation. In case of the mutant Fus^{mde1500} allele mRNA as well as protein levels are reduced (see subsection 6.3.3), suggesting reduced transcription or enhanced RNA decay.

Interestingly, interaction of FUS protein with several position specific affinity matrices (PSAM) identified in promotor regions resulted in repressed expression of downstream genes [83]. Most likely, this process is tightly controlled by other cis- and trans-acting factors. Similar mechanisms could apply for the mutant Fus^{mde1500} allele with the mutant Fus protein hypothetically mediating an impaired self-inhibition of transcriptional repression compared to the wildtype protein, resulting in decreased transcription of the mutant Fus^{mde1500} allele. Remarkably, FUS is known to bind its own mRNA [89], [192], [193], indicating control of FUS protein levels by autoregulative mechanisms during physiological conditions. Thus, impaired interaction of mutant Fus^{mde1500} protein with its own mRNA, resulting in reduced stability and accelerated RNA decay would be another explanation for decreased mutant Fus^{mde1500} levels. Moreover, FUS protein can regulate RNA decay of its own mRNA via a feed forward loop of alternatively splicing since skipping of exon 7 results in increased RNA decay [193]. Hypothetically, mutant Fus^{mde1500} protein might actively induce RNA decay by alternative splicing of certain exons or be incapable to sufficiently stabilize its own RNA compared to wildtype Fus.

The degree of RNA stability remaining is still sufficient to generate detectible levels of mutant Fus^{mde1500} protein, unlike in two lines of *Fus* knockout mice, where protein is either completely depleted [79] or drastically reduced [78]. Interestingly, the target sites and the resulting length of the potential transcript and/or protein inversely correlate with the expression levels, indicating that location of the introduced gene disruption affects transcript levels of the resulting mutant allele.

In summary, lack of 41 amino acids of the mutant Fus^{mde1500} protein C-terminal region might affect either interaction with promotor regions or binding to its own mRNA in a way that transcription or RNA stability is decreased, resulting in reduced expression levels. Inhibition of RNA decay in combination with analysis of potential alternative *fus* splicing products affecting *fus* mRNA stability would determine whether RNA stability or transcription repression mechanisms account for reduced levels of mutant Fus^{mde1500} mRNA.

7.7 Increased insolubility of the Fus^{mde1500} protein is not sufficient for inclusion formation

Differential fractionation of 6 - 24 mpf old Fus^{mde1500} mutant zebrafish brains revealed a tendency of the mutant Fus^{mde1500} protein to more insolubility than the Fus^{wildtype} protein (see subsection 6.3.5), indicating that the zebrafish Fus C-terminal domain truncated in the mutant allele is required for mediating protein solubility. Interestingly, human FUS' low complexity (LC) domain localized in the N-terminal region of the protein was reported to be necessary and sufficient for reversible polymer formation [66]. However, also ALS causing FUS mutations clustered in the C-terminal part of the FUS protein, e.g. H517Q mutation, confer flexibility loss detected by molecular dynamics simulation (MDS) resulting in elevated aggregation propensity [194], implying crucial functions of the C-terminal NLS for maintenance of flexibility and solubility. Partial shifting of the mutant Fus^{mde1500} protein from soluble to more insoluble fractions *in vitro* suggests an increased potential to form aggregates also *in vivo*. Despite an increased insolubility of the mutant Fus^{mde1500} protein, it is still distinct from the insoluble FUS protein isolated from pathological inclusions of human FTLD-FUS cases [38]. Moreover, the alterations in solubility are not sufficient to form pathological insoluble inclusions as evidenced by lack of Fus pathology in aged Fus^{mde1500} mutant brains (see subsection 6.3.5). Insolubility might increase proportionally with age or upon certain stimuli such as stress or seeding particles that would potentially initiate oligomerization and aggregation of mutant Fus^{mde1500} protein. Biochemical analysis of mutant Fus^{mde1500} protein solubility and immunohistochemistry in aged fish and after stimulation with an adequate stressor or seeding impulse will reveal whether firstly insolubility propensity increases and secondly oligomerization and aggregation of insoluble mutant Fus^{mde1500} protein can be induced.

7.8 Nuclear import regulation of the Fus^{mde1500} protein

Work in cell culture has shown that the C-terminal region of FUS, harboring the PY-NLS and the RGG3 domain, is necessary and sufficient to mediate transportin (TRN) dependent nuclear import [70]. Strikingly, fALS associated point mutations in the C-terminal domain disrupt nuclear import of FUS leading to cytosolic redistribution of FUS [70], [74]. Interestingly, the severity of the different fALS mutations regarding disease onset and progression is reflected by the degree of cytosolic redistribution

when expressed *in vitro*. Thus, severe mutations show a more pronounced cytosolic redistribution than milder mutations [70]. Since the entire PY-NLS and C-terminal parts of the RGG3 domain are lacking in the Fus^{mde1500} protein, this mutation is reminiscent of severe ALS causing mutations, therefore predicted to prominently localize to the cytosol. When transgenically expressed in embryonic zebrafish and primary cortical neurons (see Figure 6.10), mutant Fus^{mde1500} protein redistributes to cytosolic compartments, however, the main fraction is still localized to the nucleus. Subcellular fractionation analysis (see Figure 6.10) and immunohistochemistry of adult brains endogenously expressing the mutant Fus^{mde1500} protein (see subsection 6.4.5) did not yield severe cytosolic distribution of the mutant Fus rather showing only a slight tendency to shift to a more cytosolic localization whereas the main fraction of Fus protein is still nuclear. Interestingly, FUS localization can be modulated by arginine methylation of the RGG domains. Impact of methylation status on wildtype and fALS mutant FUS protein localization was analyzed by inhibiting protein arginine methylation using chemical treatment with adenosine-2,3-dialdehylde (AdOX). AdOX inhibits all S-adenosyl-methionine (SAM)-dependent enzymatic reactions, including protein arginine methylation [45], thus leading to hypomethylation. Under normal conditions, FUS is heavily methylated, whereas in FTLD-FUS cases, hypomethylation of FUS is thought to mediate cytosolic redistribution due to overly tight binding of FUS to TRN and impaired nuclear import [37]. In ALS-FUS, fALS mutations are known to mediate cytosolic distribution of FUS under normal methylation conditions. However, hypomethylation can also enable FUS harboring fALS mutations to localize to the nucleus [45], [37]. In addition, silencing of *protein N-arginine methyltransferase 1 (PRMT1)* causes nuclear localization of fALS associated FUS mutations [45] through reduction of FUS methylation levels. Thus, degree of methylation in synergy with other determinants of localization, e.g. NLS disrupting mutations regulate localization of FUS protein, extending the nuclear import signal to the PY-NLS and the RGG3 domain. Hypothetically, the tight regulation of arginine methylation is imbalanced in Fus^{mde1500} mutants due to truncation of the entire NLS and parts of the RGG3 domain leading to reduced methylation of the remaining RGG3 domain. This might lead to the unexpected nuclear localization of the truncated Fus^{mde1500} protein. Also, truncation of the NLS and parts of the RGG3 might reduce binding to TRN in general to a degree that is sufficient for nuclear import but not enough for a re-export and cytoplasmic accumulation of Fus protein as predicted in FTLD-FUS. In line with this hypothesis, RNA expression levels of the zebrafish protein N-arginine methyltransferase 1 (*prmt1*) are mildly reduced in Fus^{mde1500} mutant zebrafish compared to wildtype siblings, as ev-

idenced by an unbiased next generation sequencing (NGS) approach (data not shown). Methylation levels of Fus in Fus^{mde1500} mutants might be reduced and together with the truncated RGG3 domain possibly modulate the affinity of the mutant Fus^{mde1500} protein to the import factor TRN to a level that it is still sufficiently transported to the nucleus despite the lack of the PY-NLS.

Beside methylation, other post translational modifications are known to also modify localization of FUS under certain conditions. Upon calicheamicin γ1 (CLM) induced DNA damage, FUS is phosphorylated leading to cytosolic FUS localization in cell culture [199]. Moreover, increased DNA damage levels were found in FTLD-FUS patients [199]. Cellular stress might be a common disease mechanisms in all FUSopathies [37], thus distinct stressors including genomic stress potentially initiate specific FUS post-translational modification events leading to redistribution mechanisms and eventually to cytosolic accumulation and aggregation of FUS in sporadic ALS-FUS and FTLD-FUS. General cellular stress due to overexpression of different Fus constructs might already be sufficient to elicit translocation of the mutant Fus^{mde1500} protein, potentially being more susceptible to dysregulated posttranslational modifications than the wildtype Fus protein due to the truncation of parts of the RGG3 domain and the entire NLS.

Moreover, initial localization of endogenous mutant Fus^{mde1500} protein might be equally distributed between nucleus and cytosol but the steady state of nuclear import and cytosolic redistribution might be disturbed due to rapid proteasomal degradation of the cytosolic Fus^{mde1500} protein fraction, thus resulting in a relative nuclear accumulation of the mutant Fus^{mde1500} protein.

Analysis of posttranslational modifications, in particular methylation status and phosphorylation of mutant Fus^{mde1500} protein together with examination of human FUS' endogenous localization in ALS-FUS and FTLD-FUS cases via immunohistochemistry will provide insights into affected import mechanisms. Moreover, analysis of mutant Fus^{mde1500} protein distribution upon inhibition of the protein degradation machinery will determine whether proteasomal degradation regulation accounts for the nuclear localization of the mutant Fus^{mde1500} protein.

7.9 Concluding remarks

So far, Fus^{mde1500} mutant zebrafish have not developed any obvious phenotype, that would reveal major dysfunctions upon truncating the Fus protein, indicating that the Fus^{mde1500} mutation alone confers no pathogenicity sufficient to elicit ALS reminis-

cent symptoms in zebrafish. Since most neurodegenerative disease are age-related, $Fus^{mde1500}$ mutant zebrafish possibly will develop phenotypes and manifest symptoms upon aging and influence of additional parameters, e.g. chronic stress, environmental circumstances, and genetic risk factors.
However, mutant $Fus^{mde1500}$ protein exhibits pathological features similar to insoluble FUS protein found in pathologic inclusions in ALS-FUS and FTLD-FUS cases, i.e. the tendency to become insoluble and partial localization to the cytosol upon transgenic expression. Thus, $Fus^{mde1500}$ mutant zebrafish serves as animal model suitable for studying localization of $Fus^{mde1500}$ mutant protein, SG and inclusion formation, as well as identification of disease modifying factors in an aged whole organisms approach.

8 References

[1] Christian Haass and Dennis J Selkoe. Soluble protein oligomers in neurodegeneration: lessons from the Alzheimer's amyloid β-peptide. *Nature Reviews Molecular Cell Biology*, 8(2):101–112, February 2007.

[2] Byron Caughey and Peter T Lansbury. Protofibrils, pores, fibrils, and neurodegeneration: separating the responsible protein aggregates from the innocent bystanders. *Annu Rev Neurosci*, 26:267–98, 2003.

[3] Johnathan Cooper-Knock, Janine Kirby, Robin Highley, and Pamela J Shaw. The spectrum of c9orf72-mediated neurodegeneration and amyotrophic lateral sclerosis. *Neurotherapeutics*, 12(2):326–39, Apr 2015.

[4] Wim Robberecht and Thomas Philips. The changing scene of amyotrophic lateral sclerosis. *Nature reviews Neuroscience*, March 2013.

[5] D Neary, J S Snowden, L Gustafson, U Passant, D Stuss, S Black, M Freedman, A Kertesz, P H Robert, M Albert, K Boone, B L Miller, J Cummings, and D F Benson. Frontotemporal lobar degeneration: a consensus on clinical diagnostic criteria. *Neurology*, 51(6):1546–54, Dec 1998.

[6] Tim Van Langenhove, Julie van der Zee, and Christine Van Broeckhoven. The molecular basis of the frontotemporal lobar degeneration-amyotrophic lateral sclerosis spectrum. *Annals of medicine*, 44(8):817–828, December 2012.

[7] M L Gorno-Tempini, A E Hillis, S Weintraub, A Kertesz, M Mendez, S F Cappa, J M Ogar, J D Rohrer, S Black, B F Boeve, F Manes, N F Dronkers, R Vandenberghe, K Rascovsky, K Patterson, B L Miller, D S Knopman, J R Hodges, M M Mesulam, and M Grossman. Classification of primary progressive aphasia and its variants. *Neurology*, 76(11):1006–14, Mar 2011.

[8] Shuo-Chien Ling, Magdalini Polymenidou, and Don W Cleveland. Converging Mechanisms in ALS and FTD: Disrupted RNA and Protein Homeostasis. *Neuron*, 79(3):416–438, August 2013.

[9] A Chiò, G Logroscino, B J Traynor, J Collins, J C Simeone, L A Goldstein, and L A White. Global epidemiology of amyotrophic lateral sclerosis: a systematic review of the published literature. *Neuroepidemiology*, 41(2):118–30, 2013.

[10] Prof Matthew C Kiernan DSc, Steve Vucic PhD, Benjamin C Cheah MBiostat, Martin R Turner PhD, Prof Andrew Eisen MD, Prof Orla Hardiman MD, James R Burrell MBBS, and Margaret C Zoing BNurs. Amyotrophic lateral sclerosis. *The Lancet*, 377(9769):942–955, March 2011.

[11] Benjamin Rix Brooks. El escorial world federation of neurology criteria for the diagnosis of amyotrophic lateral sclerosis. *Journal of the Neurological Sciences*, 124(Suppl.):96–107, 1994.

[12] Asa J Wilbourn. Clinical neurophysiology in the diagnosis of amyotrophic lateral sclerosis: The lambert and the el escorial criteria. *Journal of the Neurological Sciences*, 160(1):S25–S29, October 1998.

[13] Peter Munch Andersen, Gian Domenico Borasio, Reinhard Dengler, Orla Hardiman, Katja Kollewe, Peter Nigel Leigh, Pierre-Francois Pradat, Vincenzo Silani, Barbara Tomik, and EALSC Working Group. Good practice in the management of amyotrophic lateral sclerosis: clinical guidelines. an evidence-based review with good practice points. ealsc working group. *Amyotroph Lateral Scler*, 8(4):195–213, Aug 2007.

[14] Monica Bucchia, Agnese Ramirez, Valeria Parente, Chiara Simone, Monica Nizzardo, Francesca Magri, Sara Dametti, and Stefania Corti. Therapeutic development in amyotrophic lateral sclerosis. *Clin Ther*, 37(3):668–680, Mar 2015.

[15] Patricia Lillo and John R Hodges. Frontotemporal dementia and motor neurone disease: Overlapping clinic-pathological disorders. *Journal of Clinical Neuroscience*, 16(9):1131–1135, September 2009.

[16] G M Ringholz, S H Appel, M Bradshaw, N A Cooke, D M Mosnik, and P E Schulz. Prevalence and patterns of cognitive impairment in sporadic ALS. *Neurology*, 65(4):586–590, August 2005.

[17] J R Burrell, M C Kiernan, S Vucic, and J R Hodges. Motor Neuron dysfunction in frontotemporal dementia. *Brain : a journal of neurology*, 134(9):2582–2594, September 2011.

[18] Catherine Lomen-Hoerth, Thomas Anderson, and Bruce Miller. The overlap of amyotrophic lateral sclerosis and frontotemporal dementia. *Neurology*, 59(7):1077–9, October 2002.

[19] Ian R A Mackenzie, Manuela Neumann, Eileen H Bigio, Nigel J Cairns, Irina Alafuzoff, Jillian Kril, Gabor G Kovacs, Bernardino Ghetti, Glenda Halliday, Ida E Holm, Paul G Ince, Wouter Kamphorst, Tamas Revesz, Annemieke J M Rozemuller, Samir Kumar-Singh, Haruhiko Akiyama, Atik Baborie, Salvatore Spina, Dennis W Dickson, John Q Trojanowski, and David M A Mann. Nomenclature and nosology for neuropathologic subtypes of frontotemporal lobar degeneration: an update. *Acta Neuropathologica*, 119(1):1–4, January 2010.

[20] Malcolm Proudfoot, Nick J Gutowski, Dieter Edbauer, David A Hilton, Mark Stephens, Julia Rankin, and Ian R A Mackenzie. Early dipeptide repeat pathology in a frontotemporal dementia kindred with C9ORF72 mutation and intellectual disability. *Acta Neuropathologica*, 127(3):451–458, January 2014.

[21] Rosa Rademakers, Manuela Neumann, and Ian R Mackenzie. Advances in understanding the molecular basis of frontotemporal dementia. *Nature Publishing Group*, June 2012.

[22] B Borroni, C Bonvicini, A Alberici, E Buratti, C Agosti, S Archetti, A Papetti, C Stuani, M Di Luca, M Gennarelli, and A Padovani. Mutation within TARDBP leads to frontotemporal dementia without motor neuron disease. *Human mutation*, 30(11):E974–83, November 2009.

[23] Lina Benajiba, Isabelle Le Ber, Agnès Camuzat, Mathieu Lacoste, Catherine Thomas-Anterion, Philippe Couratier, Solenn Legallic, François Salachas, Didier Hannequin, Marielle Decousus, Lucette Lacomblez, Eric Guedj, Véronique Golfier, William Camu, Bruno Dubois, Dominique Campion, Vincent Meininger, Alexis Brice, and French Clinical and Genetic Research Network on Frontotemporal Lobar Degeneration/Frontotemporal Lobar Degeneration with Motoneuron Disease. TARDBP mutations in motoneuron disease with frontotemporal lobar degeneration. *Annals of neurology*, 65(4):470–473, April 2009.

[24] Jill S Goldman, Jennifer Adamson, Anna Karydas, Bruce L Miller, and Mike Hutton. New genes, new dilemmas: Ftld genetics and its implications for families. *Am J Alzheimers Dis Other Demen*, 22(6):507–15, 2007.

[25] Serena Lattante, Sorana Ciura, Guy A Rouleau, and Edor Kabashi. Defining the genetic connection linking amyotrophic lateral sclerosis (als) with frontotemporal dementia (ftd). *Trends Genet*, 31(5):263–273, May 2015.

[26] M Hutton, C L Lendon, P Rizzu, M Baker, S Froelich, H Houlden, S Pickering-Brown, S Chakraverty, A Isaacs, A Grover, J Hackett, J Adamson, S Lincoln, D Dickson, P Davies, R C Petersen, M Stevens, E de Graaff, E Wauters, J van Baren, M Hillebrand, M Joosse, J M Kwon, P Nowotny, L K Che, J Norton, J C Morris, L A Reed, J Trojanowski, H Basun, L Lannfelt, M Neystat, S Fahn, F Dark, T Tannenberg, P R Dodd, N Hayward, J B Kwok, P R Schofield, A Andreadis, J Snowden, D Craufurd, D Neary, F Owen, B A Oostra, J Hardy, A Goate, J van Swieten, D Mann, T Lynch, and P Heutink. Association of missense and 5'-splice-site mutations in tau with the inherited dementia ftdp-17. *Nature*, 393(6686):702–5, Jun 1998.

[27] P Poorkaj, T D Bird, E Wijsman, E Nemens, R M Garruto, L Anderson, A Andreadis, W C Wiederholt, M Raskind, and G D Schellenberg. Tau is a candidate gene for chromosome 17 frontotemporal dementia. *Ann Neurol*, 43(6):815–25, Jun 1998.

[28] M G Spillantini, J R Murrell, M Goedert, M R Farlow, A Klug, and B Ghetti. Mutation in the tau gene in familial multiple system tauopathy with presenile dementia. *Proc Natl Acad Sci U S A*, 95(13):7737–41, Jun 1998.

[29] R Rademakers, M Cruts, and C van Broeckhoven. The role of tau (mapt) in frontotemporal dementia and related tauopathies. *Hum Mutat*, 24(4):277–95, Oct 2004.

[30] Matt Baker, Ian R Mackenzie, Stuart M Pickering-Brown, Jennifer Gass, Rosa Rademakers, Caroline Lindholm, Julie Snowden, Jennifer Adamson, A Dessa Sadovnick, Sara Rollinson, Ashley Cannon, Emily Dwosh, David Neary, Stacey Melquist, Anna Richardson, Dennis Dickson, Zdenek Berger, Jason Eriksen, Todd Robinson, Cynthia Zehr, Chad A Dickey, Richard Crook, Eileen McGowan, David Mann, Bradley Boeve, Howard Feldman, and Mike Hutton. Mutations in progranulin cause tau-negative frontotemporal dementia linked to chromosome 17. *Nature*, 442(7105):916–9, Aug 2006.

[31] Marc Cruts, Ilse Gijselinck, Julie van der Zee, Sebastiaan Engelborghs, Hans Wils, Daniel Pirici, Rosa Rademakers, Rik Vandenberghe, Bart Dermaut, Jean-

Jacques Martin, Cornelia van Duijn, Karin Peeters, Raf Sciot, Patrick Santens, Tim De Pooter, Maria Mattheijssens, Marleen Van den Broeck, Ivy Cuijt, Krist'l Vennekens, Peter P De Deyn, Samir Kumar-Singh, and Christine Van Broeckhoven. Null mutations in progranulin cause ubiquitin-positive frontotemporal dementia linked to chromosome 17q21. *Nature*, 442(7105):920–4, Aug 2006.

[32] Hao Deng, Kai Gao, and Joseph Jankovic. The role of FUS gene variants in neurodegenerative diseases. *Nature Publishing Group*, 10(6):337–348, May 2014.

[33] P N Leigh, H Whitwell, O Garofalo, J Buller, M Swash, J E Martin, J M Gallo, R O Weller, and B H Anderton. Ubiquitin-immunoreactive intraneuronal inclusions in amyotrophic lateral sclerosis. morphology, distribution, and specificity. *Brain*, 114 (Pt 2):775–88, Apr 1991.

[34] D R Rosen, T Siddique, D Patterson, D A Figlewicz, P Sapp, A Hentati, D Donaldson, J Goto, J P O'Regan, and H X Deng. Mutations in cu/zn superoxide dismutase gene are associated with familial amyotrophic lateral sclerosis. *Nature*, 362(6415):59–62, Mar 1993.

[35] Ian R A Mackenzie, Eileen H Bigio, Paul G Ince, Felix Geser, Manuela Neumann, Nigel J Cairns, Linda K Kwong, Mark S Forman, John Ravits, Heather Stewart, Andrew Eisen, Leo McClusky, Hans A Kretzschmar, Camelia M Monoranu, J Robin Highley, Janine Kirby, Teepu Siddique, Pamela J Shaw, Virginia M-Y Lee, and John Q Trojanowski. Pathological tdp-43 distinguishes sporadic amyotrophic lateral sclerosis from amyotrophic lateral sclerosis with sod1 mutations. *Ann Neurol*, 61(5):427–34, May 2007.

[36] Chun-Feng Tan, Hiroto Eguchi, Asako Tagawa, Osamu Onodera, Takuya Iwasaki, Akira Tsujino, Masatoyo Nishizawa, Akiyoshi Kakita, and Hitoshi Takahashi. Tdp-43 immunoreactivity in neuronal inclusions in familial amyotrophic lateral sclerosis with or without sod1 gene mutation. *Acta Neuropathol*, 113(5):535–42, May 2007.

[37] Dorothee Dormann and Christian Haass. Fused in sarcoma (FUS): An oncogene goes awry in neurodegeneration. *Molecular and cellular neurosciences*, April 2013.

[38] Manuela Neumann, Rosa Rademakers, Sigrun Roeber, Matt Baker, Hans A Kretzschmar, and Ian R A Mackenzie. A new subtype of frontotemporal lobar degener-

ation with FUS pathology. *Brain : a journal of neurology*, 132(Pt 11):2922–2931, November 2009.

[39] Manuela Neumann, Sigrun Roeber, Hans A Kretzschmar, Rosa Rademakers, Matt Baker, and Ian R A Mackenzie. Abundant FUS-immunoreactive pathology in neuronal intermediate filament inclusion disease. *Acta Neuropathologica*, 118(5):605–616, November 2009.

[40] David G Munoz, Manuela Neumann, Hirofumi Kusaka, Osamu Yokota, Kenji Ishihara, Seishi Terada, Shigetoshi Kuroda, and Ian R Mackenzie. FUS pathology in basophilic inclusion body disease. *Acta Neuropathologica*, 118(5):617–627, November 2009.

[41] T J Kwiatkowski, D A Bosco, A L Leclerc, E Tamrazian, C R Vanderburg, C Russ, A Davis, J Gilchrist, E J Kasarskis, T Munsat, P Valdmanis, G A Rouleau, B A Hosler, P Cortelli, P J de Jong, Y Yoshinaga, J L Haines, M A Pericak-Vance, J Yan, N Ticozzi, T Siddique, D McKenna-Yasek, P C Sapp, H R Horvitz, J E Landers, and R H Brown. Mutations in the FUS/TLS Gene on Chromosome 16 Cause Familial Amyotrophic Lateral Sclerosis. *Science (New York, NY)*, 323(5918):1205–1208, February 2009.

[42] C Vance, E L Scotter, A L Nishimura, C Troakes, J C Mitchell, C Kathe, H Urwin, C Manser, C C Miller, T Hortobagyi, M Dragunow, B Rogelj, and C E Shaw. ALS mutant FUS disrupts nuclear localization and sequesters wild-type FUS within cytoplasmic stress granules. *Human Molecular Genetics*, March 2013.

[43] Manuela Neumann, Eva Bentmann, Dorothee Dormann, Ali Jawaid, Mariely Dejesus-Hernandez, Olaf Ansorge, Sigrun Roeber, Hans A Kretzschmar, David G Munoz, Hirofumi Kusaka, Osamu Yokota, Lee Cyn Ang, Juan Bilbao, Rosa Rademakers, Christian Haass, and Ian R A Mackenzie. FET proteins TAF15 and EWS are selective markers that distinguish FTLD with FUS pathology from amyotrophic lateral sclerosis with FUS mutations. *Brain : a journal of neurology*, 134(Pt 9):2595–2609, September 2011.

[44] Manuela Neumann, Chiara F Valori, Olaf Ansorge, Hans A Kretzschmar, David G Munoz, Hirofumi Kusaka, Osamu Yokota, Kenji Ishihara, Lee Cyn Ang, Juan M Bilbao, and Ian R A Mackenzie. Transportin 1 accumulates specifically with FET proteins but no other transportin cargos in FTLD-FUS and is

absent in FUS inclusions in ALS with FUS mutations. *Acta Neuropathologica*, 124(5):705–716, November 2012.

[45] Dorothee Dormann, Tobias Madl, Chiara F Valori, Eva Bentmann, Sabina Tahirovic, Claudia Abou-Ajram, Elisabeth Kremmer, Olaf Ansorge, Ian R A Mackenzie, Manuela Neumann, and Christian Haass. Arginine methylation next to the PY-NLS modulates Transportin binding and nuclear import of FUS. *The EMBO journal*, pages 1–18, September 2012.

[46] Manuela Neumann, Deepak M Sampathu, Linda K Kwong, Adam C Truax, Matthew C Micsenyi, Thomas T Chou, Jennifer Bruce, Theresa Schuck, Murray Grossman, Christopher M Clark, Leo F McCluskey, Bruce L Miller, Eliezer Masliah, Ian R Mackenzie, Howard Feldman, Wolfgang Feiden, Hans A Kretzschmar, John Q Trojanowski, and Virginia M-Y Lee. Ubiquitinated tdp-43 in frontotemporal lobar degeneration and amyotrophic lateral sclerosis. *Science*, 314(5796):130–3, Oct 2006.

[47] Tetsuaki Arai, Masato Hasegawa, Haruhiko Akiyama, Kenji Ikeda, Takashi Nonaka, Hiroshi Mori, David Mann, Kuniaki Tsuchiya, Mari Yoshida, Yoshio Hashizume, and Tatsuro Oda. Tdp-43 is a component of ubiquitin-positive tau-negative inclusions in frontotemporal lobar degeneration and amyotrophic lateral sclerosis. *Biochem Biophys Res Commun*, 351(3):602–11, Dec 2006.

[48] Jemeen Sreedharan, Ian P Blair, Vineeta B Tripathi, Xun Hu, Caroline Vance, Boris Rogelj, Steven Ackerley, Jennifer C Durnall, Kelly L Williams, Emanuele Buratti, Francisco Baralle, Jacqueline de Belleroche, J Douglas Mitchell, P Nigel Leigh, Ammar Al-Chalabi, Christopher C Miller, Garth Nicholson, and Christopher E Shaw. TDP-43 mutations in familial and sporadic amyotrophic lateral sclerosis. *Science (New York, NY)*, 319(5870):1668–1672, March 2008.

[49] Michael A Gitcho, Robert H Baloh, Sumi Chakraverty, Kevin Mayo, Joanne B Norton, Denise Levitch, Kimmo J Hatanpaa, Charles L White, 3rd, Eileen H Bigio, Richard Caselli, Matt Baker, Muhammad T Al-Lozi, John C Morris, Alan Pestronk, Rosa Rademakers, Alison M Goate, and Nigel J Cairns. Tdp-43 a315t mutation in familial motor neuron disease. *Ann Neurol*, 63(4):535–8, Apr 2008.

[50] Edor Kabashi, Paul N Valdmanis, Patrick Dion, Dan Spiegelman, Brendan J McConkey, Christine Vande Velde, Jean-Pierre Bouchard, Lucette Lacomblez, Ksenia Pochigaeva, Francois Salachas, Pierre-Francois Pradat, William Camu,

Vincent Meininger, Nicolas Dupre, and Guy A Rouleau. Tardbp mutations in individuals with sporadic and familial amyotrophic lateral sclerosis. *Nat Genet*, 40(5):572–4, May 2008.

[51] Vivianna M Van Deerlin, James B Leverenz, Lynn M Bekris, Thomas D Bird, Wuxing Yuan, Lauren B Elman, Dana Clay, Elisabeth McCarty Wood, Alice S Chen-Plotkin, Maria Martinez-Lage, Ellen Steinbart, Leo McCluskey, Murray Grossman, Manuela Neumann, I-Lin Wu, Wei-Shiung Yang, Robert Kalb, Douglas R Galasko, Thomas J Montine, John Q Trojanowski, Virginia M-Y Lee, Gerard D Schellenberg, and Chang-En Yu. Tardbp mutations in amyotrophic lateral sclerosis with tdp-43 neuropathology: a genetic and histopathological analysis. *Lancet Neurol*, 7(5):409–16, May 2008.

[52] Mariely DeJesus-Hernandez, Ian R Mackenzie, Bradley F Boeve, Adam L Boxer, Matt Baker, Nicola J Rutherford, Alexandra M Nicholson, NiCole A Finch, Heather Flynn, Jennifer Adamson, Naomi Kouri, Aleksandra Wojtas, Pheth Sengdy, Ging-Yuek R Hsiung, Anna Karydas, William W Seeley, Keith A Josephs, Giovanni Coppola, Daniel H Geschwind, Zbigniew K Wszolek, Howard Feldman, David S Knopman, Ronald C Petersen, Bruce L Miller, Dennis W Dickson, Kevin B Boylan, Neill R Graff-Radford, and Rosa Rademakers. Expanded ggggcc hexanucleotide repeat in noncoding region of c9orf72 causes chromosome 9p-linked ftd and als. *Neuron*, 72(2):245–56, Oct 2011.

[53] Alan E Renton, Elisa Majounie, Adrian Waite, Javier Simón-Sánchez, Sara Rollinson, J Raphael Gibbs, Jennifer C Schymick, Hannu Laaksovirta, John C van Swieten, Liisa Myllykangas, Hannu Kalimo, Anders Paetau, Yevgeniya Abramzon, Anne M Remes, Alice Kaganovich, Sonja W Scholz, Jamie Duckworth, Jinhui Ding, Daniel W Harmer, Dena G Hernandez, Janel O Johnson, Kin Mok, Mina Ryten, Danyah Trabzuni, Rita J Guerreiro, Richard W Orrell, James Neal, Alex Murray, Justin Pearson, Iris E Jansen, David Sondervan, Harro Seelaar, Derek Blake, Kate Young, Nicola Halliwell, Janis Bennion Callister, Greg Toulson, Anna Richardson, Alex Gerhard, Julie Snowden, David Mann, David Neary, Michael A Nalls, Terhi Peuralinna, Lilja Jansson, Veli-Matti Isoviita, Anna-Lotta Kaivorinne, Maarit Hölttä-Vuori, Elina Ikonen, Raimo Sulkava, Michael Benatar, Joanne Wuu, Adriano Chiò, Gabriella Restagno, Giuseppe Borghero, Mario Sabatelli, ITALSGEN Consortium, David Heckerman, Ekaterina Rogaeva, Lorne Zinman, Jeffrey D Rothstein, Michael Sendtner, Carsten

Drepper, Evan E Eichler, Can Alkan, Ziedulla Abdullaev, Svetlana D Pack, Amalia Dutra, Evgenia Pak, John Hardy, Andrew Singleton, Nigel M Williams, Peter Heutink, Stuart Pickering-Brown, Huw R Morris, Pentti J Tienari, and Bryan J Traynor. A hexanucleotide repeat expansion in c9orf72 is the cause of chromosome 9p21-linked als-ftd. *Neuron*, 72(2):257–68, Oct 2011.

[54] Ilse Gijselinck, Tim Van Langenhove, Julie van der Zee, Kristel Sleegers, Stéphanie Philtjens, Gernot Kleinberger, Jonathan Janssens, Karolien Bettens, Caroline Van Cauwenberghe, Sandra Pereson, Sebastiaan Engelborghs, Anne Sieben, Peter De Jonghe, Rik Vandenberghe, Patrick Santens, Jan De Bleecker, Githa Maes, Veerle Bäumer, Lubina Dillen, Geert Joris, Ivy Cuijt, Ellen Corsmit, Ellen Elinck, Jasper Van Dongen, Steven Vermeulen, Marleen Van den Broeck, Carolien Vaerenberg, Maria Mattheijssens, Karin Peeters, Wim Robberecht, Patrick Cras, Jean-Jacques Martin, Peter P De Deyn, Marc Cruts, and Christine Van Broeckhoven. A c9orf72 promoter repeat expansion in a flanders-belgian cohort with disorders of the frontotemporal lobar degeneration-amyotrophic lateral sclerosis spectrum: a gene identification study. *Lancet Neurol*, 11(1):54–65, Jan 2012.

[55] Hussein Daoud, Hamid Suhail, Mike Sabbagh, Veronique Belzil, Anna Szuto, Alexandre Dionne-Laporte, Jawad Khoris, William Camu, Francois Salachas, Vincent Meininger, Jean Mathieu, Michael Strong, Patrick A Dion, and Guy A Rouleau. C9orf72 hexanucleotide repeat expansions as the causative mutation for chromosome 9p21-linked amyotrophic lateral sclerosis and frontotemporal dementia. *Arch Neurol*, 69(9):1159–63, Sep 2012.

[56] Peter E A Ash, Kevin F Bieniek, Tania F Gendron, Thomas Caulfield, Wen-Lang Lin, Mariely Dejesus-Hernandez, Marka M van Blitterswijk, Karen Jansen-West, Joseph W Paul, 3rd, Rosa Rademakers, Kevin B Boylan, Dennis W Dickson, and Leonard Petrucelli. Unconventional translation of c9orf72 ggggcc expansion generates insoluble polypeptides specific to c9ftd/als. *Neuron*, 77(4):639–46, Feb 2013.

[57] Kohji Mori, Shih-Ming Weng, Thomas Arzberger, Stephanie May, Kristin Rentzsch, Elisabeth Kremmer, Bettina Schmid, Hans A Kretzschmar, Marc Cruts, Christine Van Broeckhoven, Christian Haass, and Dieter Edbauer. The c9orf72 ggggcc repeat is translated into aggregating dipeptide-repeat proteins in ftld/als. *Science*, 339(6125):1335–8, Mar 2013.

[58] Kohji Mori, Thomas Arzberger, Friedrich A Grässer, Ilse Gijselinck, Stephanie May, Kristin Rentzsch, Shih-Ming Weng, Martin H Schludi, Julie van der Zee, Marc Cruts, Christine Van Broeckhoven, Elisabeth Kremmer, Hans A Kretzschmar, Christian Haass, and Dieter Edbauer. Bidirectional transcripts of the expanded c9orf72 hexanucleotide repeat are translated into aggregating dipeptide repeat proteins. *Acta Neuropathol*, 126(6):881–93, Dec 2013.

[59] Ian R Mackenzie, Thomas Arzberger, Elisabeth Kremmer, Dirk Troost, Stefan Lorenzl, Kohji Mori, Shih-Ming Weng, Christian Haass, Hans A Kretzschmar, Dieter Edbauer, and Manuela Neumann. Dipeptide repeat protein pathology in c9orf72 mutation cases: clinico-pathological correlations. *Acta Neuropathol*, 126(6):859–79, Dec 2013.

[60] A Crozat, P Aman, N Mandahl, and D Ron. Fusion of chop to a novel rna-binding protein in human myxoid liposarcoma. *Nature*, 363(6430):640–4, Jun 1993.

[61] T H Rabbitts, A Forster, R Larson, and P Nathan. Fusion of the dominant negative transcription regulator chop with a novel gene fus by translocation t(12;16) in malignant liposarcoma. *Nat Genet*, 4(2):175–80, Jun 1993.

[62] Adelene Y Tan and James L Manley. The tet family of proteins: functions and roles in disease. *J Mol Cell Biol*, 1(2):82–92, Dec 2009.

[63] Julien Couthouis, Michael P Hart, Renske Erion, Oliver D King, Zamia Diaz, Tadashi Nakaya, Fadia Ibrahim, Hyung-Jun Kim, Jelena Mojsilovic-Petrovic, Saarene Panossian, Cecilia E Kim, Edward C Frackelton, Jennifer A Solski, Kelly L Williams, Dana Clay-Falcone, Lauren Elman, Leo McCluskey, Robert Greene, Hakon Hakonarson, Robert G Kalb, Virginia M Y Lee, John Q Trojanowski, Garth A Nicholson, Ian P Blair, Nancy M Bonini, Vivianna M Van Deerlin, Zissimos Mourelatos, James Shorter, and Aaron D Gitler. Evaluating the role of the fus/tls-related gene ewsr1 in amyotrophic lateral sclerosis. *Hum Mol Genet*, 21(13):2899–911, Jul 2012.

[64] N Ticozzi, C Vance, A L Leclerc, P Keagle, J D Glass, D McKenna-Yasek, P C Sapp, V Silani, D A Bosco, C E Shaw, R H Brown, Jr, and J E Landers. Mutational analysis reveals the fus homolog taf15 as a candidate gene for familial amyotrophic lateral sclerosis. *Am J Med Genet B Neuropsychiatr Genet*, 156B(3):285–90, Apr 2011.

[65] H Zinszner, R Albalat, and D Ron. A novel effector domain from the rna-binding protein tls or ews is required for oncogenic transformation by chop. *Genes Dev*, 8(21):2513–26, Nov 1994.

[66] Masato Kato, Tina W Han, Shanhai Xie, Kevin Shi, Xinlin Du, Leeju C Wu, Hamid Mirzaei, Elizabeth J Goldsmith, Jamie Longgood, Jimin Pei, Nick V Grishin, Douglas E Frantz, Jay W Schneider, She Chen, Lin Li, Michael R Sawaya, David Eisenberg, Robert Tycko, and Steven L McKnight. Cell-free Formation of RNA Granules: Low Complexity Sequence Domains Form Dynamic Fibers within Hydrogels. *Cell*, 149(4):753–767, May 2012.

[67] Tina W Han, Masato Kato, Shanhai Xie, Leeju C Wu, Hamid Mirzaei, Jimin Pei, Min Chen, Yang Xie, Jeffrey Allen, Guanghua Xiao, and Steven L McKnight. Cell-free Formation of RNA Granules: Bound RNAs Identify Features and Components of Cellular Assemblies. *Cell*, 149(4):768–779, May 2012.

[68] C G Burd and G Dreyfuss. Conserved structures and diversity of functions of rna-binding proteins. *Science*, 265(5172):615–21, Jul 1994.

[69] Yuko Iko, Takashi S Kodama, Nobuyuki Kasai, Takuji Oyama, Eugene H Morita, Takanori Muto, Mika Okumura, Ritsuko Fujii, Toru Takumi, Shin-ichi Tate, and Kosuke Morikawa. Domain architectures and characterization of an rna-binding protein, tls. *J Biol Chem*, 279(43):44834–40, Oct 2004.

[70] Dorothee Dormann, Ramona Rodde, Dieter Edbauer, Eva Bentmann, Ingeborg Fischer, Alexander Hruscha, Manuel E Than, Ian R A Mackenzie, Anja Capell, Bettina Schmid, Manuela Neumann, and Christian Haass. ALS-associated fused in sarcoma (FUS) mutations disrupt Transportin-mediated nuclear import. *The EMBO journal*, 29(16):2841–2857, August 2010.

[71] Dorothee Dormann, Tobias Madl, Chiara F Valori, Eva Bentmann, Sabina Tahirovic, Claudia Abou-Ajram, Elisabeth Kremmer, Olaf Ansorge, Ian R A Mackenzie, Manuela Neumann, and Christian Haass. Arginine methylation next to the PY-NLS modulates Transportin binding and nuclear import of FUS. *The EMBO journal*, pages 1–18, September 2012.

[72] Brittany J Lee, Ahmet E Cansizoglu, Katherine E Süel, Thomas H Louis, Zichao Zhang, and Yuh Min Chook. Rules for nuclear localization sequence recognition by karyopherin beta 2. *Cell*, 126(3):543–558, August 2006.

[73] Dorothee Dormann and Christian Haass. TDP-43 and FUS: a nuclear affair. *Trends in Neurosciences*, 34(7):339–348, July 2011.

[74] D A Bosco, N Lemay, H K Ko, H Zhou, C Burke, T J Kwiatkowski, P Sapp, D McKenna-Yasek, R H Brown, and L J Hayward. Mutant FUS proteins that cause amyotrophic lateral sclerosis incorporate into stress granules. *Human Molecular Genetics*, 19(21):4160–4175, October 2010.

[75] Paul Anderson and Nancy Kedersha. Stress granules: the tao of rna triage. *Trends Biochem Sci*, 33(3):141–50, Mar 2008.

[76] H Baechtold, M Kuroda, J Sok, D Ron, B S Lopez, and A T Akhmedov. Human 75-kda dna-pairing protein is identical to the pro-oncoprotein tls/fus and is able to promote d-loop formation. *J Biol Chem*, 274(48):34337–42, Nov 1999.

[77] P Bertrand, A T Akhmedov, F Delacote, A Durrbach, and B S Lopez. Human pomp75 is identified as the pro-oncoprotein tls/fus: both pomp75 and pomp100 dna homologous pairing activities are associated to cell proliferation. *Oncogene*, 18(31):4515–21, Aug 1999.

[78] G G Hicks, N Singh, A Nashabi, S Mai, G Bozek, L Klewes, D Arapovic, E K White, M J Koury, E M Oltz, L Van Kaer, and H E Ruley. Fus deficiency in mice results in defective B-lymphocyte development and activation, high levels of chromosomal instability and perinatal death. *Nature genetics*, 24(2):175–179, February 2000.

[79] M Kuroda, J Sok, L Webb, H Baechtold, F Urano, Y Yin, P Chung, D G de Rooij, A Akhmedov, T Ashley, and D Ron. Male sterility and enhanced radiation sensitivity in TLS(-/-) mice. *The EMBO journal*, 19(3):453–462, February 2000.

[80] A Bertolotti, Y Lutz, D J Heard, P Chambon, and L Tora. htaf(ii)68, a novel rna/ssdna-binding protein with homology to the pro-oncoproteins tls/fus and ews is associated with both tfiid and rna polymerase ii. *EMBO J*, 15(18):5022–31, Sep 1996.

[81] Adelene Y Tan and James L Manley. Tls inhibits rna polymerase iii transcription. *Mol Cell Biol*, 30(1):186–96, Jan 2010.

[82] C A Powers, M Mathur, B M Raaka, D Ron, and H H Samuels. Tls (translocated-in-liposarcoma) is a high-affinity interactor for steroid, thyroid hormone, and retinoid receptors. *Mol Endocrinol*, 12(1):4–18, Jan 1998.

[83] Adelene Y Tan, Todd R Riley, Tristan Coady, Harmen J Bussemaker, and James L Manley. Tls/fus (translocated in liposarcoma/fused in sarcoma) regulates target gene transcription via single-stranded dna response elements. *Proc Natl Acad Sci U S A*, 109(16):6030–5, Apr 2012.

[84] C Calvio, G Neubauer, M Mann, and A I Lamond. Identification of hnrnp p2 as tls/fus using electrospray mass spectrometry. *RNA*, 1(7):724–33, Sep 1995.

[85] Juri Rappsilber, Ursula Ryder, Angus I Lamond, and Matthias Mann. Large-scale proteomic analysis of the human spliceosome. *Genome Res*, 12(8):1231–45, Aug 2002.

[86] Zhaolan Zhou, Lawrence J Licklider, Steven P Gygi, and Robin Reed. Comprehensive proteomic analysis of the human spliceosome. *Nature*, 419(6903):182–5, Sep 2002.

[87] A Lerga, M Hallier, L Delva, C Orvain, I Gallais, J Marie, and F Moreau-Gachelin. Identification of an rna binding specificity for the potential splicing factor tls. *J Biol Chem*, 276(9):6807–16, Mar 2001.

[88] M Hallier, A Lerga, S Barnache, A Tavitian, and F Moreau-Gachelin. The transcription factor spi-1/pu.1 interacts with the potential splicing factor tls. *J Biol Chem*, 273(9):4838–42, Feb 1998.

[89] Clotilde Lagier-Tourenne, Magdalini Polymenidou, Kasey R Hutt, Anthony Q Vu, Michael Baughn, Stephanie C Huelga, Kevin M Clutario, Shuo-Chien Ling, Tiffany Y Liang, Curt Mazur, Edward Wancewicz, Aneeza S Kim, Andy Watt, Sue Freier, Geoffrey G Hicks, John Paul Donohue, Lily Shiue, C Frank Bennett, John Ravits, Don W Cleveland, and Gene W Yeo. Divergent roles of ALS-linked proteins FUS/TLS and TDP-43 intersect in processing long pre-mRNAs. *Nature Neuroscience*, 15(11):1488–1497, November 2012.

[90] Shinsuke Ishigaki, Akio Masuda, Yusuke Fujioka, Yohei Iguchi, Masahisa Katsuno, Akihide Shibata, Fumihiko Urano, Gen Sobue, and Kinji Ohno. Position-dependent fus-rna interactions regulate alternative splicing events and transcriptions. *Sci Rep*, 2:529, 2012.

[91] Tadashi Nakaya, Panagiotis Alexiou, Manolis Maragkakis, Alexandra Chang, and Zissimos Mourelatos. Fus regulates genes coding for rna-binding proteins in

neurons by binding to their highly conserved introns. *RNA*, 19(4):498–509, Apr 2013.

[92] Boris Rogelj, Laura E Easton, Gireesh K Bogu, Lawrence W Stanton, Gregor Rot, Tomaž Curk, Blaž Zupan, Yoichiro Sugimoto, Miha Modic, Nejc Haberman, James Tollervey, Ritsuko Fujii, Toru Takumi, Christopher E Shaw, and Jernej Ule. Widespread binding of fus along nascent rna regulates alternative splicing in the brain. *Sci Rep*, 2:603, 2012.

[93] Jessica I Hoell, Erik Larsson, Simon Runge, Jeffrey D Nusbaum, Sujitha Duggimpudi, Thalia A Farazi, Markus Hafner, Arndt Borkhardt, Chris Sander, and Thomas Tuschl. RNA targets of wild-type and mutant FET family proteins. *Nature Structural & Molecular Biology*, 18(12):1428–1431, November 2011.

[94] Denise Orozco and Dieter Edbauer. Fus-mediated alternative splicing in the nervous system: consequences for als and ftld. *J Mol Med (Berl)*, 91(12):1343–54, Dec 2013.

[95] Ritsuko Fujii and Toru Takumi. TLS facilitates transport of mRNA encoding an actin-stabilizing protein to dendritic spines. *Journal of cell science*, 118(Pt 24):5755–5765, December 2005.

[96] Denise Orozco, Sabina Tahirovic, Kristin Rentzsch, Benjamin M Schwenk, Christian Haass, and Dieter Edbauer. Loss of fused in sarcoma (fus) promotes pathological tau splicing. *EMBO Rep*, 13(8):759–64, Aug 2012.

[97] Kurt R Brunden, John Q Trojanowski, and Virginia M-Y Lee. Evidence that non-fibrillar tau causes pathology linked to neurodegeneration and behavioral impairments. *J Alzheimers Dis*, 14(4):393–9, Aug 2008.

[98] Alix de Calignon, Leora M Fox, Rose Pitstick, George A Carlson, Brian J Bacskai, Tara L Spires-Jones, and Bradley T Hyman. Caspase activation precedes and leads to tangles. *Nature*, 464(7292):1201–4, Apr 2010.

[99] J E Tobin, J C Latourelle, M F Lew, C Klein, O Suchowersky, H A Shill, L I Golbe, M H Mark, J H Growdon, G F Wooten, B A Racette, J S Perlmutter, R Watts, M Guttman, K B Baker, S Goldwurm, G Pezzoli, C Singer, M H Saint-Hilaire, A E Hendricks, S Williamson, M W Nagle, J B Wilk, T Massood, J M Laramie, A L DeStefano, I Litvan, G Nicholson, A Corbett, S Isaacson, D J Burn, P F Chinnery, P P Pramstaller, S Sherman, J Al-hinti, E Drasby, M Nance, A T

Moller, K Ostergaard, R Roxburgh, B Snow, J T Slevin, F Cambi, J F Gusella, and R H Myers. Haplotypes and gene expression implicate the mapt region for parkinson disease: the genepd study. *Neurology*, 71(1):28–34, Jul 2008.

[100] H Zinszner, J Sok, D Immanuel, Y Yin, and D Ron. Tls (fus) binds rna in vivo and engages in nucleo-cytoplasmic shuttling. *J Cell Sci*, 110 (Pt 15):1741–50, Aug 1997.

[101] Ritsuko Fujii, Shigeo Okabe, Tomoe Urushido, Kiyoshi Inoue, Atsushi Yoshimura, Taro Tachibana, Toru Nishikawa, Geoffrey G Hicks, and Toru Takumi. The rna binding protein tls is translocated to dendritic spines by mglur5 activation and regulates spine morphology. *Curr Biol*, 15(6):587–93, Mar 2005.

[102] Yoshimitsu Kanai, Naoshi Dohmae, and Nobutaka Hirokawa. Kinesin transports rna: isolation and characterization of an rna-transporting granule. *Neuron*, 43(4):513–25, Aug 2004.

[103] Atsushi Yoshimura, Ritsuko Fujii, Yasuhito Watanabe, Shigeo Okabe, Kenji Fukui, and Toru Takumi. Myosin-va facilitates the accumulation of mrna/protein complex in dendritic spines. *Curr Biol*, 16(23):2345–51, Dec 2006.

[104] Ritsuko Fujii, Shigeo Okabe, Tomoe Urushido, Kiyoshi Inoue, Atsushi Yoshimura, Taro Tachibana, Toru Nishikawa, Geoffrey G Hicks, and Toru Takumi. The RNA binding protein TLS is translocated to dendritic spines by mGluR5 activation and regulates spine morphology. *Current biology : CB*, 15(6):587–593, March 2005.

[105] Tetsuro Murakami, Seung-Pil Yang, Lin Xie, Taizo Kawano, Donald Fu, Asuka Mukai, Christopher Bohm, Fusheng Chen, Janice Robertson, Hiroshi Suzuki, Gian Gaetano Tartaglia, Michele Vendruscolo, Gabriele S Kaminski Schierle, Fiona T S Chan, Aileen Moloney, Damian Crowther, Clemens F Kaminski, Mei Zhen, and Peter St George-Hyslop. ALS mutations in FUS cause neuronal dysfunction and death in Caenorhabditis elegans by a dominant gain-of-function mechanism. *Human Molecular Genetics*, 21(1):1–9, January 2012.

[106] Ji-Wu Wang, Jonathan R Brent, Andrew Tomlinson, Neil A Shneider, and Brian D McCabe. The ALS-associated proteins FUS and TDP-43 function together to affect Drosophila locomotion and life span. *The Journal of clinical investigation*, 121(10):4118–4126, October 2011.

[107] Hiroshi Sasayama, Mai Shimamura, Takahiko Tokuda, Yumiko Azuma, Tomokatsu Yoshida, Toshiki Mizuno, Masanori Nakagawa, Nobuhiro Fujikake, Yoshitaka Nagai, and Masamitsu Yamaguchi. Knockdown of the Drosophila fused in sarcoma (FUS) homologue causes deficient locomotive behavior and shortening of motoneuron terminal branches. *PloS one*, 7(6):e39483, 2012.

[108] Nicholas A Lanson, Astha Maltare, Hanna King, Rebecca Smith, Ji Han Kim, J Paul Taylor, Thomas E Lloyd, and Udai Bhan Pandey. A Drosophila model of FUS-related neurodegeneration reveals genetic interaction between FUS and TDP-43. *Human Molecular Genetics*, 20(13):2510–2523, July 2011.

[109] Yanbo Chen, Mengxue Yang, Jianwen Deng, Xiaoping Chen, Ye Ye, Li Zhu, Jianghong Liu, Haihong Ye, Yan Shen, Yan Li, Elizabeth J Rao, Kazuo Fushimi, Xiaohong Zhou, Eileen H Bigio, Marsel Mesulam, Qi Xu, and Jane Y Wu. Expression of human fus protein in drosophila leads to progressive neurodegeneration. *Protein Cell*, 2(6):477–86, Jun 2011.

[110] Edor Kabashi, Valérie Bercier, Alexandra Lissouba, Meijiang Liao, Edna Brustein, Guy A Rouleau, and Pierre Drapeau. FUS and TARDBP but Not SOD1 Interact in Genetic Models of Amyotrophic Lateral Sclerosis. *PLoS Genetics*, 7(8):e1002214, August 2011.

[111] R Fujii. TLS facilitates transport of mRNA encoding an actin-stabilizing protein to dendritic spines. *Journal of cell science*, 118(24):5755–5765, December 2005.

[112] Jacqueline C Mitchell, Philip McGoldrick, Caroline Vance, Tibor Hortobagyi, Jemeen Sreedharan, Boris Rogelj, Elizabeth L Tudor, Bradley N Smith, Christian Klasen, Christopher C J Miller, Jonathan D Cooper, Linda Greensmith, and Christopher E Shaw. Overexpression of human wild-type fus causes progressive motor neuron degeneration in an age- and dose-dependent fashion. *Acta Neuropathol*, 125(2):273–88, Feb 2013.

[113] Cao Huang, Hongxia Zhou, Jianbin Tong, Han Chen, Yong-Jian Liu, Dian Wang, Xiaotao Wei, and Xu-Gang Xia. FUS transgenic rats develop the phenotypes of amyotrophic lateral sclerosis and frontotemporal lobar degeneration. *PLoS Genetics*, 7(3):e1002011, March 2011.

[114] Dimitris Beis and Didier Y R Stainier. In vivo cell biology: following the zebrafish trend. *Trends Cell Biol*, 16(2):105–12, Feb 2006.

[115] Kerstin Howe, Matthew D Clark, Carlos F Torroja, James Torrance, Camille Berthelot, Matthieu Muffato, John E Collins, Sean Humphray, Karen McLaren, Lucy Matthews, Stuart McLaren, Ian Sealy, Mario Caccamo, Carol Churcher, Carol Scott, Jeffrey C Barrett, Romke Koch, Gerd-Jörg Rauch, Simon White, William Chow, Britt Kilian, Leonor T Quintais, José A Guerra-Assunção, Yi Zhou, Yong Gu, Jennifer Yen, Jan-Hinnerk Vogel, Tina Eyre, Seth Redmond, Ruby Banerjee, Jianxiang Chi, Beiyuan Fu, Elizabeth Langley, Sean F Maguire, Gavin K Laird, David Lloyd, Emma Kenyon, Sarah Donaldson, Harminder Sehra, Jeff Almeida-King, Jane Loveland, Stephen Trevanion, Matt Jones, Mike Quail, Dave Willey, Adrienne Hunt, John Burton, Sarah Sims, Kirsten McLay, Bob Plumb, Joy Davis, Chris Clee, Karen Oliver, Richard Clark, Clare Riddle, David Elliot, David Eliott, Glen Threadgold, Glenn Harden, Darren Ware, Sharmin Begum, Beverley Mortimore, Beverly Mortimer, Giselle Kerry, Paul Heath, Benjamin Phillimore, Alan Tracey, Nicole Corby, Matthew Dunn, Christopher Johnson, Jonathan Wood, Susan Clark, Sarah Pelan, Guy Griffiths, Michelle Smith, Rebecca Glithero, Philip Howden, Nicholas Barker, Christine Lloyd, Christopher Stevens, Joanna Harley, Karen Holt, Georgios Panagiotidis, Jamieson Lovell, Helen Beasley, Carl Henderson, Daria Gordon, Katherine Auger, Deborah Wright, Joanna Collins, Claire Raisen, Lauren Dyer, Kenric Leung, Lauren Robertson, Kirsty Ambridge, Daniel Leongamornlert, Sarah McGuire, Ruth Gilderthorp, Coline Griffiths, Deepa Manthravadi, Sarah Nichol, Gary Barker, Siobhan Whitehead, Michael Kay, Jacqueline Brown, Clare Murnane, Emma Gray, Matthew Humphries, Neil Sycamore, Darren Barker, David Saunders, Justene Wallis, Anne Babbage, Sian Hammond, Maryam Mashreghi-Mohammadi, Lucy Barr, Sancha Martin, Paul Wray, Andrew Ellington, Nicholas Matthews, Matthew Ellwood, Rebecca Woodmansey, Graham Clark, James D Cooper, James Cooper, Anthony Tromans, Darren Grafham, Carl Skuce, Richard Pandian, Robert Andrews, Elliot Harrison, Andrew Kimberley, Jane Garnett, Nigel Fosker, Rebekah Hall, Patrick Garner, Daniel Kelly, Christine Bird, Sophie Palmer, Ines Gehring, Andrea Berger, Christopher M Dooley, Zübeyde Ersan-Ürün, Cigdem Eser, Horst Geiger, Maria Geisler, Lena Karotki, Anette Kirn, Judith Konantz, Martina Konantz, Martina Oberländer, Silke Rudolph-Geiger, Mathias Teucke, Christa Lanz, Günter Raddatz, Kazutoyo Osoegawa, Baoli Zhu, Amanda Rapp, Sara Widaa, Cordelia Langford, Fengtang Yang, Stephan C Schuster, Nigel P Carter, Jennifer Harrow, Zemin Ning, Javier Herrero, Steve M J Searle, Anton Enright, Robert Geisler, Ronald H A Plasterk, Charles Lee, Monte Westerfield, Pieter J de Jong,

Leonard I Zon, John H Postlethwait, Christiane Nüsslein-Volhard, Tim J P Hubbard, Hugues Roest Crollius, Jane Rogers, and Derek L Stemple. The zebrafish reference genome sequence and its relationship to the human genome. *Nature*, 496(7446):498–503, Apr 2013.

[116] Graham J Lieschke and Peter D Currie. Animal models of human disease: zebrafish swim into view. *Nat Rev Genet*, 8(5):353–67, May 2007.

[117] Richard White, Kristin Rose, and Leonard Zon. Zebrafish cancer: the state of the art and the path forward. *Nat Rev Cancer*, 13(9):624–36, Sep 2013.

[118] Aarti Asnani and Randall T Peterson. The zebrafish as a tool to identify novel therapies for human cardiovascular disease. *Dis Model Mech*, 7(7):763–7, Jul 2014.

[119] Asha Seth, Derek L Stemple, and Inês Barroso. The emerging use of zebrafish to model metabolic disease. *Dis Model Mech*, 6(5):1080–8, Sep 2013.

[120] Amnon Schlegel and Philipp Gut. Metabolic insights from zebrafish genetics, physiology, and chemical biology. *Cell Mol Life Sci*, Jan 2015.

[121] Yung-Yao Lin. Muscle diseases in the zebrafish. *Neuromuscul Disord*, 22(8):673–84, Aug 2012.

[122] Morgan Newman, Esmaeil Ebrahimie, and Michael Lardelli. Using the zebrafish model for alzheimer's disease research. *Front Genet*, 5:189, 2014.

[123] Shunmoogum A Patten, Gary A B Armstrong, Alexandra Lissouba, Edor Kabashi, J Alex Parker, and Pierre Drapeau. Fishing for causes and cures of motor neuron disorders. *Dis Model Mech*, 7(7):799–809, Jul 2014.

[124] Andrew J Rennekamp and Randall T Peterson. 15 years of zebrafish chemical screening. *Curr Opin Chem Biol*, 24:58–70, Feb 2015.

[125] Cameron Wyatt, Ewelina M Bartoszek, and Emre Yaksi. Methods for studying the zebrafish brain: past, present and future. *Eur J Neurosci*, Apr 2015.

[126] Philipp Gut, Bernat Baeza-Raja, Olov Andersson, Laura Hasenkamp, Joseph Hsiao, Daniel Hesselson, Katerina Akassoglou, Eric Verdin, Matthew D Hirschey, and Didier Y R Stainier. Whole-organism screening for gluconeogenesis identifies activators of fasting metabolism. *Nat Chem Biol*, 9(2):97–104, Feb 2013.

[127] David Kokel, Jennifer Bryan, Christian Laggner, Rick White, Chung Yan J Cheung, Rita Mateus, David Healey, Sonia Kim, Andreas A Werdich, Stephen J Haggarty, Calum A Macrae, Brian Shoichet, and Randall T Peterson. Rapid behavior-based identification of neuroactive small molecules in the zebrafish. *Nat Chem Biol*, 6(3):231–237, Mar 2010.

[128] David Kokel, Chung Yan J Cheung, Robert Mills, Jaeda Coutinho-Budd, Liyi Huang, Vincent Setola, Jared Sprague, Shan Jin, Youngnam N Jin, Xi-Ping Huang, Giancarlo Bruni, Clifford J Woolf, Bryan L Roth, Michael R Hamblin, Mark J Zylka, David J Milan, and Randall T Peterson. Photochemical activation of trpa1 channels in neurons and animals. *Nat Chem Biol*, 9(4):257–63, Apr 2013.

[129] W Driever, L Solnica-Krezel, A F Schier, S C Neuhauss, J Malicki, D L Stemple, D Y Stainier, F Zwartkruis, S Abdelilah, Z Rangini, J Belak, and C Boggs. A genetic screen for mutations affecting embryogenesis in zebrafish. *Development*, 123:37–46, Dec 1996.

[130] P Haffter, M Granato, M Brand, M C Mullins, M Hammerschmidt, D A Kane, J Odenthal, F J van Eeden, Y J Jiang, C P Heisenberg, R N Kelsh, M Furutani-Seiki, E Vogelsang, D Beuchle, U Schach, C Fabian, and C Nüsslein-Volhard. The identification of genes with unique and essential functions in the development of the zebrafish, danio rerio. *Development*, 123:1–36, Dec 1996.

[131] A Amsterdam, S Burgess, G Golling, W Chen, Z Sun, K Townsend, S Farrington, M Haldi, and N Hopkins. A large-scale insertional mutagenesis screen in zebrafish. *Genes Dev*, 13(20):2713–24, Oct 1999.

[132] Brent R Bill, Andrew M Petzold, Karl J Clark, Lisa A Schimmenti, and Stephen C Ekker. A primer for morpholino use in zebrafish. *Zebrafish*, 6(1):69–77, Mar 2009.

[133] Cecilia B Moens, Thomas M Donn, Emma R Wolf-Saxon, and Taylur P Ma. Reverse genetics in zebrafish by tilling. *Brief Funct Genomic Proteomic*, 7(6):454–9, Nov 2008.

[134] Erno Wienholds, Stefan Schulte-Merker, Brigitte Walderich, and Ronald H A Plasterk. Target-selected inactivation of the zebrafish rag1 gene. *Science*, 297(5578):99–102, Jul 2002.

[135] Yannick Doyon, Jasmine M McCammon, Jeffrey C Miller, Farhoud Faraji, Catherine Ngo, George E Katibah, Rainier Amora, Toby D Hocking, Lei Zhang, Edward J Rebar, Philip D Gregory, Fyodor D Urnov, and Sharon L Amacher. Heritable targeted gene disruption in zebrafish using designed zinc-finger nucleases. *Nat Biotechnol*, 26(6):702–8, Jun 2008.

[136] Xiangdong Meng, Marcus B Noyes, Lihua J Zhu, Nathan D Lawson, and Scot A Wolfe. Targeted gene inactivation in zebrafish using engineered zinc-finger nucleases. *Nat Biotechnol*, 26(6):695–701, Jun 2008.

[137] Peng Huang, An Xiao, Mingguo Zhou, Zuoyan Zhu, Shuo Lin, and Bo Zhang. Heritable gene targeting in zebrafish using customized talens. *Nat Biotechnol*, 29(8):699–700, Aug 2011.

[138] Jeffrey C Miller, Siyuan Tan, Guijuan Qiao, Kyle A Barlow, Jianbin Wang, Danny F Xia, Xiangdong Meng, David E Paschon, Elo Leung, Sarah J Hinkley, Gladys P Dulay, Kevin L Hua, Irina Ankoudinova, Gregory J Cost, Fyodor D Urnov, H Steve Zhang, Michael C Holmes, Lei Zhang, Philip D Gregory, and Edward J Rebar. A tale nuclease architecture for efficient genome editing. *Nat Biotechnol*, 29(2):143–8, Feb 2011.

[139] Jeffry D Sander, Lindsay Cade, Cyd Khayter, Deepak Reyon, Randall T Peterson, J Keith Joung, and Jing-Ruey J Yeh. Targeted gene disruption in somatic zebrafish cells using engineered talens. *Nat Biotechnol*, 29(8):697–8, Aug 2011.

[140] Nannan Chang, Changhong Sun, Lu Gao, Dan Zhu, Xiufei Xu, Xiaojun Zhu, Jing-Wei Xiong, and Jianzhong Jeff Xi. Genome editing with rna-guided cas9 nuclease in zebrafish embryos. *Cell Res*, 23(4):465–72, Apr 2013.

[141] Alexander Hruscha, Peter Krawitz, Alexandra Rechenberg, Verena Heinrich, Jochen Hecht, Christian Haass, and Bettina Schmid. Efficient crispr/cas9 genome editing with low off-target effects in zebrafish. *Development*, 140(24):4982–7, Dec 2013.

[142] Woong Y Hwang, Yanfang Fu, Deepak Reyon, Morgan L Maeder, Prakriti Kaini, Jeffry D Sander, J Keith Joung, Randall T Peterson, and Jing-Ruey Joanna Yeh. Heritable and precise zebrafish genome editing using a crispr-cas system. *PLoS One*, 8(7):e68708, 2013.

[143] Woong Y Hwang, Yanfang Fu, Deepak Reyon, Morgan L Maeder, Shengdar Q Tsai, Jeffry D Sander, Randall T Peterson, J-R Joanna Yeh, and J Keith Joung. Efficient genome editing in zebrafish using a crispr-cas system. *Nat Biotechnol*, 31(3):227–9, Mar 2013.

[144] Li-En Jao, Susan R Wente, and Wenbiao Chen. Efficient multiplex biallelic zebrafish genome editing using a crispr nuclease system. *Proc Natl Acad Sci U S A*, 110(34):13904–9, Aug 2013.

[145] Bettina Schmid and Christian Haass. Genomic editing opens new avenues for zebrafish as a model for neurodegeneration. *J Neurochem*, 127(4):461–70, Nov 2013.

[146] Jimann Shin, Jiakun Chen, and Lilianna Solnica-Krezel. Efficient homologous recombination-mediated genome engineering in zebrafish using tale nucleases. *Development*, 141(19):3807–18, Oct 2014.

[147] Yao Zu, Xiangjun Tong, Zhanxiang Wang, Da Liu, Ruochuan Pan, Zhe Li, Yingying Hu, Zhou Luo, Peng Huang, Qian Wu, Zuoyan Zhu, Bo Zhang, and Shuo Lin. Talen-mediated precise genome modification by homologous recombination in zebrafish. *Nat Methods*, 10(4):329–31, Apr 2013.

[148] Dana Carroll. Genome engineering with zinc-finger nucleases. *Genetics*, 188(4):773–82, Aug 2011.

[149] Fyodor D Urnov, Edward J Rebar, Michael C Holmes, H Steve Zhang, and Philip D Gregory. Genome editing with engineered zinc finger nucleases. *Nat Rev Genet*, 11(9):636–46, Sep 2010.

[150] J Keith Joung and Jeffry D Sander. Talens: a widely applicable technology for targeted genome editing. *Nat Rev Mol Cell Biol*, 14(1):49–55, Jan 2013.

[151] Blake Wiedenheft, Samuel H Sternberg, and Jennifer A Doudna. Rna-guided genetic silencing systems in bacteria and archaea. *Nature*, 482(7385):331–8, Feb 2012.

[152] Martin Jinek, Krzysztof Chylinski, Ines Fonfara, Michael Hauer, Jennifer A Doudna, and Emmanuelle Charpentier. A programmable dual-rna-guided dna endonuclease in adaptive bacterial immunity. *Science*, 337(6096):816–21, Aug 2012.

[153] Patrick R Blackburn, Jarryd M Campbell, Karl J Clark, and Stephen C Ekker. The crispr system–keeping zebrafish gene targeting fresh. *Zebrafish*, 10(1):116–8, Mar 2013.

[154] Tennore Ramesh, Alison N Lyon, Ricardo H Pineda, Chunping Wang, Paul M L Janssen, Benjamin D Canan, Arthur H M Burghes, and Christine E Beattie. A genetic model of amyotrophic lateral sclerosis in zebrafish displays phenotypic hallmarks of motoneuron disease. *Dis Model Mech*, 3(9-10):652–62, 2010.

[155] Stacey A Sakowski, J Simon Lunn, Angela S Busta, Sang Su Oh, Grettel Zamora-Berridi, Madeline Palmer, Andrew A Rosenberg, Stephen G Philip, James J Dowling, and Eva L Feldman. Neuromuscular effects of g93a-sod1 expression in zebrafish. *Mol Neurodegener*, 7:44, 2012.

[156] Barbara Solchenberger, Claire Russell, Elisabeth Kremmer, Christian Haass, and Bettina Schmid. Granulin knock out zebrafish lack frontotemporal lobar degeneration and neuronal ceroid lipofuscinosis pathology. *PLoS One*, 10(3):e0118956, 2015.

[157] Bettina Schmid, Alexander Hruscha, Sebastian Hogl, Julia Banzhaf-Strathmann, Katrin Strecker, Julie van der Zee, Mathias Teucke, Stefan Eimer, Jan Hegermann, Maike Kittelmann, Elisabeth Kremmer, Marc Cruts, Barbara Solchenberger, Laura Hasenkamp, Frauke van Bebber, Christine Van Broeckhoven, Dieter Edbauer, Stefan F Lichtenthaler, and Christian Haass. Loss of als-associated tdp-43 in zebrafish causes muscle degeneration, vascular dysfunction, and reduced motor neuron axon outgrowth. *Proc Natl Acad Sci U S A*, 110(13):4986–91, Mar 2013.

[158] Channa A A Hewamadduma, Andrew J Grierson, Taylur P Ma, Luyuan Pan, Cecilia B Moens, Philip W Ingham, Tennore Ramesh, and Pamela J Shaw. Tardbpl splicing rescues motor neuron and axonal development in a mutant tardbp zebrafish. *Hum Mol Genet*, 22(12):2376–86, Jun 2013.

[159] Edor Kabashi, Li Lin, Miranda L Tradewell, Patrick A Dion, Valérie Bercier, Patrick Bourgouin, Daniel Rochefort, Samar Bel Hadj, Heather D Durham, Christine Vande Velde, Guy A Rouleau, and Pierre Drapeau. Gain and loss of function of als-related mutations of tardbp (tdp-43) cause motor deficits in vivo. *Hum Mol Genet*, 19(4):671–83, Feb 2010.

[160] Angela S Laird, Annelies Van Hoecke, Louis De Muynck, Mieke Timmers, Ludo Van den Bosch, Philip Van Damme, and Wim Robberecht. Progranulin is neurotrophic in vivo and protects against a mutant tdp-43 induced axonopathy. *PLoS One*, 5(10):e13368, 2010.

[161] Nicholas A Lanson, Jr and Udai Bhan Pandey. Fus-related proteinopathies: lessons from animal models. *Brain Res*, 1462:44–60, Jun 2012.

[162] Jacques A Villefranc, Julio Amigo, and Nathan D Lawson. Gateway compatible vectors for analysis of gene function in the zebrafish. *Dev Dyn*, 236(11):3077–87, Nov 2007.

[163] Christian Mosimann, Charles K Kaufman, Pulin Li, Emily K Pugach, Owen J Tamplin, and Leonard I Zon. Ubiquitous transgene expression and cre-based recombination driven by the ubiquitin promoter in zebrafish. *Development*, 138(1):169–77, Jan 2011.

[164] M C Mullins, M Hammerschmidt, P Haffter, and C Nüsslein-Volhard. Large-scale mutagenesis in the zebrafish: in search of genes controlling development in a vertebrate. *Curr Biol*, 4(3):189–202, Mar 1994.

[165] C B Kimmel, W W Ballard, S R Kimmel, B Ullmann, and T F Schilling. Stages of embryonic development of the zebrafish. *Dev Dyn*, 203(3):253–310, Jul 1995.

[166] J Karlsson, J von Hofsten, and P E Olsson. Generating transparent zebrafish: a refined method to improve detection of gene expression during embryonic development. *Mar Biotechnol (NY)*, 3(6):522–7, Nov 2001.

[167] Tripti Gupta and Mary C Mullins. Dissection of organs from the adult zebrafish. *J Vis Exp*, (37), 2010.

[168] S C Baraban, M R Taylor, P A Castro, and H Baier. Pentylenetetrazole induced changes in zebrafish behavior, neural activity and c-fos expression. *Neuroscience*, 131(3):759–68, 2005.

[169] Fatma O Kok, Masahiro Shin, Chih-Wen Ni, Ankit Gupta, Ann S Grosse, Andreas van Impel, Bettina C Kirchmaier, Josi Peterson-Maduro, George Kourkoulis, Ira Male, Dana F DeSantis, Sarah Sheppard-Tindell, Lwaki Ebarasi, Christer Betsholtz, Stefan Schulte-Merker, Scot A Wolfe, and Nathan D Lawson. Reverse genetic screening reveals poor correlation between morpholino-induced and mutant phenotypes in zebrafish. *Dev Cell*, 32(1):97–108, Jan 2015.

[170] Dominik Paquet, Ratan Bhat, Astrid Sydow, Eva-Maria Mandelkow, Stefan Berg, Sven Hellberg, Johanna Fälting, Martin Distel, Reinhard W Köster, Bettina Schmid, and Christian Haass. A zebrafish model of tauopathy allows in vivo imaging of neuronal cell death and drug evaluation. *The Journal of clinical investigation*, 119(5):1382–1395, May 2009.

[171] T Ishikawa, M Morita, and I Nakano. Constant blood flow reduction in premotor frontal lobe regions in als with dementia - a spect study with 3d-ssp. *Acta Neurol Scand*, 116(5):340–4, Nov 2007.

[172] M Tanaka, S Kondo, S Hirai, X Sun, T Yamagishi, and K Okamoto. Cerebral blood flow and oxygen metabolism in progressive dementia associated with amyotrophic lateral sclerosis. *J Neurol Sci*, 120(1):22–8, Dec 1993.

[173] Farida Emran, Jason Rihel, and John E Dowling. A behavioral assay to measure responsiveness of zebrafish to changes in light intensities. *J Vis Exp*, (20), 2008.

[174] David Kokel, Jennifer Bryan, Christian Laggner, Rick White, Chung Yan J Cheung, Rita Mateus, David Healey, Sonia Kim, Andreas A Werdich, Stephen J Haggarty, Calum A Macrae, Brian Shoichet, and Randall T Peterson. Rapid behavior-based identification of neuroactive small molecules in the zebrafish. *Nature chemical biology*, 6(3):231–237, March 2010.

[175] Jason Rihel and Alexander F Schier. Behavioral screening for neuroactive drugs in zebrafish. *Dev Neurobiol*, 72(3):373–85, Mar 2012.

[176] Eva Bentmann, Manuela Neumann, Sabina Tahirovic, Ramona Rodde, Dorothee Dormann, and Christian Haass. Requirements for stress granule recruitment of fused in sarcoma (fus) and tar dna-binding protein of 43 kda (tdp-43). *J Biol Chem*, 287(27):23079–94, Jun 2012.

[177] L Van Den Bosch, P Van Damme, E Bogaert, and W Robberecht. The role of excitotoxicity in the pathogenesis of amyotrophic lateral sclerosis. *Biochim Biophys Acta*, 1762(11-12):1068–82, 2006.

[178] Eva Bentmann, Christian Haass, and Dorothee Dormann. Stress granules in neurodegeneration–lessons learnt from tar dna binding protein of 43 kda and fused in sarcoma. *FEBS J*, 280(18):4348–70, Sep 2013.

[179] A Y Tan and J L Manley. The TET Family of Proteins: Functions and Roles in Disease. *Journal of Molecular Cell Biology*, 1(2):82–92, November 2009.

[180] Miler T Lee, Ashley R Bonneau, and Antonio J Giraldez. Zygotic genome activation during the maternal-to-zygotic transition. *Annu Rev Cell Dev Biol*, 30:581–613, 2014.

[181] Mary Lou King, Timothy J Messitt, and Kimberly L Mowry. Putting rnas in the right place at the right time: Rna localization in the frog oocyte. *Biol Cell*, 97(1):19–33, Jan 2005.

[182] Christine E Holt and Simon L Bullock. Subcellular mrna localization in animal cells and why it matters. *Science*, 326(5957):1212–6, Nov 2009.

[183] Gaku Kumano. Polarizing animal cells via mrna localization in oogenesis and early development. *Dev Growth Differ*, 54(1):1–18, Jan 2012.

[184] Jennifer A Schisa. Effects of stress and aging on ribonucleoprotein assembly and function in the germ line. *Wiley Interdiscip Rev RNA*, 5(2):231–46, 2014.

[185] Jennifer A Schisa. New insights into the regulation of rnp granule assembly in oocytes. *Int Rev Cell Mol Biol*, 295:233–89, 2012.

[186] G Dreyfuss, M J Matunis, S Piñol-Roma, and C G Burd. hnrnp proteins and the biogenesis of mrna. *Annu Rev Biochem*, 62:289–321, 1993.

[187] A M Krecic and M S Swanson. hnrnp complexes: composition, structure, and function. *Curr Opin Cell Biol*, 11(3):363–71, Jun 1999.

[188] Hong Joo Kim, Nam Chul Kim, Yong-Dong Wang, Emily A Scarborough, Jennifer Moore, Zamia Diaz, Kyle S MacLea, Brian Freibaum, Songqing Li, Amandine Molliex, Anderson P Kanagaraj, Robert Carter, Kevin B Boylan, Aleksandra M Wojtas, Rosa Rademakers, Jack L Pinkus, Steven A Greenberg, John Q Trojanowski, Bryan J Traynor, Bradley N Smith, Simon Topp, Athina-Soragia Gkazi, Jack Miller, Christopher E Shaw, Michael Kottlors, Janbernd Kirschner, Alan Pestronk, Yun R Li, Alice Flynn Ford, Aaron D Gitler, Michael Benatar, Oliver D King, Virginia E Kimonis, Eric D Ross, Conrad C Weihl, James Shorter, and J Paul Taylor. Mutations in prion-like domains in hnrnpa2b1 and hnrnpa1 cause multisystem proteinopathy and als. *Nature*, 495(7442):467–73, Mar 2013.

[189] Kohji Mori, Sven Lammich, Ian R A Mackenzie, Ignasi Forné, Sonja Zilow, Hans Kretzschmar, Dieter Edbauer, Jonathan Janssens, Gernot Kleinberger, Marc Cruts, Jochen Herms, Manuela Neumann, Christine Van Broeckhoven, Thomas

Arzberger, and Christian Haass. hnrnp a3 binds to ggggcc repeats and is a constituent of p62-positive/tdp43-negative inclusions in the hippocampus of patients with c9orf72 mutations. *Acta Neuropathol*, 125(3):413–23, Mar 2013.

[190] Ritsuko Fujii and Toru Takumi. Tls facilitates transport of mrna encoding an actin-stabilizing protein to dendritic spines. *J Cell Sci*, 118(Pt 24):5755–65, Dec 2005.

[191] Jake N Miller and David A Pearce. Nonsense-mediated decay in genetic disease: friend or foe? *Mutat Res Rev Mutat Res*, 762:52–64, 2014.

[192] Jessica I Hoell, Erik Larsson, Simon Runge, Jeffrey D Nusbaum, Sujitha Duggimpudi, Thalia A Farazi, Markus Hafner, Arndt Borkhardt, Chris Sander, and Thomas Tuschl. Rna targets of wild-type and mutant fet family proteins. *Nat Struct Mol Biol*, 18(12):1428–31, Dec 2011.

[193] Yueqin Zhou, Songyan Liu, Guodong Liu, Arzu Oztürk, and Geoffrey G Hicks. Als-associated fus mutations result in compromised fus alternative splicing and autoregulation. *PLoS Genet*, 9(10):e1003895, Oct 2013.

[194] Balu Kamaraj, Vidya Rajendran, Rao Sethumadhavan, Chundi Vinay Kumar, and Rituraj Purohit. Mutational analysis of fus gene and its structural and functional role in amyotrophic lateral sclerosis 6. *J Biomol Struct Dyn*, 33(4):834–44, 2015.

[195] Annelies M A van der Laan, Alice M C van Gemert, Roeland W Dirks, Jasprina N Noordermeer, Lee G Fradkin, Hans J Tanke, and Carolina R Jost. mrna cycles through hypoxia-induced stress granules in live drosophila embryonic muscles. *Int J Dev Biol*, 56(9):701–9, 2012.

[196] Soong Ho Kim, Willie K Dong, Ivan Jeanne Weiler, and William T Greenough. Fragile x mental retardation protein shifts between polyribosomes and stress granules after neuronal injury by arsenite stress or in vivo hippocampal electrode insertion. *J Neurosci*, 26(9):2413–8, Mar 2006.

[197] Katie Moisse, Kathryn Volkening, Cheryl Leystra-Lantz, Ian Welch, Tracy Hill, and Michael J Strong. Divergent patterns of cytosolic tdp-43 and neuronal progranulin expression following axotomy: implications for tdp-43 in the physiological response to neuronal injury. *Brain Res*, 1249:202–11, Jan 2009.

[198] L Amaducci and G Tesco. Aging as a major risk for degenerative diseases of the central nervous system. *Curr Opin Neurol*, 7(4):283–6, Aug 1994.

[199] Qiudong Deng, Christopher J Holler, Georgia Taylor, Kathryn F Hudson, William Watkins, Marla Gearing, Daisuke Ito, Melissa E Murray, Dennis W Dickson, Nicholas T Seyfried, and Thomas Kukar. Fus is phosphorylated by dna-pk and accumulates in the cytoplasm after dna damage. *J Neurosci*, 34(23):7802–13, Jun 2014.

[200] J S Eisen and J C Smith. Controlling morpholino experiments: don't stop making antisense. *Development (Cambridge, England)*, 135(10):1735–1743, April 2008.

[201] Babykumari P Chitramuthu, David C Baranowski, Denis G Kay, Andrew Bateman, and Hugh Pj Bennett. Progranulin modulates zebrafish motoneuron development in vivo and rescues truncation defects associated with knockdown of survival motor neuron 1. *Mol Neurodegener*, 5:41, 2010.

[202] Marjo J den Broeder, Herma van der Linde, Judith R Brouwer, Ben A Oostra, Rob Willemsen, and René F Ketting. Generation and characterization of fmr1 knockout zebrafish. *PLoS One*, 4(11):e7910, 2009.

[203] Ben Tucker, Robert I Richards, and Michael Lardelli. Contribution of mglur and fmr1 functional pathways to neurite morphogenesis, craniofacial development and fragile x syndrome. *Hum Mol Genet*, 15(23):3446–58, Dec 2006.

[204] Manuela Neumann, Chiara F Valori, Olaf Ansorge, Hans A Kretzschmar, David G Munoz, Hirofumi Kusaka, Osamu Yokota, Kenji Ishihara, Lee-Cyn Ang, Juan M Bilbao, and Ian R A Mackenzie. Transportin 1 accumulates specifically with fet proteins but no other transportin cargos in ftld-fus and is absent in fus inclusions in als with fus mutations. *Acta Neuropathol*, 124(5):705–16, Nov 2012.

[205] Cuong Q Diep, Dongdong Ma, Rahul C Deo, Teresa M Holm, Richard W Naylor, Natasha Arora, Rebecca A Wingert, Frank Bollig, Gordana Djordjevic, Benjamin Lichman, Hao Zhu, Takanori Ikenaga, Fumihito Ono, Christoph Englert, Chad A Cowan, Neil A Hukriede, Robert I Handin, and Alan J Davidson. Identification of adult nephron progenitors capable of kidney regeneration in zebrafish. *Nature*, 470(7332):95–100, Feb 2011.

[206] Sumeet Pal Singh, Jennifer E Holdway, and Kenneth D Poss. Regeneration of

amputated zebrafish fin rays from de novo osteoblasts. *Dev Cell*, 22(4):879–86, Apr 2012.

[207] Matthew Gemberling, Travis J Bailey, David R Hyde, and Kenneth D Poss. The zebrafish as a model for complex tissue regeneration. *Trends Genet*, 29(11):611–20, Nov 2013.

[208] Ching-Ling Lien, Michael R Harrison, Tai-Lan Tuan, and Vaughn A Starnes. Heart repair and regeneration: recent insights from zebrafish studies. *Wound Repair Regen*, 20(5):638–46, 2012.

[209] Catherina G Becker and Thomas Becker. Adult zebrafish as a model for successful central nervous system regeneration. *Restor Neurol Neurosci*, 26(2-3):71–80, 2008.

[210] Veronika Kuscha, Sarah L Frazer, Tatyana B Dias, Masahiko Hibi, Thomas Becker, and Catherina G Becker. Lesion-induced generation of interneuron cell types in specific dorsoventral domains in the spinal cord of adult zebrafish. *J Comp Neurol*, 520(16):3604–16, Nov 2012.

[211] Rebecca Schmidt, Uwe Strähle, and Steffen Scholpp. Neurogenesis in zebrafish - from embryo to adult. *Neural Dev*, 8:3, 2013.

[212] Caghan Kizil, Jan Kaslin, Volker Kroehne, and Michael Brand. Adult neurogenesis and brain regeneration in zebrafish. *Dev Neurobiol*, 72(3):429–61, Mar 2012.

[213] Sorana Ciura, Serena Lattante, Isabelle Le Ber, Morwena Latouche, Hervé Tostivint, Alexis Brice, and Edor Kabashi. Loss of function of c9orf72 causes motor deficits in a zebrafish model of amyotrophic lateral sclerosis. *Ann Neurol*, 74(2):180–7, Aug 2013.

[214] Edor Kabashi, Valérie Bercier, Alexandra Lissouba, Meijiang Liao, Edna Brustein, Guy A Rouleau, and Pierre Drapeau. Fus and tardbp but not sod1 interact in genetic models of amyotrophic lateral sclerosis. *PLoS Genet*, 7(8):e1002214, Aug 2011.

[215] Robin Lemmens, Annelies Van Hoecke, Nicole Hersmus, Veerle Geelen, Isabel D'Hollander, Vincent Thijs, Ludo Van Den Bosch, Peter Carmeliet, and Wim Robberecht. Overexpression of mutant superoxide dismutase 1 causes a motor axonopathy in the zebrafish. *Hum Mol Genet*, 16(19):2359–65, Oct 2007.

[216] Michelle L McWhorter, Umrao R Monani, Arthur H M Burghes, and Christine E Beattie. Knockdown of the survival motor neuron (smn) protein in zebrafish causes defects in motor axon outgrowth and pathfinding. *J Cell Biol*, 162(5):919–31, Sep 2003.

[217] Dominik Paquet, Ratan Bhat, Astrid Sydow, Eva-Maria Mandelkow, Stefan Berg, Sven Hellberg, Johanna Fälting, Martin Distel, Reinhard W Köster, Bettina Schmid, and Christian Haass. A zebrafish model of tauopathy allows in vivo imaging of neuronal cell death and drug evaluation. *J Clin Invest*, 119(5):1382–95, May 2009.

[218] Ping Song and Sanjay W Pimplikar. Knockdown of amyloid precursor protein in zebrafish causes defects in motor axon outgrowth. *PLoS One*, 7(4):e34209, 2012.

9 Acknowledgements

In everyone's life, at some time, our inner fire goes out. It is then burst into flame by an encounter with another human being. We should all be thankful for those people who rekindle the inner spirit. **Albert Schweitzer**

I am especially grateful to...

... **Prof. Christian Haass** for scientifically supervising my thesis and being my "Dr. Father". Thank you for your motivating enthusiasm, constant support and the opportunity to conduct my thesis in your institute.

... **Dr. Bettina Schmid** for the direct scientific supervision, fruitful discussions, helpful input and constant support. Your door was always open.

... **Prof. Thomas Misgeld** and **Prof. Rüdiger Klein** for their interest in my work and for scientific discussions during Thesis Advisory Committee Meetings and beyond.

... the **Hans and Ilse Breuer Foundation** and the **International Max Planck Research School for life sciences** for financial support.

... **Dr. Elisabeth Kremmer** for generation and supply of antibodies

... **Dr. Thomas Arzberger** and **Brigitte Kraft** for medical and scientific input as well as technical IHC support.

... **Dr. Dorothee Dormann**, **Dr. Eva Bentmann** and **Dr. Marc Calvet Suarez** for sharing interest in FUS and for the supply with constructs and antibodies.

... **Dr. Benjamin Schwenk** for expertise in and supply with rat primary cortical neurons, constructs, antibodies, and staining protocols.

... **Sabine Odoy** and **Barbara Kassner** for the excellent lab management and help with all

kinds of paper work.

... **all current zebrafish lab members and alumni** for the fish solidarity, inspiring atmosphere, constructive discussions and technical support.

... **all current Haass lab members and alumni** for the friendly working atmosphere, scientific input, technical advice.

... **Dr. Benjamin Schwenk** and **Dr. Katrin Strecker** for critically reading parts of this thesis.

... **Lulu, Mummy, Dad and you precious ones** supporting me through the ups and downs of research, for believing in me and my strengths and encouraging me to follow my dreams.